

Doctoral School of Material Sciences and Technologies

MODELING LEAD-FREE INTERCONNECT RELIABILITY UNDER CREEP IN ADVANCED PACKAGING

OE-BGK Student's name: Ramiro Sebastian Vargas Cruz

ATDI Registration number: T000382/FI12904/D

2025 Supervisor's name: Viktor Gonda



Doctoral School of Material Sciences and Technologies

STUDENT DECLARATION

The undersigned student hereby declares that the thesis as his results, the literature, and the tools used can be identified. Results in the achieved thesis may be used for the purposes and tasks of the university awarding institution free of charge, subject to any restrictions on encryption.

Budapest, June 13th, 2025

Student's Signature

Abstract

In the constant evolution of electronic packaging, downscaled electronic boards will lead to smaller, faster, and more function rich electronics. The soldered interconnects are crucial in the reliability of electronics, and new soldering materials are developed for the various demands. Various lead-free, microalloyed solders are introduced, and it is essential to analyze whether an alloy would provide the required performance at both mechanical and electrical requirements without compromising the mechanical and electronic integrity. In such a performance analysis, computational simulations of the performance may accelerate developments. This work aims to compare different lead-free soldering materials using Anand's Creep mathematical model in Finite Element Analysis (FEA) software.

Initially, SAC (Sn-Ag-Cu, tin-silver-copper) solders 305, 387, and Sn3.5Ag were compared to the eutectic SnPb solder. This foundational study revealed advantageous creep strain behavior under thermal and mechanical loads. The geometry considered for this purpose was largely simplified in order to provide insight into the deformation behavior within a chip stack. Furthermore, a reverse engineering approach was defined to intercalculate material parameters between the Anand and Power Law creep models.

Since SAC305 alloys are widely successful, besides their behavior may be largely influenced by the delivery state, a comparison of several Anand Parameter sets for SAC305 was conducted. Despite using the same composition, six papers reported different sets of Anand parameters. Furthermore, the geometry was improved to better align with recent developments in electronic packaging. Fan-out wafer-level packaging was incorporated into the study. Based on the results, the optimal set of parameters regarding agreement with other sets and simulation time was determined. Additionally, doped SAC solders were included in the comparison to assess whether creep behavior can be compared. The advantages of incorporating bismuth (Bi), nickel (Ni), and antimony (Sb) into SAC solders were demonstrated by the creep strain energy based analysis.

While investigating similar studies in FEA, it was noticed that most researchers employ idealized geometries at the solder—solder pad vicinity in the modeling. Microscopic images show that copper pad edges may not be ideally sharp due to the

subtractive processing steps, the real shape might be better approximated by a chamfer or fillet shape. In addition, Intermetallic compound layers (IMC) were usually neglected in the simulations. For these reasons, for a new set of comparisons were defined for the pad geometry and interfacial properties involved. Results displayed a significant reduction in creep strain and more stable curves, adding variations in the copper pad edge. This change in geometry also leads to a more evident difference in creep strain energy density between SAC305 and doped SAC solders. Creep strain energy density is critical for reliability prediction. As for the IMC inclusion, a 5% increment in creep curves was reported.

Finally, all the geometrical models briefly described above were designed in 2-D to optimize computing resources versus the computationally cost demanding 3-D simulation, which would provide may accurate results at significantly higher computation times. Thus, a pseudo-3-D model was designed for a comparison where the following parameters were varied: soldering material, copper pad geometry, interfacial layer quality, and simulation domain: 2-D vs. pseudo-3-D. Creep strain curves and stress vs. strain curves displayed a significant change. Values from the curves obtained from the pseudo-3-D model were leaser than those obtained from the 2-D model. Further changes could be implemented to the model presented in this research to approximate experimental results accurately. This research suggests that IMC layers can be neglected when analyzing a broader scale, and doped SAC solders present a notorious advantage over SAC305. It also proves the importance of not idealizing the geometry of the copper pad edge.

Acknowledgments

"The definition of insanity is doing the same thing over and over,

Albert Einstein

and expecting different results."

I want to thank many people and institutions, but I will keep it short by mentioning the most valuable contributions:

My family, Patricio, Carmita, and Valeria, unconditional support throughout the process.

Dr. Viktor Gonda, my supervisor. I firmly believe that Hungary needs more lecturers like him.

Stipendium Hungaricum for their initiative in bringing international students to Hungary.

CONTENTS

A	bstract		i
A	cknowledg	gments	iii
1.	. Introdu	ection	1
	1.1 Sc	oldering Materials	2
	1.1.1	Solder Modeling Evolution	4
	1.1.2	Importance of time-dependent variables analysis	5
	1.2 Cı	reep Material Models	6
	1.2.1	Creep definition	6
	1.2.2	Five Power Law Model	7
	1.2.3	Diffusive Creep	8
	1.2.4	Harper-Dorn Creep Model	8
	1.2.5	Anand Creep Model	9
	1.3 O	utline of the thesis	10
	1.4 O	bjectives	11
2.	. Fundar	mental thermal-mechanical behavior of soldered Stacks	13
	2.1 In	troduction	13
	2.1.1	Comparison of lead-free vs. lead-containing solders	14
	2.2 Si	mulation Setup	15
	2.2.1	Geometry description	15
	2.2.2	Material Properties	16
	1.1.1	Load Case	17
	2.2.3	Boundary Conditions	18
	2.2.4	Point of analysis	18
	2.2.5	Power-law creep parameters	19
	2.3 Re	esults and Discussion	19
	2.3.1	Eutectic Lead-containing vs. Lead-free solders comparison	19
	2.3.2	Power-law Creep Parameters Proposal	21

	2.4	Conclusions	23
3.	Effe	ect of Anand parameters on the behavior of soldered stacks	25
	3.1	Introduction	2
	3.1.	1 Fan-Out Wafer Level Packaging	2
	3.1.	2 SAC Solders	2
	3.1.	3 Doped SAC solders	2
	3.2	Simulation Setup	30
	3.2.	1 Geometry description	30
	3.2.	2 Material Properties	3
	3.2.	3 Load Case and Job Parameters	32
	3.3	Results and Discussion	33
	3.3.	1 SAC305 variation of Anand parameters	3
	3.3.	2 SAC305 vs. SACX solders	3:
	3.4	Conclusions	3
4.	Ana	alysis of reliability models and first estimation of reliability indicators	39
	4.1	Introduction	39
	4.1.1	Failure prediction models	39
	4.2	Simulation Setup	4
	4.2.	1 Geometry of the Copper Pad	4
	4.2.	2 Initial and Boundary Conditions	4
	4.2.	3 Material Properties	4
	4.2.	4 Overview of the studied cases	4
	4.3	Results and Discussion	4:
	4.3.	1 Effect of the Bond Pad Geometry	40
	4.3.	2 Reliability prediction analysis	4
	4.4	Conclusions	4
5.	Effi	cient modeling framework for estimation of reliability indicators	50
	5.1	Introduction	50
	5.2	Simulation Setup	52

	5.2.1	Model geometry	52
	5.2.2	Material Models and Properties	54
	5.2.3	Boundary conditions	55
	5.2.4	Summary of Parameters Variation	56
5	.3 Re	sults and Discussion	57
	5.3.1	General Observations	57
	5.3.2	Creep Strain and Creep Strain Energy Density	59
	5.3.3	Von Mises and Shear Stresses	61
	5.3.4	Hysteresis Curves	63
	5.3.5	Reliability-Related Predictions	64
5	.4 Cc	onclusions	65
6.	Summa	ry of New Scientific Results	67
7.	List of	Publications	69
7	.1 Ar	ticles in internationally reviewed academic journals	69
7	.2 Pa	pers at international scientific conferences.	69
8.	Recomi	mendations and Outlook	70
Figu	ıres		71
Tab	les		73
Dof	oroncos		75

1. Introduction

Recent regulations on Waste from Electrical and Electronic Equipment (WEEE) and Restrictions on Hazardous Substances (RoHS) have limited the usage of Pb (lead) in electronic applications [1], [2]. One of the critical lead-containing components in the electronics industry is the soldering material; the eutectic Sn-Pb (tin-lead) solder had to be replaced by lead-free soldering materials. Typically, solder joints are subjected to temperatures around 80% of their melting temperature during their service life [3]. A significant change in the composition of the soldering material increases the melting temperature, but this should not compromise the electronic device's performance and reliability.

One of the first compositions that replaced lead-containing solders was the near-eutectic Sn-Ag-Cu (tin-silver-copper), widely known as SAC solder [4]. Varying the percentage by weight (wt.%) and composition of the alloys, different SAC solders have been commercialized (e.g., SAC305, SAC405, SAC105) [5]. In the automotive industry, thermal requirements have been defined for Integrated Circuits (ICs) that undergo harsh working environments where temperature loads may reach over 150°C [6]. Consequently, new solder materials, called doped-SAC or SAC-X, were developed [7].

Currently, electronic equipment reliability is linked to performance and security [8]. Therefore, it is essential to understand reliability tests and mathematical models that can effectively predict the lifetime of materials. Regarding thermal cycling reliability tests, recent studies have proved the accuracy of Finite Element Analysis (FEA) on IC simulations with lifetime prediction errors of less than 20% [9]. Lead-free solder joint reliability is of great interest in accurately predicting the service life of an electronic device.

Solder materials are the main components of electronic circuit boards, along with semiconductors, ceramics, plastics, and composites. Due to its advantageous characteristics, eutectic SnPb solder was initially predominant in printed circuit boards (PCBs) manufacturing. With the introduction of lead-free solder materials, the solder selection should be based on considerations of thermal-mechanical reliability.

Printed Circuit Board (PCB) working conditions can result in irreversible deformations after a significant period. To assess the reliability of solder joints, a model proposed by Dudek [10] conceives viscoplastic deformation behavior as the sum of elastic, rate-independent plastic, and creep strain at constant stress above $0.5T_{\rm m}$ ($T_{\rm m}$: absolute melting temperature). However, under continuous thermo-mechanical loads, Zhang [11] suggests that rate-independent plasticity and primary creep deformation are negligible. Numerous mathematical models and simulations have been carried out considering creep to predict failures due to cyclic loads at a constant temperature.

1.1 Soldering Materials

The first patents and concepts of the printed circuit board (PCB) were introduced by Charles L. in 1925 [12]. It consisted of a copper layer shaped like a path that interconnected electronic components. This concept replaced the traditional wiring process in circuit manufacturing. However, a joining material was needed to secure the circuit after mounting the electronic components on the PCB. This material, known as solder, is a fusible alloy with a low melting temperature and is usually eutectic. The solder provides the mechanical and electrical connection between the copper path and the electronic component. Moreover, the electricity that flows through the solder and the surrounding environment causes a slight cycling thermal load. According to the application of electronic packaging, some of the most common temperature ranges are detailed in Table 1.1.

Table 1.1. Thermal environments for solder in several electronic packages [13].

Use conditions	Thermal e	xcurs	ion (°C)
Consumer electronics	0	to	60
Computers	15	to	60
Telecommunications	-40	to	85
Commercial aircraft	- 55	to	95
Military aircraft	- 55	to	125
Space	-40	to	85
Automotive – Passenger compartment	- 55	to	65
Automotive – Under the hood	- 55	to	150

For over 50 years, eutectic tin-lead (SnPb) solder has been valued for its unique combination of outstanding properties and reliability. While lead is economically suitable, it poses health hazards. Specifically, lead can interfere with the reproductive and cardiovascular systems, among other issues [14]. Consequently, in 2002, the

European Parliament enacted the Restriction of Hazardous Substances Directive (RoHS) to limit lead usage in electrical and electronic equipment [2]. This regulatory document was revised in 2011 [15] to include more specific weight percentages and some exceptions. RoHS impacted European industries and markets in China, Japan, South Korea, Turkey, and the United States. As the 2006 deadline for implementing such restrictions approached, tin-silver-copper (SnAgCu), commonly known as SAC-solder, emerged as the best alternative to eutectic SnPb solder [16]. Among the major companies, Philips reported their initial test results regarding SAC405 (Ag 4% and Cu 0.5%) in 2004. They encountered challenges related to solder pre-heat time, which damaged the plastic housing of electro/magnetic components. Furthermore, they recommended changes to design rules regarding round pad dimensions [17]. Solder materials must meet precise characteristics for high performance and long-lasting PCB longevity. Some of the most pertinent manufacturing, reliability, and performance properties to consider before selecting solder material are detailed in Table 1.2.

Table 1.2. Essential properties of solder alloys [18].

Properties relevant to manufacturing	Properties relevant to reliability and performance
Melting/liquidus temperature Wettability (of copper) Cost Environmental friendliness Availability and number of suppliers Manufacturability using current processes Ability to be made into balls Copper pick-up rate Recyclability Ability to be made into a paste	 Electrical conductivity Thermal conductivity Coefficient of thermal expansion Shear properties Tensile properties Creep resistance Fatigue properties Corrosion and oxidation resistance Intermetallic compound formation

Early studies conducted by Hwang in 2001 on SAC alloys showed promising results. SAC alloys present an overall finer microstructure that lengthens the life of a solder joint [19]. Nevertheless, PCB manufacturing also comprises electronic components and solder paste. Thus, the melting temperature is a primary concern for solder paste manufacturers as they recommend a high-temperature peak value for favorable wetting. On the other hand, component manufacturers suggest a low-temperature peak value not to damage the component itself [20]. Considering these two recommendations, Salam et al. [21] concluded that the maximum melting temperature should not exceed 230°C. Additionally, the time above liquidus should

be 40s for the ramp-soak-spike reflow profile and 50 to 70s for the ramp-to-spike reflow profile.

1.1.1 Solder Modeling Evolution

Various simulations and models have been evaluated since 2006, the deadline for applying the RoHS regulations. Hongtao [22], referred to several sources to evaluate the accuracy of material constants applied to the Garofalo hyperbolic and Dorn power-law creep model. After comparing the results with experimental procedures, Hongtao concluded that SAC405 solder had a higher creep resistance than Sn–Pb solder at the same stress level and testing temperature [22].

Although creep is usually analyzed when the temperature exceeds fifty percent of melting point (T_m) , several works have been carried out to evaluate creep at low temperatures. Cheng et al. -2005 evaluated the Anand model for Sn3.5Ag solder, suggesting some improvements that agreed better with experimental results [23].

Lee et al. – 2011 proved that shear modulus, temperature dependency, and grain size play an important role in the creep model. The three proposed models fit better with the experimental data as compared to the classic models like Anand and Power-law [24]. On the other hand, Zhang et al. – 2013 ran experiments on low-temperature creep. Although creep deformation is mainly analyzed with temperatures above half of the melting temperature, their study proves that solder alloys creep significantly at low temperatures rather than only deform elastically [25]. This study is of great interest for designing circuit boards that work at between room temperature and the solder's melting temperature.

More recent studies, like the one conducted by Subhasis et al. – 2016 reveal some disadvantages of phenomenological/empirical constitutive creep models for solders. Such models are relatively easy to use but omit microstructural and loading parameters. Subhasis et al. suggested a hybrid approach with mechanistic deformation to provide a more realistic model [26]. The latest research conducted by Thambi et al. – 2017 with the SAC387 revealed important conclusions. Thambi et al. highlighted that activation energy dependency on stress is crucial for creep equation development. Incorporating the steady-state flow stress concept considers the intercept of sub-grain structure. Thus, a better relation between creep deformation and microstructural

features was achieved [27]. However, as solder works under electricity flow, further research must also consider current density. The experimental study carried out by Yao et al. – 2017 suggests that current density affects both micro and macro mechanical properties and, consequently, creep behavior [28]. Long et al. – 2018 proposed a relation between the activation energy and the squared of current density to improve Norton's creep model for solders [29].

According to Ramachandran et al. – 2018 the most accepted creep models for soldering materials are Anand model and Garofalo-Arrhenius model (hyperbolic sine creep) [30]. Nevertheless, the second model (Garofalo-Arrhenius) has been found to have more sophisticated and generous results by considering the modified energy density [31].

All in all, creep behavior modeling is still a topic of interest since solder joints are subjected to multiple loads. Thermal, mechanical, and electrical loads have been found to affect macro and microstructural, mechanical properties, which leads to a change in the analysis of creep behavior. Some modifications to the existing models are still widely studied for SAC solders. However, researchers and institutes suggest going further in the analysis of solders containing In, Bi, and Zn.

1.1.2 Importance of time-dependent variables analysis

Time-dependent failures are a critical topic in material performance. For instance, steel is one of the main alloys for multidisciplinary applications. The International Organization for Standardization released a norm under reference 6303 in 1981. This norm established the procedures to determine and assess parameters for long-time stress rupture. Such parameters used to be obtained with a high variability, depending on the country [32]. Thus, ISO 6303 aims to minimize differences in estimation to ensure higher material durability. Similarly, in 1981, the European Creep Collaborative Committee (ECCC) was founded with 12 European countries. In 2011, the ECCC started to work on a joint industrial Project [33]. Currently, creep and more time-dependent variables are becoming of great interest due to their multiple applications in manufacturing and the expectation of a better long-lasting performance.

1.2 Creep Material Models

Before going through the fundamentals of creep, some definitions regarding alloys should be mentioned. An alloy represents the combination of different metals in different percentages, affecting the original components' phase diagram. The phase diagrams of alloys present several changes in temperature. However, alloys can be classified into two main types based on the similarity of creep behavior to pure metals. On one hand, Class I (also known as Class A) comprises alloys whose creep behavior highly differs from pure metals. On the other hand, Class II (also known as Class M) comprises alloys with a similar creep behavior in comparison with pure metals [34].

1.2.1 Creep definition

Creep is defined as the time-dependent plastic strain at constant stress above half the melting temperature (T_m) [35].

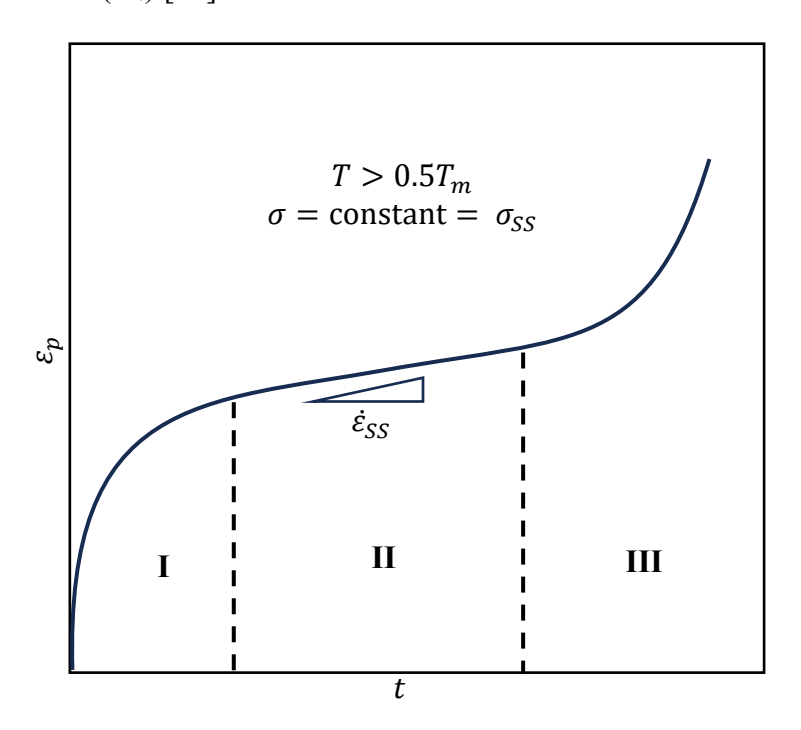


Figure 1.1 Constant true stress and constant strain rate creep behavior [35].

Creep comprises three stages: primary, secondary, and tertiary (see Figure 1.1). Along the primary stage (strain-hardening), the strain rate decreases, as hardening of the metal becomes more difficult. During the secondary stage, the strain rate is constant, this is usually called steady-state (SS) creep rate ($\dot{\varepsilon}_{SS}$). Finally, in the tertiary stage, the strain rate rises exponentially and eventually leads to a material fracture [36].

According to Kassner [35], creep can be discussed in the context of:

- 5 Power law creep.
- Diffusional creep.
- Harper-Dorn creep.
- 3-power viscous glide creep.

1.2.2 Five Power Law Model

Creep during the secondary state exhibits a direct proportion to temperature and stress. Thus, the basic power law (also known as Norton's Law) can be expressed as in (1.1).

Norton's Law:

$$\dot{\varepsilon}_{ss} = B\sigma^n \tag{1.1}$$

where B is a temperature-dependent material parameter and n depends on the material. After mathematical modelling, Ahmad et al. [37] expanded (1.1) into $\dot{\varepsilon}^c = A\sigma^n T^p$ where A and p are both characteristic constants of the material. Additionally, Brown and Ashby [38] suggests a strong logarithmic relation between Dorn constant (A) and the exponent n. Parameter n from (1.1) is 4 to 5 for pure metals (for that reason called "five" power law). It is also associated with dislocation creep (n = 4-5) and purely diffusive creep (n = 1) [39]. From the power law, multiple equations have been derived using several parameters that belong to the material of interest. Equation (1.2) details the generalized power-law equation for the creep strain rate, $\dot{\varepsilon}_{cr}$, which may incorporate, besides stress and temperature dependency, strain and time dependency as well, for non-linear, non-steady-state creep.

Generalized Power Law Equation:

$$\dot{\varepsilon}_{cr} = A(\sigma^m)(\varepsilon^n)(T^p)(q \cdot t^{q-1})$$
where,

A : Creep constant

m: Stress dependent exponent.

n : Creep strain dependent exponent.p : Temperature-dependent exponent.

q: Time dependent exponent.

1.2.3 Diffusive Creep

In terms of microstructure, a lattice plane contains at least three nonlinear lattice points. Diffusional creep involves changes in lattice planes that consequently affect vacancies [40]. According to the research done by Mesarovic [41], depending on the temperature and stress level, several micro-mechanisms of creep can be distinguished (see Table 1.3).

Table 1.3. Micro-mechanism of Creep.

Creep	Description
Nabarro-Herring [42], [43], [44]	Diffusion of vacancies through the crystalline
	lattice and complementary diffusion of atoms through the vacancy-atom exchange mechanism, leads to the creation of new lattice layers on some boundaries and disappearance of lattice layers on other boundaries.
Coble [44], [45]	
	Diffusion of vacancies/atoms along grain boundaries with the same outcome: lattice growth/disappearance.
Dislocation	Vacancy diffusion enables dislocation climb and glide.

1.2.4 Harper-Dorn Creep Model

In 1957, Harper and Dorn [46] suggested a new model for materials subjected to low stresses. Harper and Dorn found that the steady-state creep rate increased linearly with applied stress. After several experiments on aluminum, the equation (1.3) was proposed [47].

Harper-Dorn model:

$$\dot{\varepsilon}_{SS} = A_{HD} \left(\frac{D_1 G b}{kT} \right) \left(\frac{\sigma}{G} \right)^1 \tag{1.3}$$

where D_1 is the diffusion coefficient for lattice self-diffusion, G is the shear modulus, D is the Burger's vector, D is Boltzmann's constant, D is the absolute temperature, D is the applied stress, and D is a dimensionless constant of the order of D^{-11} . The early results of the Harper-Dorn model were later confirmed with tests in pure aluminum by Barrett et al. [48] and Mohamed et al. [49].

1.2.5 Anand Creep Model

In 1982 Anand [50] proposed two evolution equations from the flow equation (1.4) based on earlier theories suggested by Lee and Zaverl [51]. The primary purpose of this research was to analyze the deformation of metals at elevated temperatures above $0.5 T_m$ (absolute melting temperature). However, in 1985, after considering the second tensor (1.5) as another parameter, which characterizes the plastic state of a material, (1.6) and (1.7) where finally proposed [52].

Flow equation:

$$\dot{\varepsilon_p} = A \cdot \exp\left(-\frac{Q}{RT}\right) \left(\sinh\left(\xi \frac{\sigma}{s}\right)\right)^{1/m} \tag{1.4}$$

where

A : Pre-exponential factor.

Q : Activation energy.

R: Boltzmann constant.

 ξ : Multiplier of stress.

s : Deformation resistance.

m : Strain rate sensitivity of stress.

Second tensor equation

$$B = 1 - \frac{s}{s^*} \tag{1.5}$$

where

s* : Saturation resistance.

Evolution equations

$$\dot{\mathbf{s}} = \{h_0 | \mathbf{B} |^a \operatorname{sgn}(\mathbf{B})\} \dot{\varepsilon_p} \tag{1.6}$$

$$s^* = \hat{s} \left(\frac{\varepsilon_p}{A} \exp\left(\frac{Q}{RT} \right) \right)^n \tag{1.7}$$

where

h₀: Hardening constant.

a : Strain rate sensitivity of hardening.

\$: Deformation resistance saturation coefficient.

n : Strain rate sensitivity of saturation.

To sum up, the Anand model involves nine material parameters: A, Q, ξ , m, h_0 , \hat{s} , n, m, and s_0 , which is the initial value of the deformation resistance needed to

determine the evolution of the deformation resistance. All those values can be determined following Brown's procedure [53] who suggest at least two sets of three strain rate jump tests performed at different temperatures.

1.3 Outline of the thesis

The body of the following thesis work has been subdivided into four chapters.

Chapter Two summarizes the initial conceptualization of creep analysis in soldered stack. The simplified geometry used here emulates a ball-grid layout. The Anand model used for the solder, while external loads were combines thermal and mechanical load (vibration), and deformation and stress analyses were performed.

Besides eutectic SnPb solder material used as a reference, Anand's properties of leadfree solders as SAC387, SAC305, and Sn3.5Ag, were used. A reverse engineering approach for the intercalculation between Anand's and Power-Law model constants for SAC305 were demonstrated.

In Chapter Three, an enhanced interconnect geometry was employed in 2-D domain. A fan-out wafer-level packaging was modeled, and the analysis of material properties focused on SAC305 and doped SAC solders. From the initial results in Chapter Two, it was found that SAC305 has been widely characterized. Six different sets of Aanand parameters were reported by various authors who used different experiments and material treatments on the samples. Additionally, it was noted that the performance of novel alloys of lead-free solders were promising. The automotive industry has driven developments in SAC solders with added bismuth (Bi), nickel (Ni), and antimony (Sb) to endure harsh thermal working conditions.

Chapter Three aimed to compare the simulation results focusing on SAC305 where six different sets of Anand parameters were taken from the literature. After selecting an optimal certain set of parameters for SAC305, an additional comparison with SAC-X solders was conducted, introducing initial concepts of creep strain energy density for reliability approximation.

Chapter Four extends reliability models based on plastic deformation. Additionally, a more refined geometry is proposed. Similar studies revealed that the copper pad edge is idealized as sharp. By examining the solder stack's X-ray microscopic inspection, a fillet edge was incorporated into the original FOWLP

geometry. Variations in geometry and solder composition properties yielded numerous combinations that were compared. Overall, results concerning creep strain energy density for reliability prediction were presented, highlighting the significance of copper pad edge geometry.

In Chapter Five, two modifications were introduced to the previous geometry. First, to reduce the element's complexity, the chamfer edge replaced the fillet edge studied earlier. Second, two layers of intermetallic compound (IMC) were added, representing a new approach in the expansive field of Finite Element Analysis, where most authors overlook IMC layers in simulations. Finally, a pseudo-3-D approach was employed to approximate volume deformation similar to 3-D simulation. All 16 variations resulted in simulations considering only SAC305 and SACQ for the solder ball. The summary included the effects of variation in IMC inclusion, copper pad edge geometry, and element domain. Both stress and creep curves, along with relevant reliability values, were calculated.

In summary, this thesis focusses on the effect of geometrical, and materials evaluations, furthermore a domain simplification approach in FEA to create a cost effective framework for reliability predictions.

1.4 Objectives

Based on the outline of the following manuscript, this research aims to:

Utilize Anand's creep model to simulate the time- and temperature-dependent plastic deformation of solder joints under thermal and mechanical loads, allowing for accurate prediction of material behavior in electronic packaging.

Evaluate the mechanical responses of SnPb and lead-free solders (Sn-3.5Ag, SAC305, SAC387) under cyclic thermal and mechanical loading, identifying SAC305 as the most reliable lead-free alternative based on creep strain metrics.

Analyze six different sets of Anand parameters for SAC305 to identify the most computationally efficient and physically accurate set for simulation, and extend the study to include doped SAC solders (SACQ, SACR, InnoLot) to enhance reliability.

Examine the effects of idealized (sharp) versus realistic (fillet and chamfered) copper pad geometries on stress distribution and creep strain energy density, demonstrating that realistic geometries significantly enhance reliability predictions.

Incorporate IMC layers and develop a pseudo-3-D modeling framework to evaluate their influence on creep behavior and reliability indicators, concluding that while IMC layers have minor effects, pseudo-3-D models provide more realistic and reliable results than traditional 2-D simulations.

2. Fundamental thermal-mechanical behavior of soldered Stacks

The environmental hazards of conventional lead-tin solders have driven the transition to lead-free solder compositions. Among the alternatives, tin-silver-copper (SAC) alloys, such as Sn-3.5Ag, SAC305, and SAC387, are widely used because of their favorable electrical, mechanical, and thermal properties. With higher melting temperatures, these lead-free solders must endure thermal-mechanical loads, which can lead to significant deformations and stress in soldered electronic assemblies during thermal cycling.

The following chapter examines the thermal-mechanical creep behavior and structural integrity of electronic packages that contain solder joints. A Finite Element Model (FEM) was developed to simulate thermal cycling loads on a simplified package configuration, employing the Anand material model to characterize the creep behavior of the solders. Stress and strain analyses were conducted for the three types of lead-free solders, providing a comparative assessment of their mechanical responses. The results highlight the importance of understanding the mechanical behavior of lead-free solders to ensure the durability and integrity of electronic assemblies.

2.1 Introduction

Electronic assemblies are subjected to multiple thermal and mechanical loads during manufacturing and service, which can affect their reliability. Besides semiconductors, ceramics, plastics, and composites; solder materials can be considered the main components of electronic circuit boards. Integrated Circuits (ICs) and electronic components had external lead pins attached to the encapsulated circuit. After mounting the electronic components over the PCB, a joining material was needed to fix the circuit to the board. This material, known as solder, is a fusible alloy with a low melting temperature and commonly has a eutectic chemical composition. Due to downscaling, smaller electronic components were developed, and new surface-mounting technologies were introduced. External lead pins attached to the electronic components were replaced by metalized pads (see Figure 2.1). The Flip Chip (FC) assembly was one of the most advantageous in space optimization.

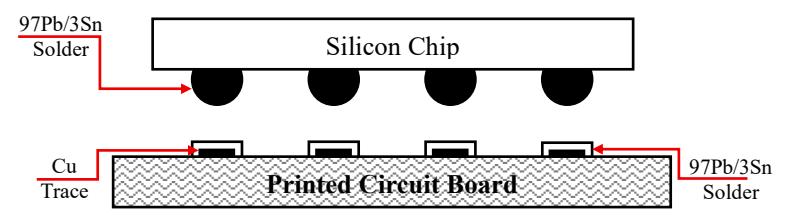


Figure 2.1 Flip Chip placement operation [54].

Due to its advantageous characteristics, the eutectic SnPb solder has been predominant in printed circuit board (PCB) manufacturing. However, international regulations have been launched to replace or limit the hazardous materials in electronic devices [2], such as the lead present in soldering materials. With the introduction of lead-free solder materials, the selection should be based on considerations of thermal-mechanical reliability.

PCB working conditions can lead to irreversible deformations after a prolonged period. To assess the reliability of solder joints, a model proposed by Dudek [10] conceives viscoplastic deformation behavior as the sum of elastic, rate-independent plastic, and creep strain at constant stress above $0.5T_{\rm m}$ ($T_{\rm m}$: absolute melting temperature). However, under constant thermo-mechanical loads, Zhang [11] suggests that rate-independent plasticity and primary creep deformation are negligible. Numerous mathematical models and simulations have been carried out considering creep to predict failures due to cyclic loads at a constant temperature.

2.1.1 Comparison of lead-free vs. lead-containing solders

Substituting the lead-containing solders, the candidates to replace them involved a challenging readjustment in the manufacturing processes. Failures to accomplish the new requirement implied significant business, financial, and legal implications [55]. To address this global concern, research and development activities focused on finding new alloys that replace conventional solder without affecting production costs. Selected publications about lead-free solders analysis and performance, among numerous articles and books, are detailed in Table 2.1. The main results generally reveal the advantages of lead-free solders in terms of creep resistance under cycling thermal loads.

Indeed, a primary requirement for lead-free solders is that their thermal-mechanical performance should reach or outperform that of conventional SnPb solder. Kotadia *et al.* [56] stressed that one of the main concerns of lead-free solders is to keep

the melting temperature around 183°C with eutectic or near-eutectic composition (see Table 2.2). Although SAC alloys are frequently used as a replacement for lead-containing solders, some other solder compositions are available with a lower melting temperature range.

Table 2.1. Selected studies on lead-free solders.

Author	Author Results					
Amagai <i>et al</i> . [57]	Considering drop, bend, and thermal cycling performance, 1.0 to 1.5 Ag is an optimum percentage for Sn-Ag-based solders. Sn-Ag-Cu is an optimum alloy for reducing intermetallic compounds and revealing high-reliability performance for dynamic loads like drop tests.					
Liang et al. [58] For isothermal low-cycle fatigue with modest strain ranges, Pb-fro outperform SnPb eutectic alloys. However, under thermal-moderate conditions, Pb-free alloys show significant deterioration of reliability large thermal strain or stress is encountered.						
Clech [59]	SAC solders are more creep-resistant than SnPb under low to medium stress					
Hongtao Ma et al. [60] From experiments of room-temperature aging, SAC405 shows less creep the SAC305, whereas SnPb solder with rather less stress than SAC shows a high creep strain (nearly fifty percent higher). Furthermore, the creep strain rates f SnPb seem to nearly stabilize with larger aging times, while SAC allowed continue to rise rapidly.						

Table 2.2. Composition and melting point of Pb-free solder alloys [56].

Alloy system		Composition				
Melting temperature below 180°C						
Bi-In	Bi-33In (eutectic)		109			
Sn-In	Sn-52In		118			
	Sn50In		118 - 125			
Sn-Bi	Sn-58Bi (eutectic)		138			
Melting tempera	ature range 180 – 20	00°C				
Sn-Bi-In	Sn-20Bi-10In		143 – 193			
Sn-Zn-Bi	Sn-8Zn3Bi		189 - 199			
Sn-Zn	Sn-Zn Sn-9Zn (eutectic)					
Melting tempera	ature range 180 – 23	80°C				
Sn-Ag	Sn-3.5Ag (eutection	e)	221			
	Sn-2Ag		221 - 226			
Sn-Ag-Cu	Sn-3.8Ag-0.7Cu	(SAC387)	217			
	(near eutectic)					
	Sn-3.9Ag-0.6Cu		~217			
	Sn-1Ag-0.5Cu	~217				
	Sn-3Ag-0.5Cu	~217				
	Sn-4Ag-0.5Cu	~217				
Sn-Cu	Sn-0.7Cu (eutection	227				

2.2 Simulation Setup

2.2.1 Geometry description

The following case study compares the equivalent creep strain and stress of three leadfree solders with the eutectic thin-lead solder. The modelled 2-D cross-section shown in Figure 2.2 comprises part of a Flip Chip assembly where the housing material of the electronic component is assumed to be ceramic [61].

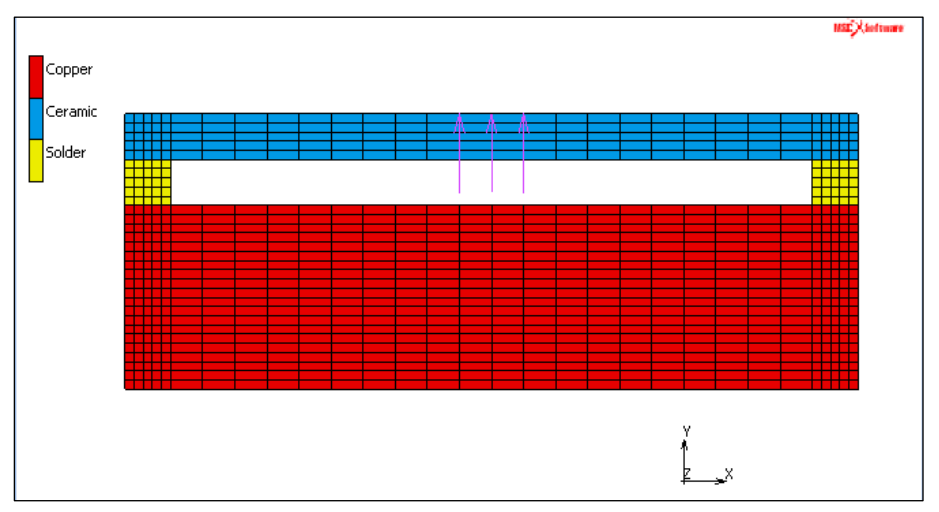


Figure 2.2 Flip-Chip Structural setup and materials description of the sample.

The software package used to run the simulations was MARC Mentat, which offers two options for processing creep analysis within its viscoplasticity properties: Power Law and Anand Model. Since the Anand model implies more parameters, this method was chosen to have more accurate results.

2.2.2 Material Properties

As this research describes creep behavior using the Anand Model, viscoplastic properties must be established. The elastic-plastic parameters for the eutectic SnPb solder, as well as for the three lead-free solders of interest, are detailed in

Table 2.3. Melting Temperature (T_m) was included to highlight the considerable variation between eutectic SnPb and unleaded solders (over 30°C). Additionally, Anand's parameters are listed in Table 2.4. It should be noted that most authors do not tabulate the activation energy; we computed it using the Boltzmann constant.

Table 2.3. Thermomechanical properties.

Material	T range (°C)	E (GPa)	ν	α (ppm/°C)	T_m (°C)
Sn3.5Ag [62]	20 – 150	48 - 25	0.40	20.2 - 21.7	221
SAC 305 [63]	25 - 125	90 - 38	0.42	16 - 22.4	217
SAC 387 [64]	20 - 100	46 - 35	0.40	17.6	217
SnPb [65]	25 - 125	22 - 12	0.40	21	183
Cu [4, 9]	-	1.3	0.34	17	1084
Ceramic [61]	_	0.375	0.22	5.36	_

Table 2.4. Material parameters for Anand model.

Description	Sn3.5Ag[67]	SAC 305 [68]	SAC 387 [69]	SnPb [61]
s ₀ (MPa)	0.65	21	37.1	56.33
$A(s^{-1})$	344.716	3 501	65.92	$1.49 \cdot 10^7$
ξ	3	4	8	11
m	0.143	0.25	0.346	0.303
h_0 (MPa)	23 241	180 000	86 442.8	2 640.75
ŝ (MPa)	26	30.2	80.8	80.42
n	0.0447	0.01	0.0002	0.0231
a	1.46	1.78	1.29	1.34
$Q\left(J\cdot \text{mol}^{-1}\right)$	54 364	77 490.78	55 307.8	90 040

1.1.1 Load Case

The center of the ceramic part (see Figure 2.2) was subjected to a vibration displacement load with an amplitude of 0.5 mm. The mechanical load consisted of a four-cycle sinusoidal oscillation running for 120 s, see Figure 2.3.

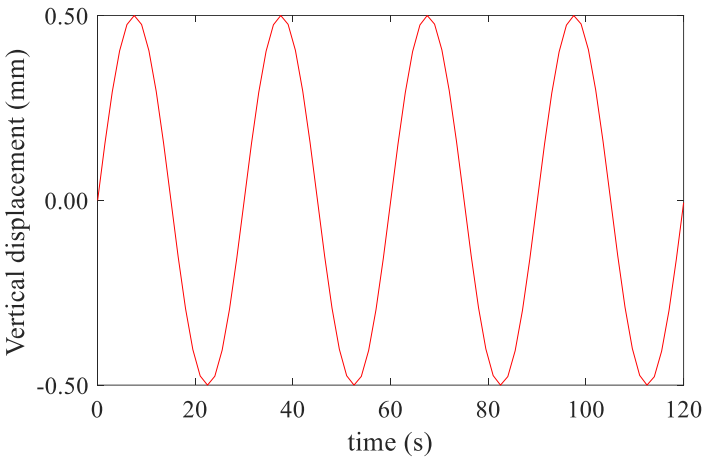


Figure 2.3 Sinusoidal Structural: Displacement vs Time.

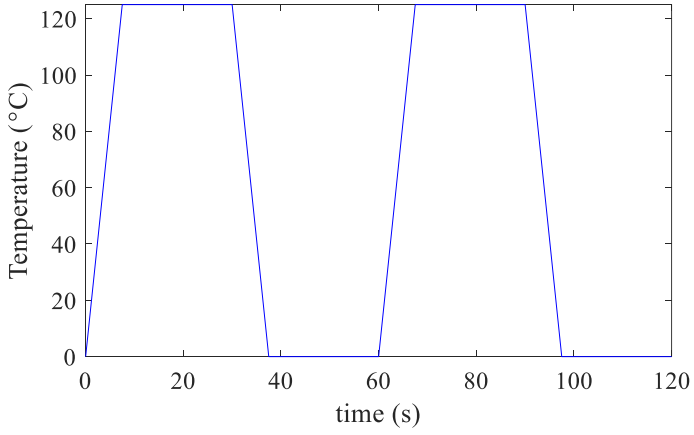


Figure 2.4 Thermal load: Temperature vs Time.

Simultaneously, a thermal load that changes the temperature of the entire sample from 0 to 125°C is also applied, describing two cycles (see Figure 2.4).

2.2.3 Boundary Conditions

As the vibration load case results in displacement, the bottom part of the copper layer must be fixed. Thus, restrictions regarding displacement and rotation in all three axes were applied to the bottom part of the sample (see Figure 2.5).

The cross-section is graphically described in Figure 2.2, and emulates only part of an entire Flip Chip assembly. A vibration load was applied in the center of the ceramic part to obtain critical values. Thus, displacement restriction in the horizontal axis *x* was used on both sides of the model (see Figure 2.6).

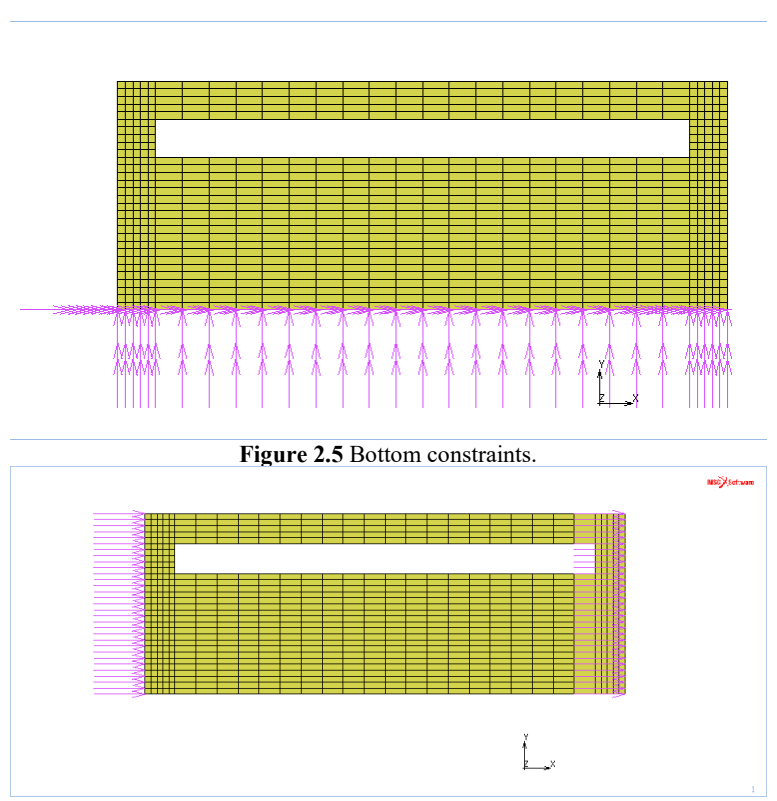


Figure 2.6 Horizontal boundary condition.

2.2.4 Point of analysis

As the main interest of this research is to determine the creep behavior of the solder materials, a middle inner point was selected to collect the data (see Figure 2.7). Equivalent Creep Strain (ECS), Total Equivalent Creep Strain (TECS), and Total Equivalent Stress (TES) data were collected from the previously described node.

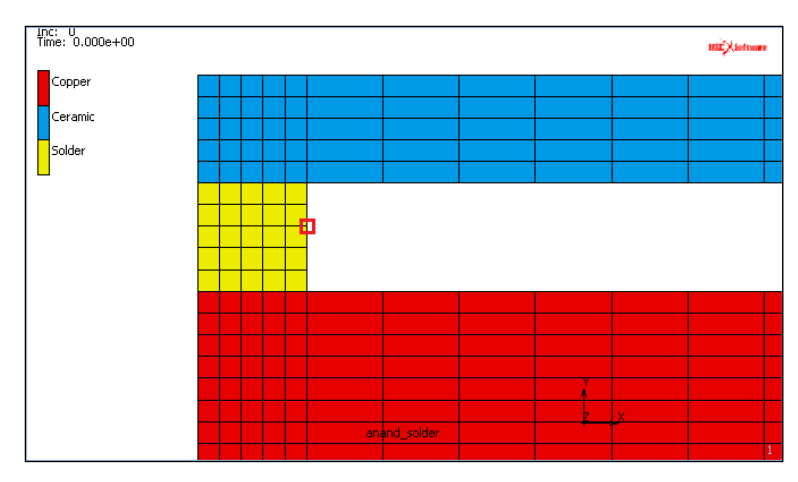


Figure 2.7 Point of analysis.

2.2.5 Power-law creep parameters

As detailed in the section 2.2.1 Marc Mentat offers creep analysis with only two mathematical models: Anand and Power-law. Therefore, theoretical Power Law creep parameters were calculated for SAC305 based on the SAC305 Anand results. Time, temperature, stress, and strain values were taken from the simulation using the Anand Model. These values from the first ten seconds were replaced in the equation (1.2) and then compared with the total equivalent creep strain from the simulation. The relative error was minimized to reach acceptable parameters, and consequently, a new simulation was run to verify the power-law parameters. After several iterations, the power-law constants were evaluated.

2.3 Results and Discussion

2.3.1 Eutectic Lead-containing vs. Lead-free solders comparison

Since a fixed number of samples per cycle did not allow the software to run the simulation, automatic calculations were set regarding job parameters. This resulted in different data sets between 50 and 130 samples per node, as summarized in Table 2.5.

Table 2.5. Data set obtained per soldering material.

Number of samples
127
116
91
54

Equivalent Creep Strain curves (Figure 2.8) describe four cycles, similar to the vibration load. However, curves present a constant difference in values only until the 60 s of the total analysis. For instance, between 80 s and 90 s, the curve for SnPb should have displayed a crest. Likewise, between 95 s and 105 s, the Sn3.5Ag and SAC305 crests are not high enough as expected due to the previous trend.

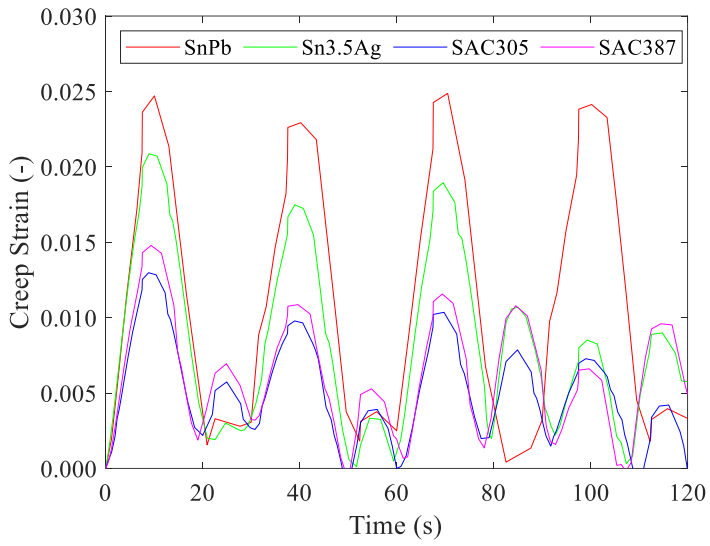


Figure 2.8 Equivalent Creep Strain - Comparison.

Furthermore, Figure 2.9 shows the evolution of the total equivalent creep strain, where after 120 s, the final values were as follows: SnPb: 0.23, Sn3.5Ag 0.18, SAC305: 0.12, and SAC387: 0.14. SAC305 exhibits the minimum total equivalent creep strain, which is nearly 48% less than the SnPb value. However, the three lead-free solders still describe a lesser total equivalent creep strain as compared to SnPb.

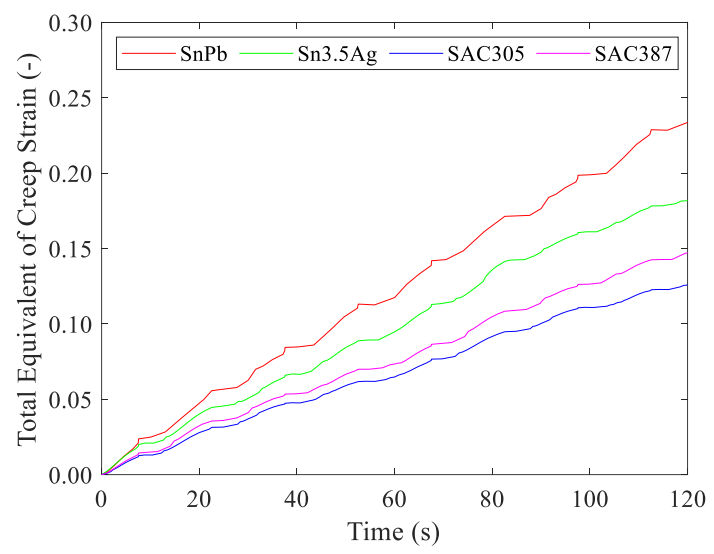


Figure 2.9 Total Equivalent Creep Strain - Comparison

Unlike creep strain curves, Figure 2.10 describes only two cycles of oscillating stress. As the temperature increases, the stress decreases, in contrast with Figure 2.4. Moreover, Sn3.5Ag and SAC387 curves present the minimum and maximum values, respectively, along most of the graph.

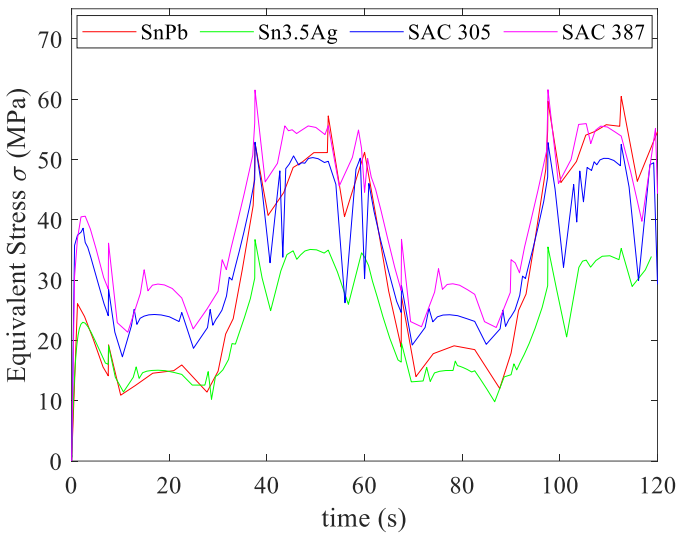


Figure 2.10 Total Equivalent Stress.

Average and maximum values of the Equivalent Creep Strain, as well as Total Equivalent Stress, are summarized in Table 2.6. Certainly, SAC305 shows the minimum average creep strain (4.8·10⁻³), whereas SnPb shows the maximum average value (12.1·10⁻³). On the other hand, regarding total equivalent stress, Sn3.5Ag shows the minimum average value (19.70 MPa), whereas SAC387 shows the maximum average value (39.38 MPa).

Table 2.6. Main values of equivalent creep and stress

		SnPb	Sn3.5Ag	SAC305	SAC387
Creep	Max	24.9	20.9	13.0	14.8
(10^{-3})	Av	12.1	7.03	4.80	5.64
Stress	Max	60.46	36.72	52.87	61.57
(MPa)	Av	33.57	19.70	34.66	39.98

2.3.2 Power-law Creep Parameters Proposal

As SAC305 creeps the least, its dataset was considered for calculating the power-law parameters. Although Anand's model is the primary focus for further comparisons, theoretical Power Law parameters are considered beneficial for broadening creep analysis. An extract of the data set taken from the first ten seconds of the simulation is shown in Table 2.7. The strain for this case was set as a constant value of 0.001. Additionally, the simulation results (Creep Strain Anand) and the result from the

equation (1.2) were listed to calculate the relative error. After numerous adjustments, power-law parameters were set to achieve an average relative error of nearly 5%.

Table 2.7. Anand Model vs. Power-law equation.

			Cree	Err.	
t	T	σ	Anand	Power-law	e
0	0	0	0	0	-
0.6	10	35.76	0.0006	0.00056	0.014
•	•				•
8.85	125	21.38	0.0131	0.01256	0.038
10.39	125	17.28	0.0130	0.01291	0.008

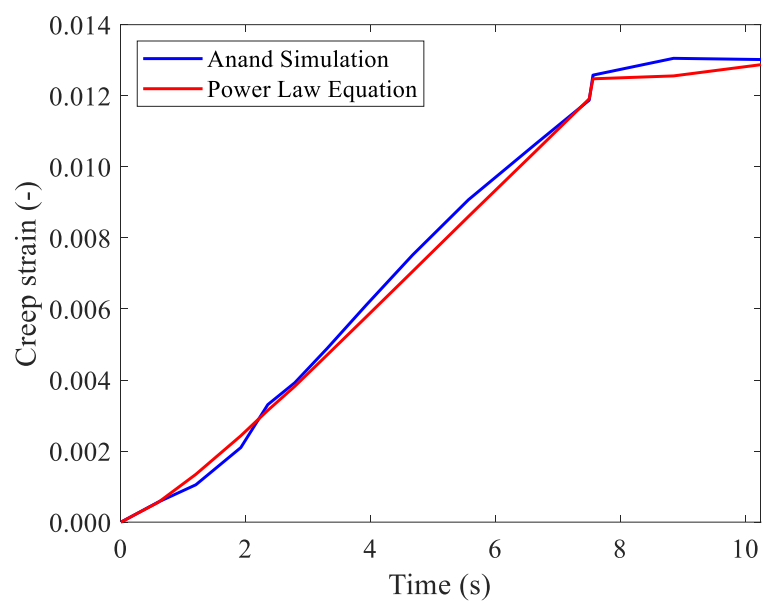


Figure 2.11 Comparison of total equivalent creep strain results.

Anand Model vs. power-law model.

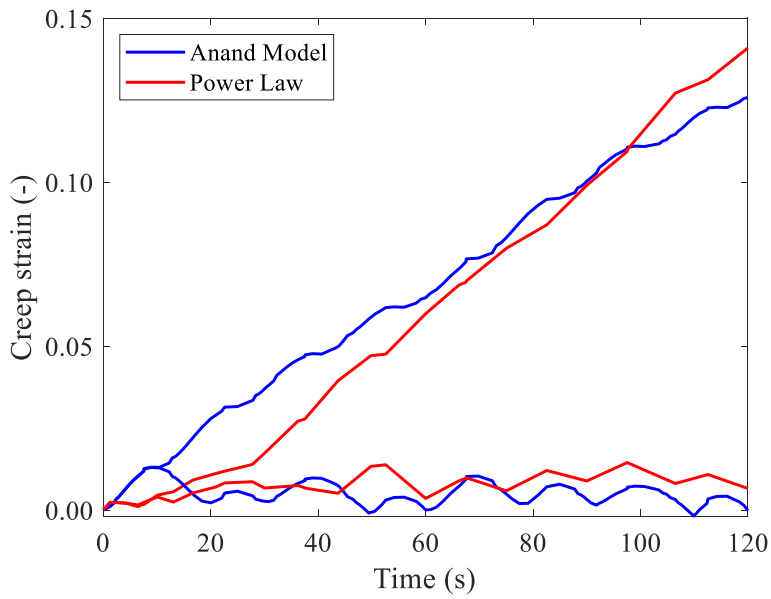


Figure 2.12 Total and equivalent creep strain for SAC305. Anand and power-law creep models.

The graphical comparison of the calculated results with the values from the simulation is shown in Figure 2.11. Once the experimental error was acceptable, the new power-law variables were set as follows: A = 3501, m = 0.25, n = 4, p = 0.75, and q = 1.5. A new dataset was acquired using those parameters as required in the viscoplastic properties. The accuracy of the results, with an average relative error over 10% regarding the final value of the total equivalent creep strain, is displayed in Figure 2.12.

2.4 Conclusions

Creep strain is a complex, time-dependent mechanical behavior that must be considered for the proper functioning of electronic boards. The eutectic solder material SnPb has a low melting temperature, which is favorable for manufacturing electronic printed circuit boards (PCBs) and has proven to be long-lasting. However, due to new international regulations, lead-free compositions are replacing the eutectic SnPb solder. The performance of unleaded solders under thermomechanical loads must be discussed to ensure correct, long-lasting, and efficient operation.

A sample was subjected to cyclic mechanical and thermal loads through a simulation. The thermal load presented two entire cycles, whereas the vibration load oscillated four times.

From the equivalent creep strain comparison, it is evident that the mechanical load governs the creep behavior rather than the thermal load. From the results in terms of total equivalent creep strain, unleaded solders present a favorable value, nearly fifty percent less than that of the eutectic solder. SAC305 and SAC387 appear to have a high degree of similarity in terms of thermomechanical properties. However, the total equivalent creep strain of SAC305 is less than that of SAC387, with a final total equivalent creep strain of 0.12 and 0.14, respectively.

On the other hand, the total equivalent stress graph correlates with the thermal load, displaying two cycles. Regarding the total equivalent stress, Sn3.5Ag presents the minimum values, whereas SAC387 presents the maximum. Indeed, the curve described by the eutectic solder is not significantly different from that of the SAC solders. Additionally, the average stress of the eutectic solder is slightly less than that of the SAC305 and SAC387.

Using the results from the Anand Model, theoretical power-law parameters were obtained for SAC305 solder. The accuracy of the results is acceptable, with an error of nearly 10% compared to the simulation values.

To summarize, lead-free solder materials exhibit lower creep strain curves under thermomechanical loads compared to eutectic SnPb solder. Yet, further analysis should be carried out to determine which one presents better performance in another time-dependent variable and still exhibits acceptable creep behavior.

3. Effect of Anand parameters on the behavior of soldered stacks

3.1 Introduction

Since 1947, when the first working transistor was announced by AT&T (American Telephone and Telegraph) at Bell Laboratories, the electronics industry has become a crucial sector for technology development. However, the leakage current at higher temperatures did not completely switch off the Germanium transistors. Hence, silicon transistors later developed by Texas Instruments were more reliable [70]. In 1957, the American firm Texas Instruments patented the first working silicon integrated circuit [71].

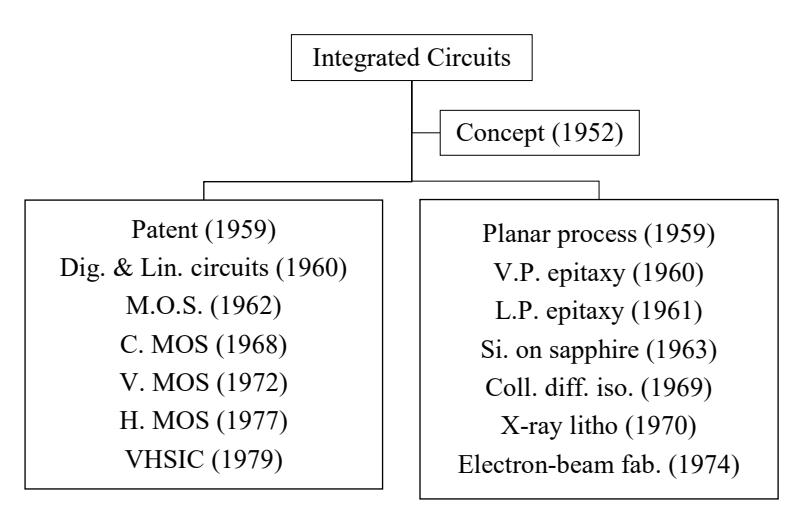


Figure 3.1 History of Integrated Circuits [71].

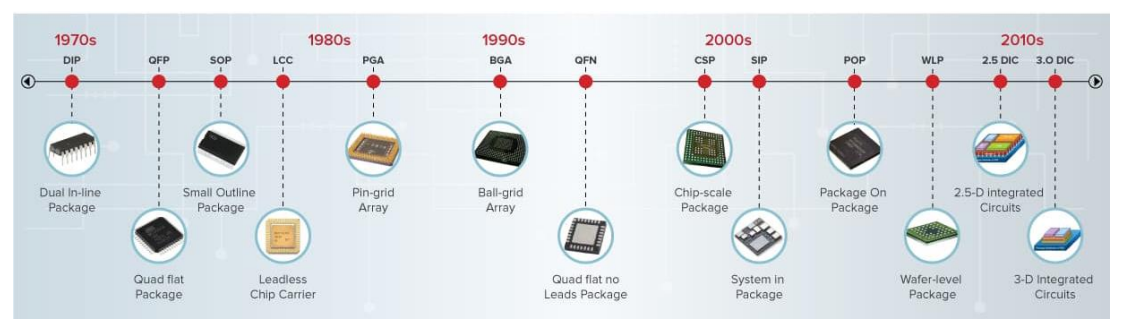


Figure 3.2 History of IC Semiconductor packaging evolution [72].

The chronological history of Integrated Circuits from their first development in 1052 till 1979 is presented in Figure 3.1. Whereas a scheme that details the evolution of electronic packaging from 1970 to the present day is shown in Figure 3.2. Since 1970, Integrated Circuits (ICs) have been integral to the evolution of technologies and the computing industry. However, the need for more efficient ICs motivates the industry to increase the number of input/output (I/O) pins while downscaling ICs.

3.1.1 Fan-Out Wafer Level Packaging

Over the last decade, Wafer Level Packaging (WLP) has been explored to increase the number of I/Os while rapidly downscaling ICs. Lau et al. [73] presented a concise review of the materials and trends regarding Fan-In and Fan-Out – WLP. Some of the advantages are substrate-less package, lower thermal resistance, and higher performance due to shorter interconnects [74]. Two basic Fan-Out WLP (FOWLP) structures can be identified: Mold first and Redistribution Layer (RDL) first, depending on the flow process (see Figure 3.3).

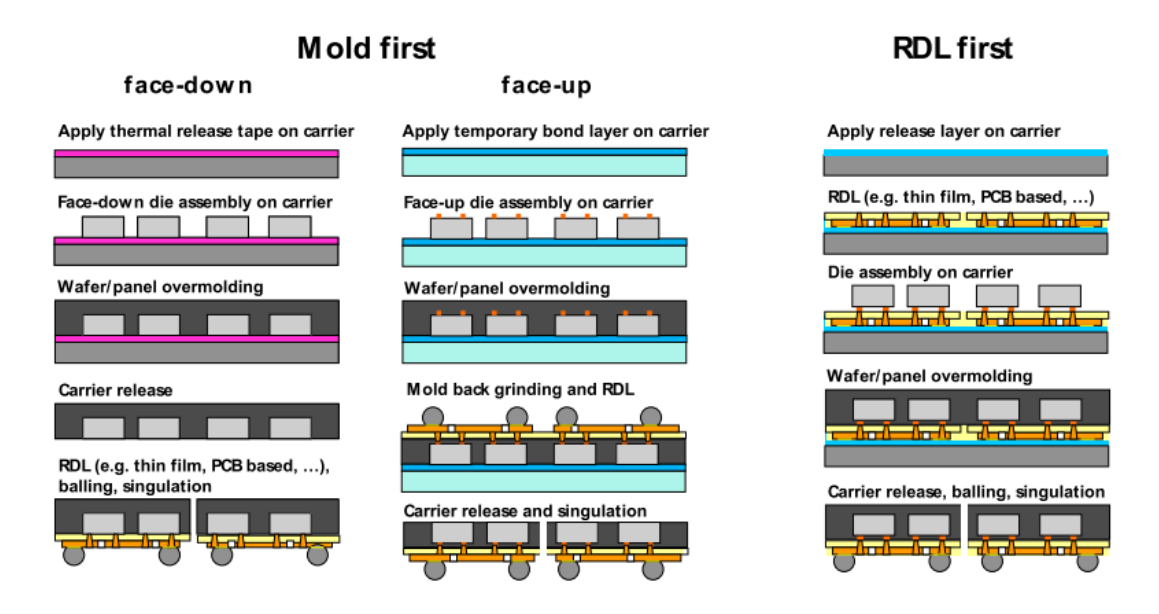


Figure 3.3 Semiconductor packaging evolution [75].

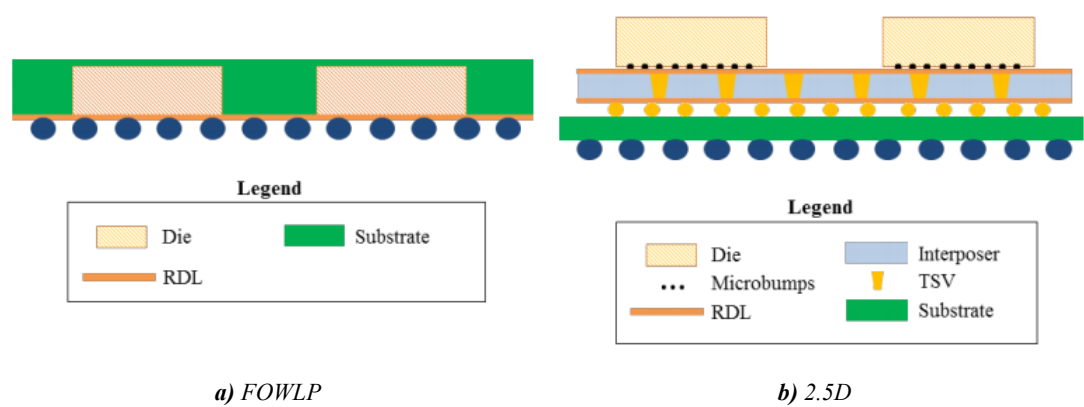


Figure 3.4 Cross-section of Electronic Packaging [76]. *TSV - Through Silicon Via

Mold first FOWLP is already in mass production. Its advantage is related to the heterogeneous components required in panel assemblies for energy harvesting [75]. Recent electrical studies suggest that RLD first-FOWLP could potentially replace some 3D IC applications [77]. However, RDL 1st is facing challenges to enhance wafer warpage and RDL scaling [78].

Chet et al.[76] presented a concise comparison in terms of yield and cost for FOWLP vs. 2.5D. The primary layer distribution of each packaging is detailed in Figure 3.4. In FOWLP, the good die is covered by the substrate, whereas in 2.5D packaging, the die and interposers can be tested before the final packaging. Thus, a 2.5D die is less likely to be discarded due to manufacturing defects.

3.1.2 SAC Solders

SAC solder compositions have been considered the most suitable candidate to replace the eutectic Sn-Pb solder in many applications. Its reliability in terms of long-lasting work periods is still widely analyzed. Some selected SAC compositions are detailed in Table 3.1.

Table 3.1. Some typical SAC Solder Compositions [79].

Allow	Weight percentage - wt%				
Alloy	Sn	Ag	Cu		
SAC 305	96 - 97	2.8 - 3.2	0.3 - 0.7		
SAC 387	95 - 96	3.6 - 4.0	0.5 - 0.9		
SAC 405	95 - 96	3.8 - 4.2	0.3 - 0.7		

SAC solders possess a relatively higher melting temperature (>217°C) than the eutectic Sn-Pb solder (183°C). SAC solders have proved a higher creep resistance under the thermal cycling load. Under vibration loads, SAC solders presented a lower fatigue life [80].

Numerous studies have characterized the properties of SAC (Sn-Ag-Cu) solder alloys, with a particular focus on commonly used variants such as SAC305 and SAC405. Comparative reliability assessments between these two alloys under cyclic thermal loading conditions ranging from 0°C to 100°C have shown no statistically significant differences in performance [81]. However, other investigations have highlighted that SAC405 may offer superior characteristics over SAC305, especially in mobile device applications where mechanical and thermal reliability are critical [82].

Different creep tests were executed in experimental works, and visco-plastic characterizations were carried out to report Anand parameters for the SAC305 composition. Mysore et al. [83] obtained their Anand parameters from a solder interconnect specimen, tabulating normal stress vs. strain rate under different

temperatures. Herkommer et al. [84] obtained their Anand parameters from a specimen under shear stress, tabulating shear stress vs. shear strain rate under different temperatures. Basit et al. [68] used Reflowed (RF) and Water Quenched (WQ) uniaxial tension specimens ($80 \times 3 \times 0.5$ mm). Based on the concepts of Ultimate Tensile Stress (UTS), Basit et al. not only reported Anand parameters for RF and WQ SAC305 but also the effect of aging on Anand parameters. Alam et al. [85] used reflowed uniaxial tension specimens ($80 \times 3 \times 0.5$ mm) to perform a stress-strain test on SAC305 and compared the results with doped SAC solders. Finally, Lall et al. [86] utilized uniaxial tension specimens ($40 \times 5 \times 0.5$ mm). A model prediction showed an acceptable correlation with the experiment.

The six sets of Anand parameters used for the simulations presented in this chapter are summarized in Table 3.2. Additionally, while reviewing the papers on SAC305 Anand parameters, a discrepancy was found regarding the alloy used. Yuwen et al. [87] performed their simulation using SAC305 Anand parameters taken from Wang et al. [88]. However, the solder used by Wang et al. was 95.7Sn3.8Ag0.5Cu, which, according to Table 3.1, does not correspond to SAC305.

Table 3.2. Anand parameters for SAC305 in various sources.

	Year	2004	2009	2013	2015	2015	2018
	Author	Janz [89]	Mysore [83]	Herkommer [84]	Basit [68]	Lall [86]	Alam [85]
s_0	MPa	45.9	2.15	1.0665	21	32.39	6.5
A	s^{-1}	5870000	17.994	1.43E+08	3501	1100	3700
ξ		2	0.35	1.472	4	6	4
m		0.0942	0.153	0.1414	0.25	0.39	0.47
h_0	MPa	9350	1525.98	5023.9	180000	174130	70000
s	MPa	58.3	2.536	20.2976	30.2	67.7	7.72
n		0.015	0.028	0.0324	0.01	0.0008	0.0315
a		1.5	1.69	1.12	1.78	1.75	1.9
Q	$J \cdot mol^{-1}$	62026.17	82895.56	88581.38	77491.14	33258	95616.75

3.1.3 Doped SAC solders

SAC-solders (Sn-Ag-Cu) successfully replaced SnPb solders in the last decade. The automotive industry now requires ICs that operate in harsh working environments, where temperature loads can exceed 150°C [6]. Consequently, new solder materials, called doped-SAC or SAC-X, were developed. Sudan et al. [90] performed an Energy Dispersive X-ray spectroscopy (EDX) to determine the composition of these new doped-SAC solders developed by private companies. The percentage of each component in the doped SAC solder is summarized in Table 3.3. SAC-R does not

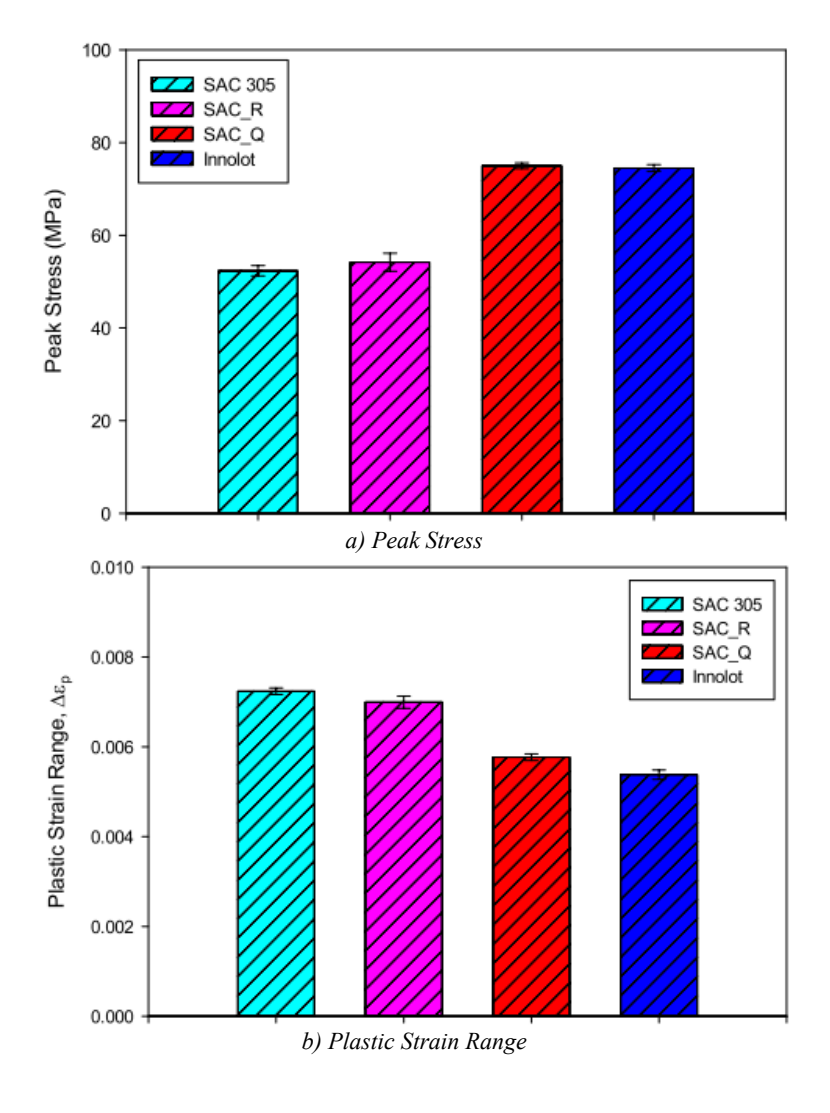
contain silver, making it the most economically viable substitute for eutectic solder and previous versions of SAC solders.

Table 3.3. Doped-SAC solders composition wt% [90].

Solder	Sn	Ag	Cu	Bi	Ni	Sb
SAC-R (Ecolloy)	96.62	0.00	0.92	2.46	0.00	0.00
SAC-Q (CycloMax)	92.77	3.41	0.52	3.30	0.00	0.00
InnoLot	90.95	3.80	0.70	3.00	0.15	1.40

Mohammad [91] compared how the mechanical behavior of SAC305 and some doped materials are affected in thermomechanical tests. Aging under different temperatures revealed that SAC305 properties (degradation in terms of Ultimate Tensile Stress and Elastic Modulus) change with higher portions than SACQ and InnoLot. According to Mahmudur et al. [92] InnoLot shows the least plastic strain range (average increment on plastic strain per cycle) in comparison with SAC-R, SAC-Q, and SAC305. However, InnoLot peak stress is higher than SAC305, see

Figure 3.5.



3.2 Simulation Setup

3.2.1 Geometry description

For the finite element modeling, a 167GJJ Package from Texas Instruments [93] was selected. This FO-WLP package includes a fine pitch Ball Grid Array (BGA). The main dimensions are shown in Figure 3.6. Half of the package was modeled, as boundary conditions were applied on the left edge to achieve symmetry with constrained displacements in the x-direction. A vertical constraint was placed on the left bottom corner concerning the y-direction displacements to ensure a unique mathematical solution (see Figure 3.7). Nine replicates of the simulation were run by changing the visco-plastic properties of the solder for comparison purposes (Table 3.2 and Table 3.5)

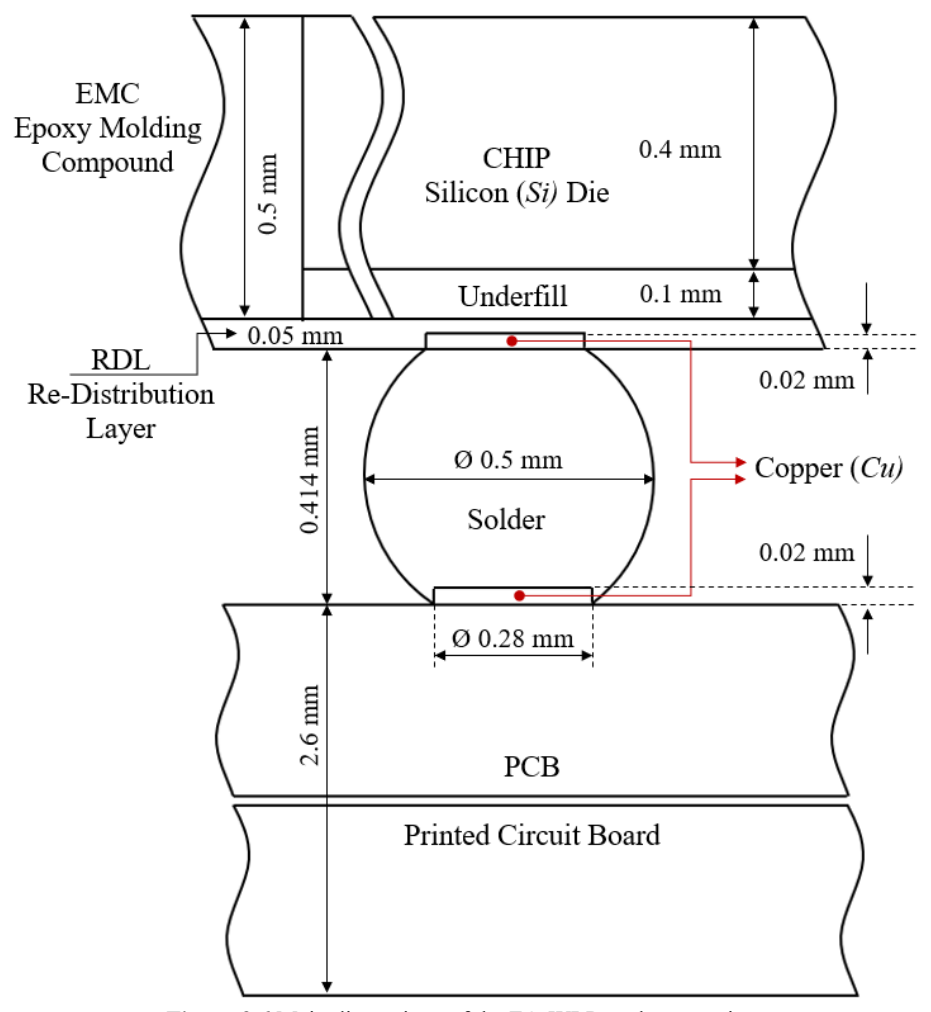


Figure 3.6 Main dimensions of the FO-WLP package section.

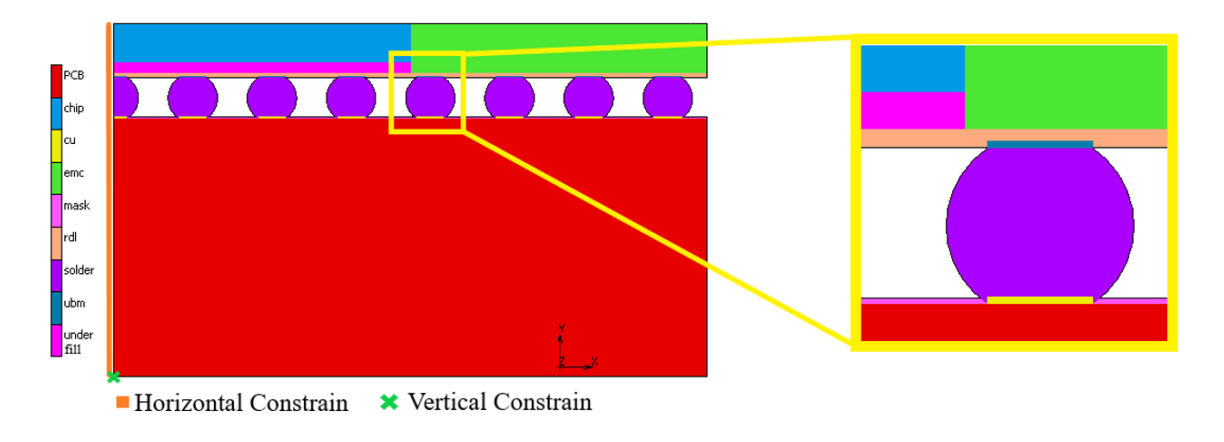


Figure 3.7 2D Model (Half cross-section of the chip).

3.2.2 Material Properties

Young's Modulus (E), Poisson's Ratio (υ), and Coefficient of Thermal Expansion (CTE) properties were set according to Table 3.4. For the solder material, temperature-dependent, E and CTE were set (Figure 3.8) the necessary sets of visco-plastic parameters for SACX solders (Table 3.5).

Table 3.4. Material parameters [94].

Material	Young's Modulus (GPa)	Poisson's Ratio	CTE ¹ (ppm/°C)	Tg ² (°C)
Si (chip)	131	0.3	2.8	
EMC	T < Tg: 18.5; T > Tg: 1.2	0.3	T < Tg: 9; T > Tg: 18	163
Dielectrics	T < Tg: 0.92; T > Tg: 0.1	0.3	T < Tg: 80 T > Tg: 227	205
Cu	117	0.34	17	
Underfill	T < Tg: 3.8; T > Tg: 0.125	0.3	T < Tg: 44; T > Tg: 119	141
Solder Mask	T < Tg: 2.4; T > Tg: 0.23	0.3	T < Tg: 60; T > Tg: 161	100
PCB (Printed Circuit Board)	For x,y: 25; For z: 11	For xy 0.11 for xz, yz 0.39	For x, y: 15 For z: 46	

¹Coefficient of Thermal Expansion, ²Glass Transition Temperature

Table 3.5. SAC-X material parameters for the Anand creep model.

Tuble bio. 5710 71 material parameters for the 7 mana creep model.					
Description	SACQ [95]	SACR [90]	InnoLot [90]		
s ₀ (MPa)	0.405	34.72	32.42		
A (s ⁻¹)	$2.45 \cdot 10^{8}$	1000	25 000		
ξ	0.068	6	7		
m	0.36	0.15	0.35		
h_0 (MPa)	3521.56	145 640	88 875		
ŝ (MPa)	0.638	71.71	56.76		
n	0.0056	0.001	0.0097		
a	1.243	1.55	1.45		
$Q\left(J\cdot \text{mol}^{-1}\right)$	112 313.8	92290.52	13.9		

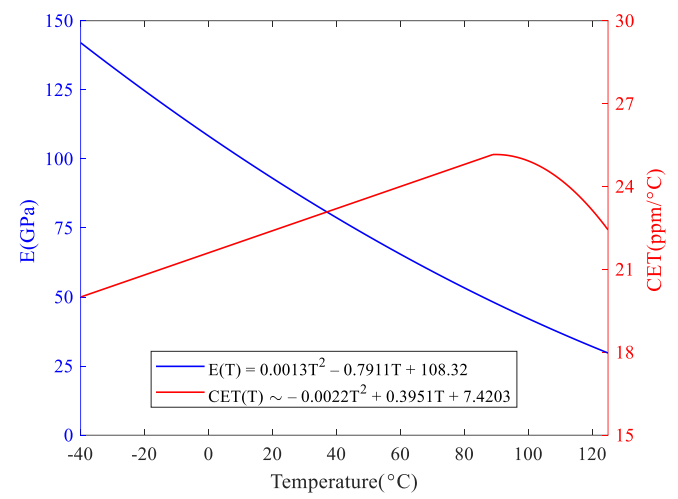


Figure 3.8 SAC305 temperature-dependent modulus and CTE [63].

3.2.3 Load Case and Job Parameters

An oscillating thermal load ranging from –40°C to 125°C, with three cycles, was used. This temperature range and cyclic timing are in accordance with the Joint Electron Device Engineering Council (JEDEC) standards [96], and the maximum temperature surpasses 0.5 T_m. Additionally, since there is a mismatch in CTE among the different materials, expansion or compression during the thermal load leads to mechanical stress, and no extra vibration or external force is required for comparison.

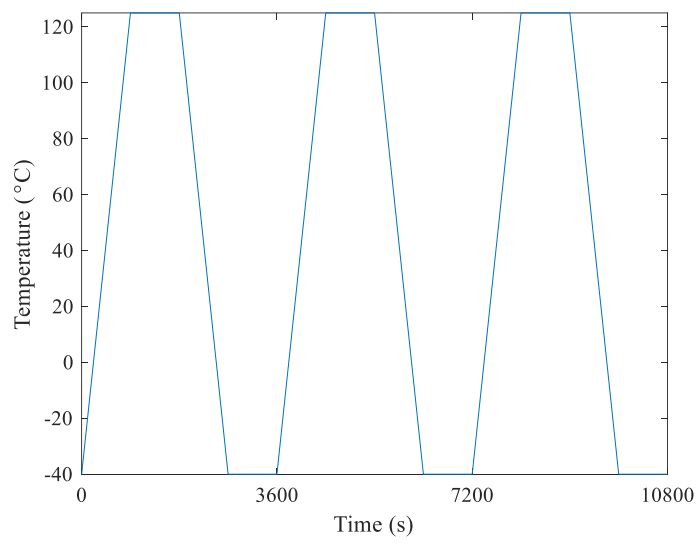


Figure 3.9 Thermal load.

Ideally, a constant time step for all the simulations would be advantageous for comparison purposes. Nevertheless, since there are several different simulations, a multi-criteria time-stepping option was chosen to ensure good convergence of the nonlinear solutions. The solver determines the actual time step, and only the criteria

conditions were fine-tuned to achieve at least a hundred time steps in a single thermal cycle.

3.3 Results and Discussion

Values of the Equivalent Creep Strain (ECS) and Total Equivalent Creep Strain (TECS) were analyzed from all the simulations. TECS can be understood as the accumulation in time of ECS (see Figure 3.11). At the end of the third cycle, the nodes with high values of TECS were found to be located at the bottom corners of each solder ball (see Figure 3.10).

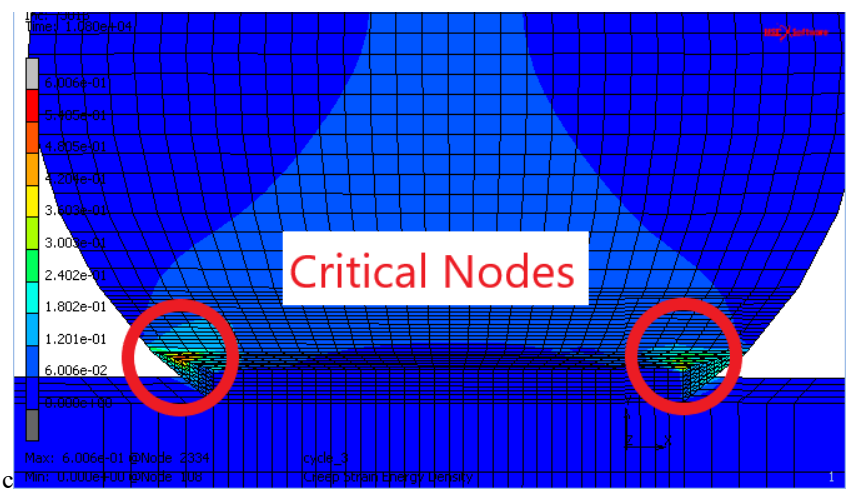


Figure 3.10 Contour band graph.

TECS distribution at the end of the 3rd thermal cycle.

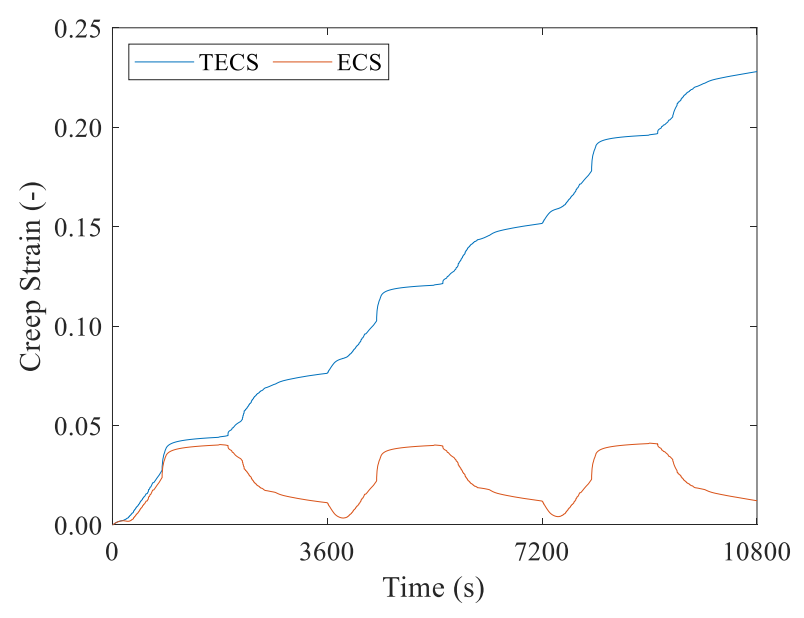


Figure 3.11 ECS and TECS vs time at critical location. Anand parameters for SAC305 taken from *Alam et al.*

As expected, the nine different simulations (due to different viscoplastic properties) agreed on the node with the maximum TECS. This node was in the bottom right corner of the outer solder ball (the most distant point from the axis of symmetry). ECS and TECS curves were retrieved from the nine simulations for comparison purposes.

3.3.1 SAC305 variation of Anand parameters

Three main waves in ECS correspond to the three thermal cycles (Figure 3.12). There is a considerable similarity during the high-temperature dwell segment. The Alam, Basit, and Janz curves show high agreement during this period. On the other hand, Lall's values align with those of the other authors only at the end of every thermal cycle. Evidently, during the low-temperature dwell segment, all curves display divergent values, except for Herkommer and Janz during the third thermal cycle.

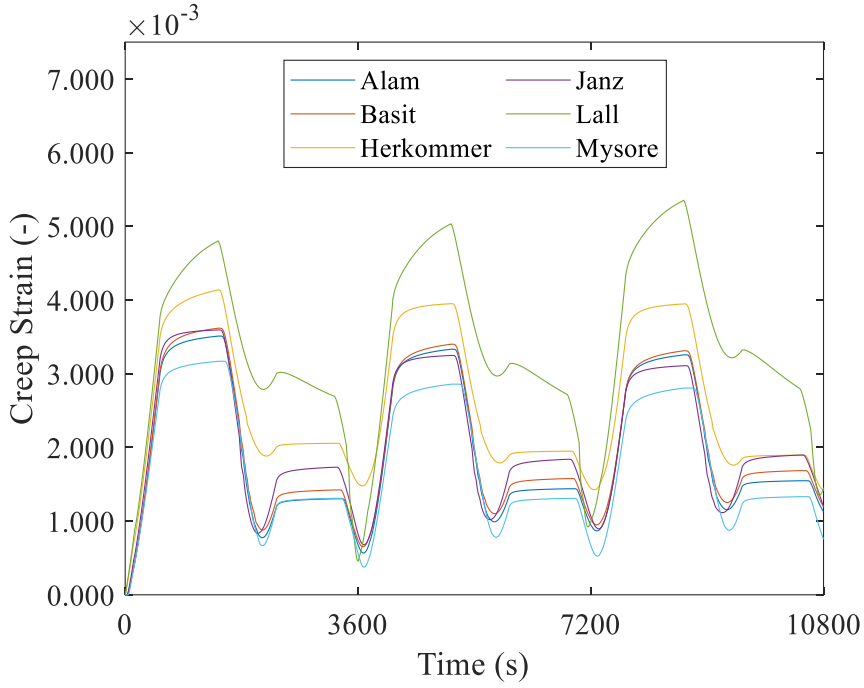


Figure 3.12 ECS at critical location.

Regarding the TECS curve (Figure 3.13), a significant agreement of values can be observed among the different curves, except for Lall. While the Mysore final TECS is approximately 0.025, the Lall final TECS is roughly 0.047. An increase of nearly 90% would result in higher creep deformation, and therefore, a shorter life spam.

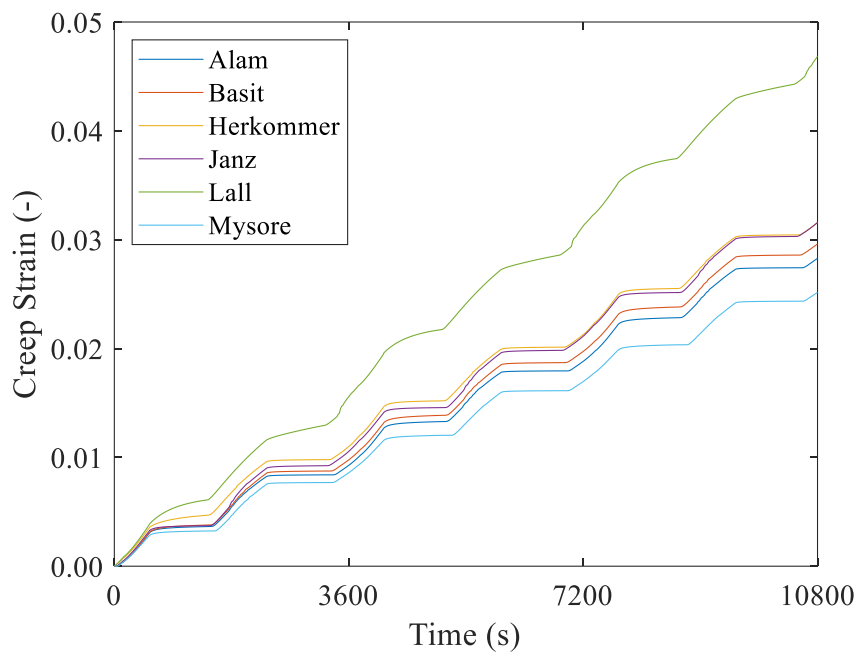


Figure 3.13 TECS at critical location.

3.3.2 SAC305 vs. SACX solders

Creep strain energy density (CSED) data were collected from the four simulation replicates (SAC305 – Basit properties and SACX solders). The bottom corner locations of each solder ball exhibited a high CSED in all scenarios. The location with the most critical value of CSED (see Figure 3.14) was situated in the bottom right corner of the outer solder ball (the most distant point from the line of symmetry).

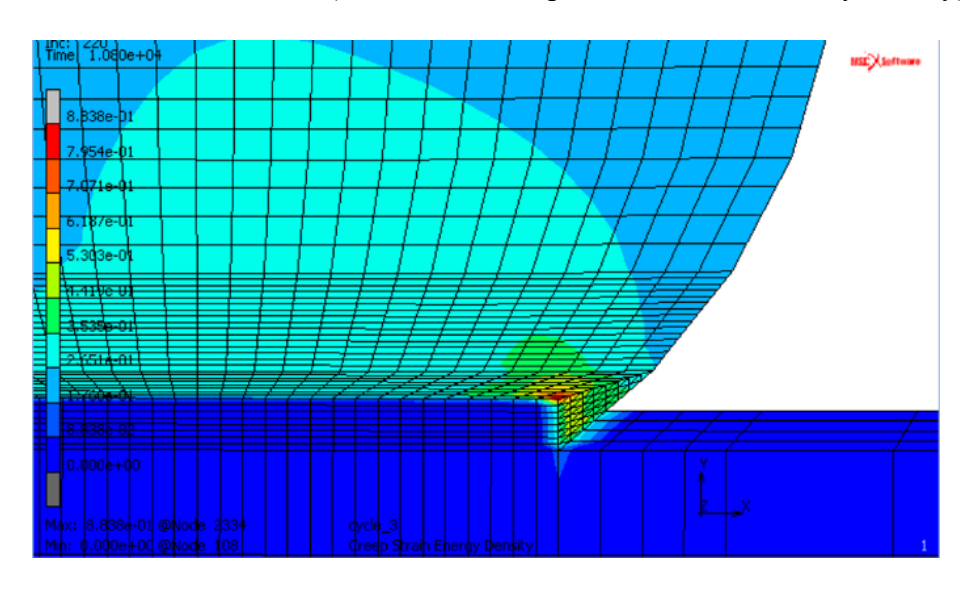


Figure 3.14 Creep Strain Energy Density. Contour Band at the critical location (SAC305 - *Basit*).

As the multi-criteria was utilized for time-stepping, each CSED vs. time curve presented a different number of steps: SAC305 - *Basit*, 1808 steps; SACQ, 4135 steps; InnoLot, 1669 points; and SACR, 579 steps. The number of steps was directly proportional to the simulation time, which varied from nearly one hour to over five hours.

The CSED vs. time curves from the critical location (Figure 3.14) of each replicate were summarized in Figure 3.15. It is worth noting that SACQ presents the lowest CSED accumulation among the different soldering materials and the highest expected resolution due to the large number of steps. Additionally, InnoLot and SAC305 curves display a similar behavior during the first two thermal cycles. Nevertheless, the approximation of the average of CSED only considers the CSED subtraction between the third and second thermal cycle (calculated in Table 3.6).

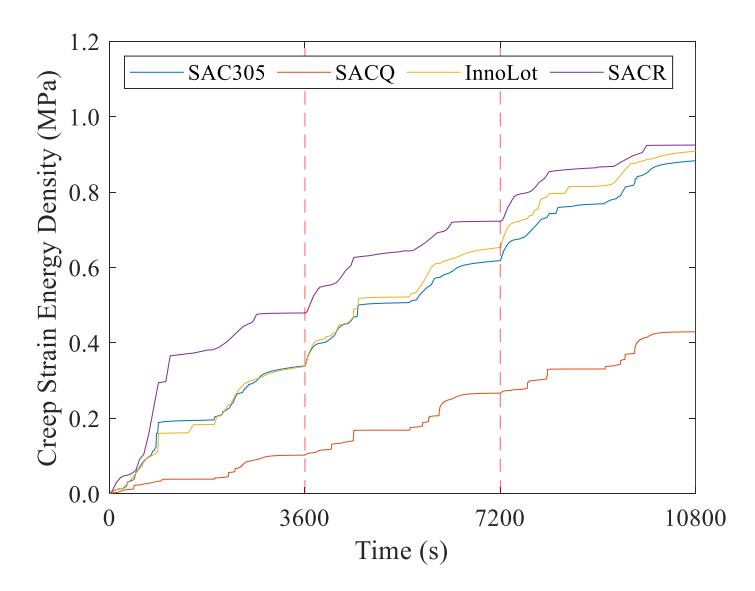


Figure 3.15 Creep Strain Energy Density Comparison.

The comparison aims to address creep-based reliability. For this purpose, average creep strain energy density, ΔW_{av} is considered a key parameter of the number of cycles to failure calculation. According to Che and Pang [97], three thermal cycles are enough to obtain a stable plastic work density that approximates the average creep strain energy density. It can be computed by taking the values at the end of the third and second thermal cycles as detailed in (3.1).

Calculation of average creep strain energy density (ΔW_{av}) [97]:

$$\Delta W_{av} = W_{3^{\text{rd}}TC} - W_{2^{\text{nd}}TC} \tag{3.1}$$

Where: ΔW_{av} , average creep strain energy density; $W_{3^{\rm rd}TC}$ and $W_{2^{\rm nd}TC}$ Creep strain energy density at the end of the third and second thermal cycles (TC).

The computed approximation of average CSED shows that SACQ presents the lowest value, whereas SAC305 displays the highest value (see Table 3.6). Based on Morrow's reliability model [98], the number of cycles to failure is inversely proportional to the average of CSED. Therefore, SACQ would resist the most extended working lifetime, followed by SACR, InnoLot, and SAC305. These results agree with a similar experimental comparison performed by Wei et al. [99] where SAC305 endured the least number of cycles to failure than SACQ, SACR, and InnoLot, under stress-controlled conditions.

A more comprehensive explanation of reliability models and the use of plastic strain energy density is provided in the section 4.1.1.

Table 3.6. Approximation of the Average of Creep Strain Energy Density (MPa).

CSED	SAC305	SACQ	InnoLot	SACR
Cycle 1	0.339020	0.102072	0.337066	0.479284
Cycle 2	0.617905	0.266476	0.653259	0.722654
Cycle 3	0.883068	0.429206	0.908353	0.924602

3.4 Conclusions

This research aims to present a simulation-based comparison of Anand parameters for SAC305. An optimal combination of mesh and time step should be set up for the six simulations to minimize the time required. From the simulation results, the following conclusions are drawn:

Despite differences in the six sets of viscoplastic parameters, all six simulations agreed on the location of the critical node at the conclusion of the three cycles. This comparison has not been found in the extensive literature database examined.

There is a significant difference in the ECS curves during the low-temperature dwell segment (-40°C); however, there is a considerable similarity among four of the six TECS curves (Alam, Basit, Herkommer, and Janz). Since TECS is the cumulative value of ECS, analyzing TECS solely could lead to a misinterpretation regarding a thorough comparison.

Since Alam, Basit, and Herkommer present a significant similarity of curves with a substantial range of time-steps, it is advisable to use the set of viscoplastic parameters that takes the shortest time (Basit) for simulation purposes.

The critical location regarding CSED is commonly situated at the outermost solder ball. This conclusion strengthens the Distance to Neutral Point theory extended in section 4.1.1.

Doped SAC solders are more advantageous than SAC305 solder in terms of working lifetime. The qualitative results suggest that SACQ has a significant advantage in the operational lifetime compared to SACR, InnoLot, and SAC305.

4. Analysis of reliability models and first estimation of reliability indicators

4.1 Introduction

Solder joint reliability is critical in the design of advanced microelectronic packaging. Predictions of reliability by thermo-mechanical simulations can accelerate the evaluations of advanced packaging and the introduction of novel solder materials. In this chapter, a finite element model of a thermally loaded Fan-Out Wafer Level Package (FO-WLP) was built and analyzed, focusing on the creep behavior of the solder balls and the consequent effect on the reliability of the package. The lead-free soldering materials in the analyses were either from a widely used SAC305 or novel doped SAC solders such as SAC-R, SAC-Q, and InnoLot. Visco-plastic (Anand creep) properties for the solders were defined as study parameters, where six variations were used for the described SAC305 and a further three sets for the doped SAC solders, respectively. Identifying a stress concentration at the sharp bond pad edges by modeling ideal geometries, a refined geometry was introduced and evaluated. Simulations for a 3-cycle thermal load were conducted. Results were collected and analyzed for Creep Strain and Strain Energies in critical positions in the solder, and reliability prediction was performed based on Morrow's model. Results show the benefit of the refined compositions of Doped SAC solders on the mechanical behavior and improved reliability.

4.1.1 Failure prediction models

Reliability of ICs subjected to cycling thermal loads has been a core research topic, with thermal fatigue analysis by predicting the number of cycles to failure. Initially, Distance to the Neutral Point (DNP) was identified as a key parameter; hence, the farthest solder joint from the neutral point of the IC possesses a risk due to the highest thermo-mechanical loads and a geometry that limits the size of the packaging and number of I/Os [100]. However, the accuracy of the approach has been intensely debated because electronic packaging layouts have undergone significant improvements. Lau [101] reported that the DNP approach presents some limitations. For instance, DNP failure prediction has been proved to be valid for packaging without underfill; however, it has been incorrectly applied where underfill is used [102].

The state of the art of reliability models used for solder joint reliability is summarized in Table 4.1. The number of cycles before failure is related either to strain or energy-type parameters. Li *et al.* [103] successfully conducted a simulation to evaluate the thermal fatigue life of a SAC solder material. Creep strain and creep strain energy density were used for the lifetime prediction. From the results, creep strain energy density using the hyperbolic-sine model approached the experimental data more accurately.

Recently, Clech [104] summarized research that compares the Coffin-Manson model and critical Distance to Neutral Point (DNP). According to Norris et al. [105], constant n was observed to be 2 for most metals. This mathematical approach has been widely studied. Zubelewicz et al. [106] stressed that the Coffin-Manson law does not fit experimental data well for high strain rates.

Table 4.1 Overview of solder joint reliability models.

M	odel	Variable's description
Coffin-Manson [107] $N_f (\Delta \epsilon_p)^n = C$		N_f (-), Cycles to failure. n (-), Empirical constant. $\Delta \epsilon_p$ (-), Inelastic strain range. C (-), Proportionality factor / Fatigue ductility coefficient.
	ow [98] $V_p = A$	n' (-), Fatigue exponent. A (MJ/m ³), Material ductility coefficient. W_p (MPa), Inelastic strain energy density.
Monkman-Grant [108] $t_r = \frac{\varepsilon_f}{\dot{\varepsilon}_{cr}}$		t_r (s), time to rupture. ε_f (-), creep ductility. $\dot{\varepsilon}_{cr}$ (s ⁻¹), creep strain rate.
Darveaux	et al. [109]	
Crack Initiation $N_0 = K_1 \Delta W_{ave}^{K_2}$ $\frac{da}{dN} = K_3 \Delta W_{ave}^{K_4}$		N_0 (-), Number of cycles before crack initiation. ΔW_{ave} (MPa), Average strain energy density. $\frac{da}{dN}$ (m/cycle), Crack growth rate per cycle. a (m), Critical length exposed to crack propagation.
Energy De $N_f = N_f$	ensity Model $\frac{a}{a} + \frac{dA}{\left(\frac{dA}{dN}\right)}$	K_{1-4} , Constants based on the element size of the solder.

Table 4.2 Employed creep and reliability models in highlighted references

	Creep Model		Reliability Model		
Author	Hyperbolic Sine	Anand	Morrow	Darveaux	Coffin Manson
Lui et al. [100]		X	X		
Che [110]	×		X		
Chen [94]	×				
Guven [111]		X		×	
Lin [112]		×	×		
Che and Pang [97]	×		X		×
Rahangadale et al. [113]		X	X		

Pang *et al.* [114] presented research where tables for n, n', C and A are listed. Additionally, they included a new approach that includes frequency dependency. Syed [115] proposed employing the Monkman-Grant model to predict the number of cycles to failure based on accumulated creep strain and creep strain energy density per cycle. Using the Power-law and Hyperbolic-sine creep model, his founding demonstrates that both accumulated creep and energy density can effectively predict the lifetime of solder stacks.

Although the Darveaux model was not available in commercial simulation programs, Ramachandran et al. later corroborated that his approach was more accurate than the Coffin-Manson model [31].

For creep material models, either hyperbolic-sine law or Anand's type of models are often used. A more detailed list of creep-based material characterization experiments is summarized in Table 4.2. The authors who used the hyperbolic-sine model stressed the lack of articles reporting Anand's constants.

4.2 Simulation Setup

This section provides a detailed description of the parameters for the electronic packaging simulations. First, the model's geometry and boundary conditions are described, and then the material properties. The simulations were carried out in Marc Mentat finite element software.

4.2.1 Geometry of the Copper Pad

Various simulations in advanced packaging, including SAC solders, have been presented in the last decade. A thorough analysis of simulations and experimental work demonstrates that the crack initiates in the vicinity where the solder ball meets the copper pad [116]. Therefore, it is relevant to consider a more suitable geometry for the copper pad edge that approximates experimental results with greater accuracy.

For the sake of simplicity in geometry, the authors represent the bottom copper pad using a sharp edge. Based on x-ray microscopic inspections, the corner pad can better approximate real microchips with a non-sharp corner (see Figure 4.1). The current chapter proposes two different edges, sharp and fillet.

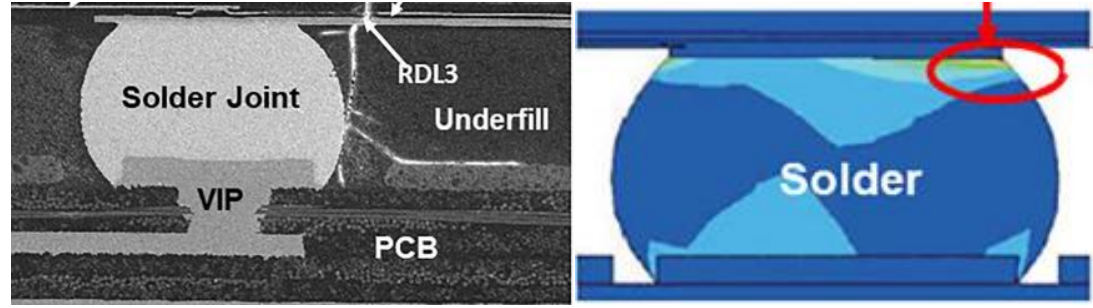
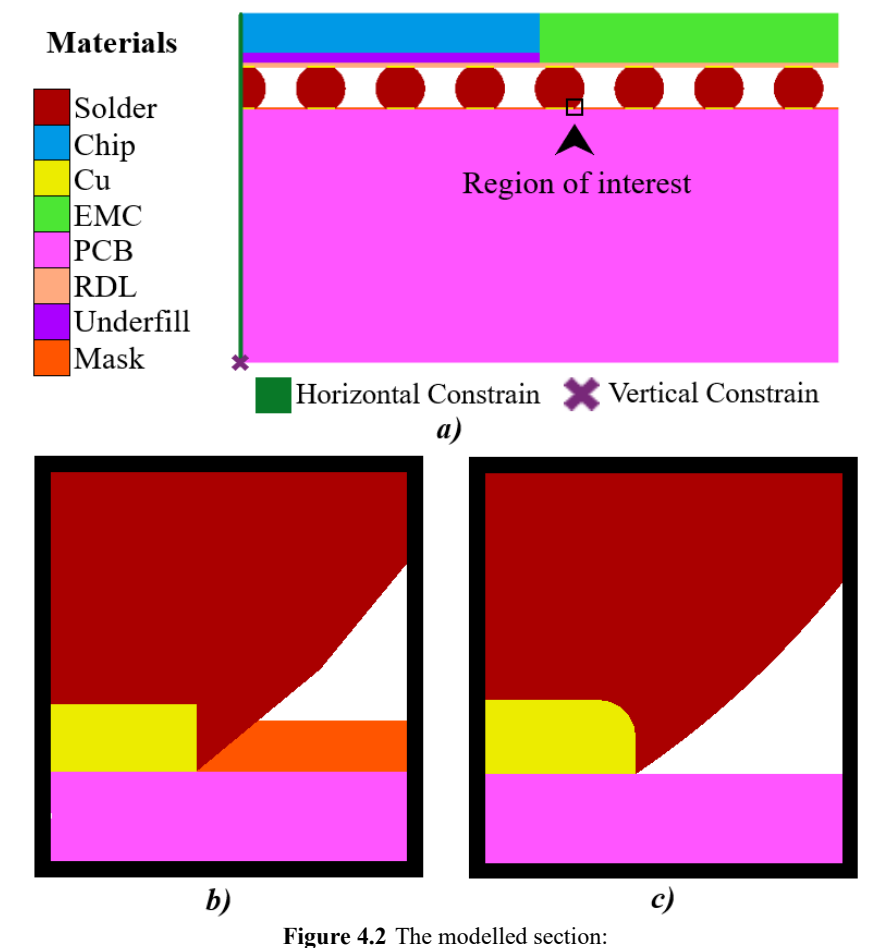


Figure 4.1 Microscopic image of real packaging vs a 2D model [116]. RDL (Re-distribution Layer), PCB (Printed Circuit Board), and VIP (Via in PCB pad)

The bottom copper layer was modeled with sharp pad edges (see Figure 3.7) considering an ideal geometry in previous works [117], [118]. However, this edge may become blunt during the soldering process; therefore, a second variant was modeled using a fillet on the copper pad. For simplicity, the model with the sharp-edged pad will be referred to as "squared" while the model with fillet-edged pad will be referred to as "rounded" (see Figure 4.2 and Figure 4.3). Additionally, due to the complexity of the mesh, a mask layer was included in the squared model, whereas the same mask layer was excluded in the rounded model.



a) Materials description and boundary conditions, b) Augmented view of the squared Cu pad profile, and c) Augmented view of the rounded Cu pad profile.

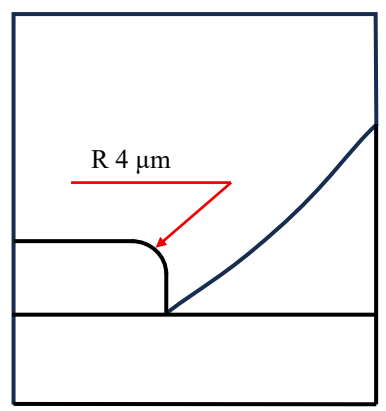


Figure 4.3 Copper pad filet edge radius.

The complexity of the mesh utilized is not visible in Figure 4.2. The modeled layout is shown with the incorporated materials. The squared model was created using a ruled mesh, while the rounded model was created using mesh seeds due to the fillet on the copper pad. The mesh contains over 200,000 elements and 115,000 nodes, respectively.

4.2.2 Initial and Boundary Conditions

For mechanical boundary conditions, mirror symmetry was considered by constraining the horizontal displacement on the model's left side. Constraints to vertical displacement were applied to the bottom left node for a unique solution (Figure 4.2). No extra mechanical loads were applied, as the coefficient of thermal expansion mismatch would produce mechanical stress in the solder.

Cyclic thermal loading was applied to the modeled section. Previous studies on failure prediction have shown that a stable plastic work density is reached within three thermal cycles [119]. An average strain and strain energy density can be computed, taking values at the second and third thermal cycles. Hence, a three-hour thermal load was applied to all the nodes in the model. The same thermal load used in the section 3.2.3 (Figure 3.9) was used for the new set of simulations. A temperature of -40°C was set for all nodes for initial thermal conditions. The temperature ranged from -40°C to 125°C. This temperature range is in accordance with the Joint Electron Device Engineering Council (JEDEC) standards [96], and the maximum temperature surpasses 0.5 T_m.

4.2.3 Material Properties

The material properties of Young's Modulus (E), Poisson's Ratio (v), and Coefficient of Thermal Expansion (CTE) are summarized in Table 3.4 for the materials, excluding the solder. These properties were considered time and temperature-independent, except for the Glass transition temperature (Tg) for specific materials. Under Bump Metallization (UBM) typically consists of Copper (Cu) coated with a noble metal to avoid corrosion, e.g., Gold (Au) [120]. For simplification, the UBM pad was modeled entirely of copper.

This work considered four different lead-free Sn-Ag-Cu (Tin-Silver-Copper) type soldering materials: SAC305 and three doped SAC solders (SACX) (see Table 3.1 and Table 3.3). Temperature-dependent E and CTE were set for SAC305 (see Figure 3.8).

For creep modeling, Anand parameters for the SACX solders from Table 3.5 were used. While six different Anand Parameters for SAC305 were used (Table 3.2) for comparison purposes.

4.2.4 Overview of the studied cases

Altogether, 11 cases are defined and summarized in Table 4.3. The main parameters were the material properties of the solder and the solder pad geometry. The initial step was to compare the different sets of Anand parameters for SAC305 (Case 01 - 06) already discussed in section 3.3.1. Next, SAC305 and Doped SAC solders were compared (Case 07 - 09), similarly detailed in section 3.3.2. Once the results were analyzed, selected material properties were simulated with the round pad profile (Cases 10 and 11).

Edge Shape Edge Shape Material Material Case Case Ro. Sq. Ro. Sq. Doped SAC Solders SAC305 Authors Comparison SACQ Alam 02 08 SACR Basit × × 03 Herkommer × 09 InnoLot 04 Janz × Edge shape comparison purposes 05 Lall 10 Basit 06 Mysore × 11 SACQ

Table 4.3 Summary of the main studied parameters.

4.3 Results and Discussion

The contour band graph of the Total Equivalent of Creep Strain (TECS) at the end of the simulation is shown in Figure 4.4. The node with the highest TECS is located on the outer bottom side of the solder ball. This result agrees with experimental data presented in [116], where in packaging including UBM cracking initiates in the bottom corners, while in packages without UBM cracking initiates in the upper corners. The magnified image in the bottom part of Figure 4.4 shows a significant change of the critical node location and the maximum value reached (0.22 for the squared profile and 0.09 for the rounded profile).

The second most critical point occurred in the middle solder ball (4th from right to left on Figure 4.4). This result can be explained by the high number of materials in the vicinity of the solder ball. In addition, a mismatch of CTE increases the stress generated in the solder ball. The levels of TECS in the upper side of the solder balls display a high concentration of strain under the EMC layer (see Figure 4.2 and Figure 4.4). Compared to experimental results, simulations on Wafer Level Chip Scale Package (WLCSP) support this phenomenon since solder crack initiated in the outer upper part of the solder ball [31].

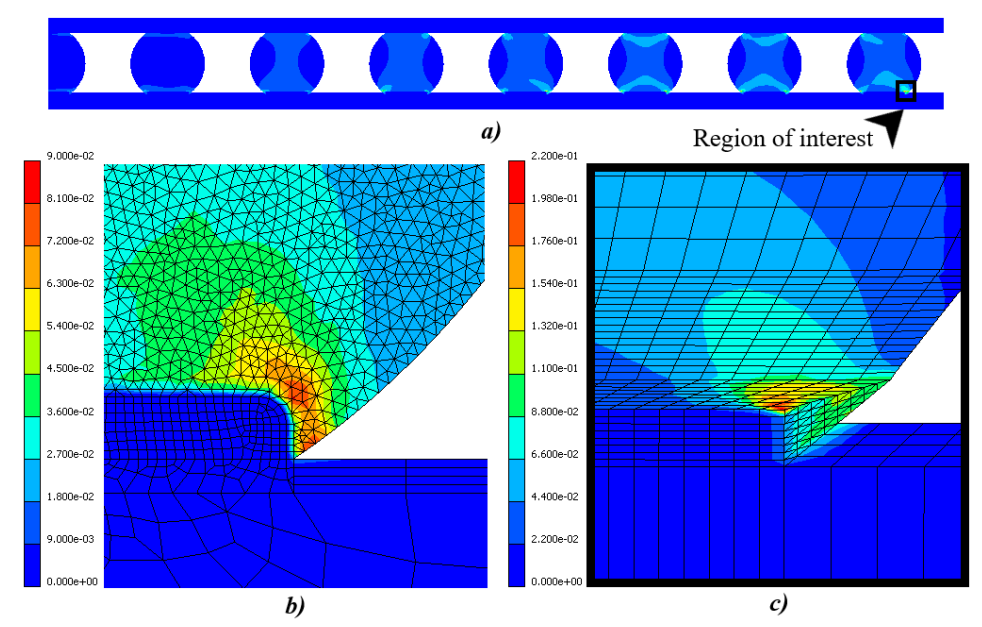


Figure 4.4. TECS at the end of the three cycles

a) TECS distribution along the solder balls (cropped image), Augmented contour band graph of TECS distribution at the vicinity of the critical node b) rounded Cu pad profile and, c) squared Cu pad profile.

4.3.1 Effect of the Bond Pad Geometry

A comparison regarding the copper pad profile was carried out. Since the geometry of the modified model became too complex, the mask layer was neglected following similar study cases [121]. The fillet radius was assumed to be 20% of the copper pad width (Figure 4.3) based on X-ray inspections taken from Lau [116].

Creep strain curves (Equivalent of Creep Strain – ECS and TECS) from the critical node are presented in Figure 4.5. Like the squared profile, the location of the critical node remained the same.

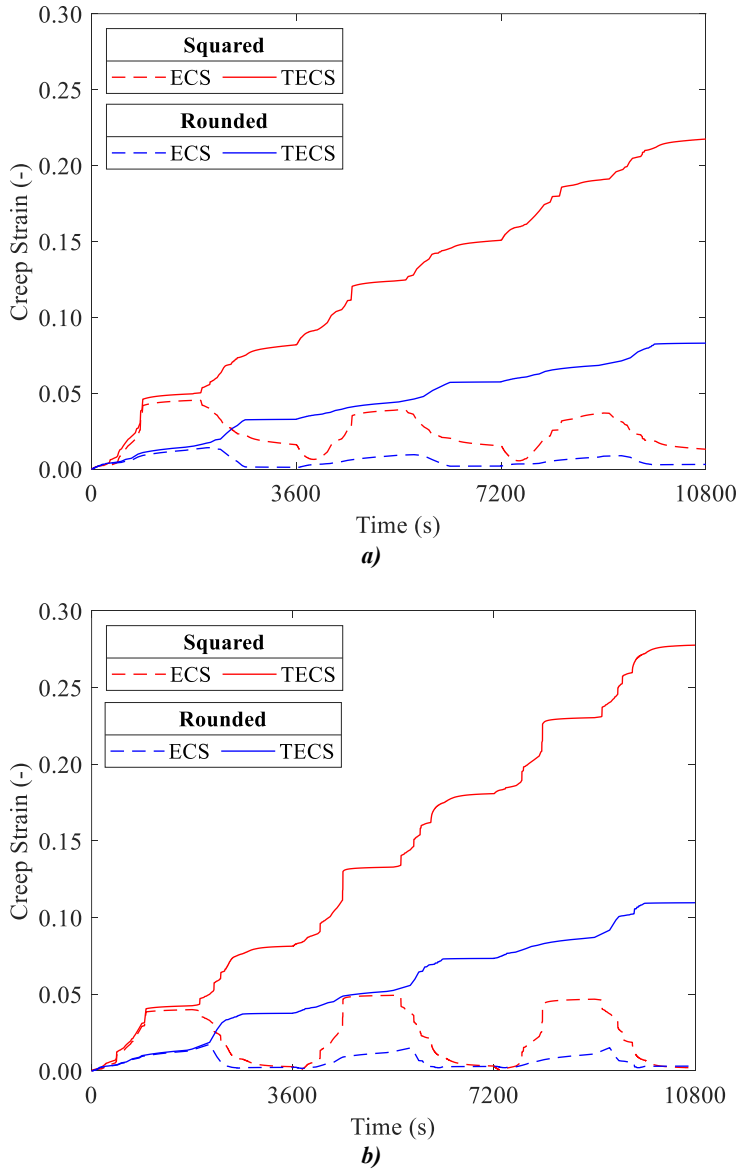
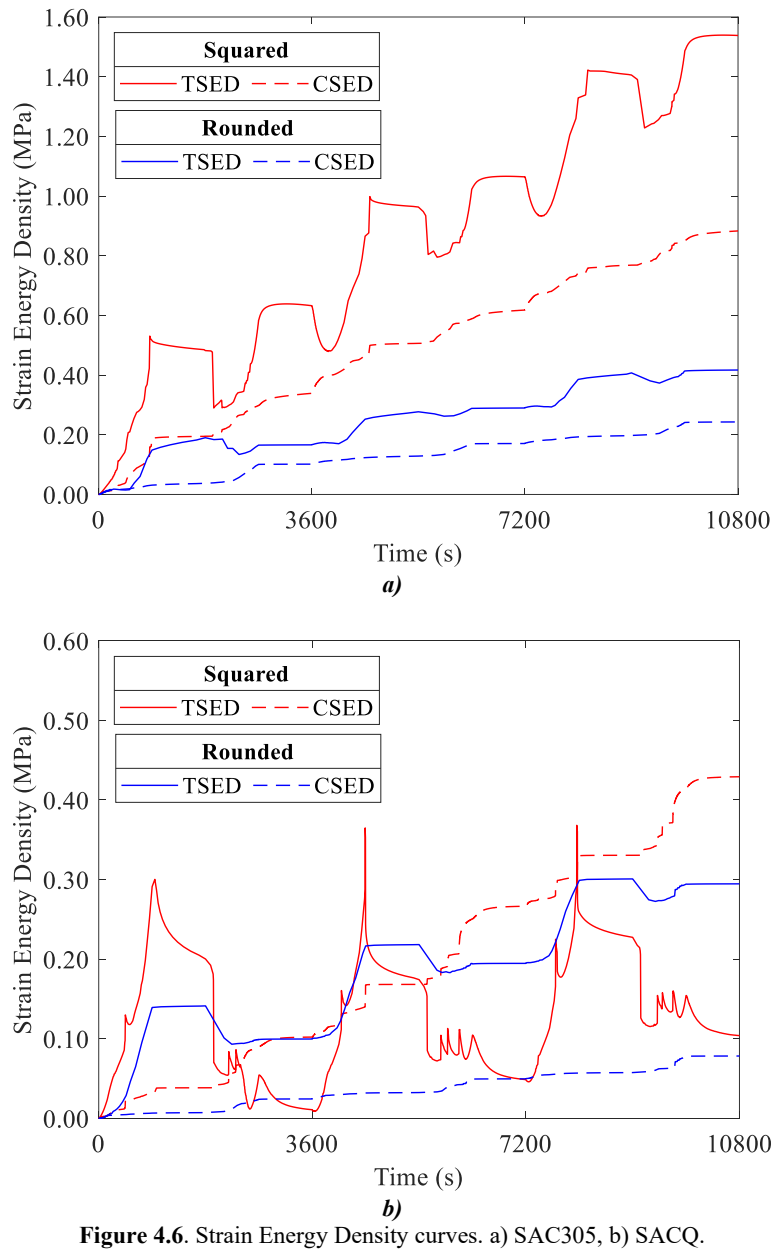


Figure 4.5. Creep Strain Curves. a) SAC305, b) SACQ.



The variation of change in profile within the same composition and between compositions are presented in Table 4.4. The column variations (Table 4.4) represent the difference of TECS between materials, while the row variations represent the variation due to the change in profile shape. It is clear to notice that in both compositions, the decrement due to shape is nearly 60%. On the other hand, a rounded profile accentuates the TECS difference between materials by 2.66%.

Table 4.4 Total Equivalent of Creep Strain final value variation

	SAC305	SACQ	variation
Squared	0.2174	0.2776	21.68%
Rounded	0.0829	0.1096	24.34%
variation	61.85%	60.51%	

Table 4.5 Total Strain Energy Density final value variation

	SAC305	SACQ	variation
Squared	0.8830	0.4292	51.40%
Rounded	0.2429	0.0782	67.79%
variation	72.49%	81.77%	

Regarding Creep Strain Energy Density (CSED) and Total Strain Energy Density (TSED), curves are presented in Figure 4.6. In the case of SACQ, TSED for the squared profile presents several unstable peaks, and the general TSED values are not greater than those of CSED. On the other hand, TSED values are constantly greater than the CSED values for the rounded profile, and the curves follow a more stable pattern. In both cases, SAC305 and SACQ squared profile; the peaks show a time dependency and relaxation.

4.3.2 Reliability prediction analysis

Following Che and Pang's procedure [97] (subtraction between final values of the third and second cycle), values of the approximation of average strain and energy variation were computed (see Table 4.6). It should be noticed that all values decreased due to a change in copper pad geometry. High values can be observed for the squared profile with a significant reduction for the rounded profile. However, a more stable curve regarding TSED in SACQ increased inelastic strain energy density.

Table 4.6 Approximation of average of creep strain and energy density.

	SAC305		SACQ	
	W_p $\Delta \varepsilon_p$		W_p	$\Delta arepsilon_p$
Squared	0.4738	0.0667	0.0552	0.0968
Rounded	0.1272	0.0255	0.0999	0.0363

Recent studies have reported Morrow and Coffin-Manson constant for estimation of the number of cycles to failure. It has been shown that the temperature, frequency, and aging may potentially affect the constants [114]. Morrow and Coffin-Manson constants for SAC305 and SACQ aging dependent have been reported in the last two years [122]. Nevertheless, temperature and frequency dependency is needed for an accurate estimation using Table 4.6.

4.4 Conclusions

The reliability of the solder ball can compromise the functionality of the entire Integrated Circuit. Repetitive thermal loading of a complex FO-WLP package was modeled, varying the copper profile and solder ball material viscoplastic properties.

Based on the results, the following conclusion can be drawn in addition the ones mentioned in section 3.4:

Solder masks can be neglected in the geometry of the electronic packaging since it does not significantly affect creep results.

A change in the copper pad profile shape (squared to rounded) shows a stress reduction and, therefore, more stable creep curves. Additionally, it accentuates the difference of creep values between materials by nearly 16% regarding creep strain values.

Filet copper pad edge might seem advantageous; however, it greatly impacts the mesh complexity. Therefore, longer simulation time is needed and special attention to unlink nodes should be paid.

Since reliability models are inversely related to inelastic strain energy, SACQ presented the most promising working time, followed by SACR, Innolot, and SAC305 in that order.

5. Efficient modeling framework for estimation of reliability indicators

5.1 Introduction

Accurate and efficient modeling and simulation of thermo-mechanical behavior of advanced electronic packaging structures, incorporating lead-free solder interconnects, require accurate geometry and material model parameters as well as relevant simplifications and assumptions.

Since the introduction of Restrictions of Hazardous Substances (RoHS) [123], several new lead-free soldering materials with high tin (Sn) content have been developed [124] in the challenging search for a suitable combination to replace the eutectic tin–lead (SnPb) solder. Thus far, tin–silver–copper (Sn-Ag-Cu, SAC) compositions have proven beneficial for electronic and mechanical properties despite an increase of about 30 °C in melting temperature compared to the conventional SnPb eutectic alloy.

In electronic packages, repetitive thermo-mechanical loads during manufacturing and service life cause deformation and stress in the solder interconnections by the mismatch of the coefficient of thermal expansion (CTE) [125] of the dissimilar materials. In some applications, the introduction of lead-free soldering materials was found to compromise the reliability [126].

Intermetallic compound (IMC) layers form between the solder and the Cu (copper) pad in a compound of Cu6Sn5 or (Cu,Ni)6Sn5 (η-phase) and Cu3Sn (ε-phase), which compromises the integrity of the solder ball [127], [128]. Consequently, novel (micro) alloying elements, such as antimony (Sb), bismuth (Bi), and nickel (Ni), may be incorporated to reduce mechanical detriment. These recently developed doped-SAC solders proved higher reliability under thermo-mechanical loads [129], [130].

Failure prediction plays an essential role in electronic packaging design. The Distance to Neutral Point (DNP) concept limited the size of the board and the number of In-put/Outputs (I/O). This theory was based on the distance from the neutral point to the furthest solder bump, where the highest thermo-mechanical load occurs [100]. For the lifetime prediction of electronic packages, reliability models typically based

on low cycle fatigue models, e.g., strain-based Coffin-Manson [107], strain energy-based Morrow [98], and Monkman-Grant [108] models have been frequently used. As the solder material behaves in a time-dependent manner, creep strain and creep strain energy density are needed to estimate the number of cycles to failure in the above-mentioned models.

Finite element modeling (FEM) is widely used to analyze the thermomechanical behavior of multi-material electronic packaging structures [131]. In electronic packaging simulations, often either a 2-D model of the main diagonal cross-section or a 3-D model of one-quarter of the chip geometry is simulated to optimize computational costs [132], [133]. The cross-sectional layout is typically idealized using a sharp-edged geometry, and IMC layers are rarely included in the simulations [116], [134]. For extensive parameter studies, a computational cost-effective simulation is preferred to run several replicates. Previous works show the advantage of such replicates to compare the creep behavior of undoped and doped SAC solders in advanced electronic packaging [135], [136], [137].

A computational cost-effective modeling framework is proposed in the present work, a simple and efficient tool that can be applied for extensive parameter studies for solder interconnect analysis. A Fan Out—Wafer Level Packaging (FO-WLP) model was built and analyzed using multiple simulation replicates in a thermal testing environment to evaluate geometry-related modeling aspects; and materials-related modeling aspects. Four main parameters were contemplated for a comprehensive comparison.

- (1) Regarding the solder materials, SAC305 and SACQ were selected for the analysis. A critical location of the model is the bond pad edge, which is prone to induce stress concentrations with ideal sharp edges, while real geometry is often blunt [116], [134].
- (2) Therefore, a model geometry with a chamfered bond pad edge was built and compared to the sharp edge configuration in the simulations.
- (3) A pseudo-3-D modeling domain was also constructed from the previous 2-D model to employ a combined plane strain plane stress analysis to improve the accuracy without compromising computational costs.

(4) Finally, the effect of incorporating thin IMC layers was analyzed, contrasting with simulations that dismiss IMC layers.

The impact of the parameter variations was evaluated on the creep strain and creep strain energy densities presented in the results section, together with the analyses of von Mises and shear stresses in the critical locations of the solder. Reliability prediction for low cycle fatigue requires strain or strain energy-based reliability indicators; furthermore, an averaging scheme, which was proposed in this work, is dedicated to the modeling framework.

5.2 Simulation Setup

Finite element simulations were set up for thermal and mechanical analysis in MSC Marc Mentat. In this section, the modeled geometry is described, including the bond pad edge variations and the incorporation of IMC, followed by material models and properties and the boundary conditions with the thermal load.

5.2.1 Model geometry

An advanced FO-WLP—Redistribution Layer First (RDL First) package was modeled based on a modified 167GJJ layout of Texas Instruments' design [93]. The ball grid array arrangement for the solder bumps consists of 15 bumps distributed horizontally with a pitch of 0.8 mm and a central solder bump. The main dimensions in the vicinity of a solder bump are displayed in a cross-section view in Figure 3.6.

Bond pad edges are often modeled with idealized sharp edges, while real geometries shown in Scanning Electron Microscopy (SEM) images [116] may become blunt in the final assembly as a consequence of the patterning process steps. The edge shape can strongly influence stress distributions in the solder balls; hence, two different edge shapes were proposed in this study: sharp and blunt (chamfered), as shown in Figure 5.1. The chamfer dimensions are: 4 µm at 45°.

Additionally, two extra layers were optionally included to analyze the variation related to IMC formation at the bond pad–solder interface. An estimated 10% of the copper pad's total thickness, 2 μ m, was established for each IMC layer's (Cu₆Sn₅ and Cu₃Sn) thickness with idealized smooth geometries at the interfaces.

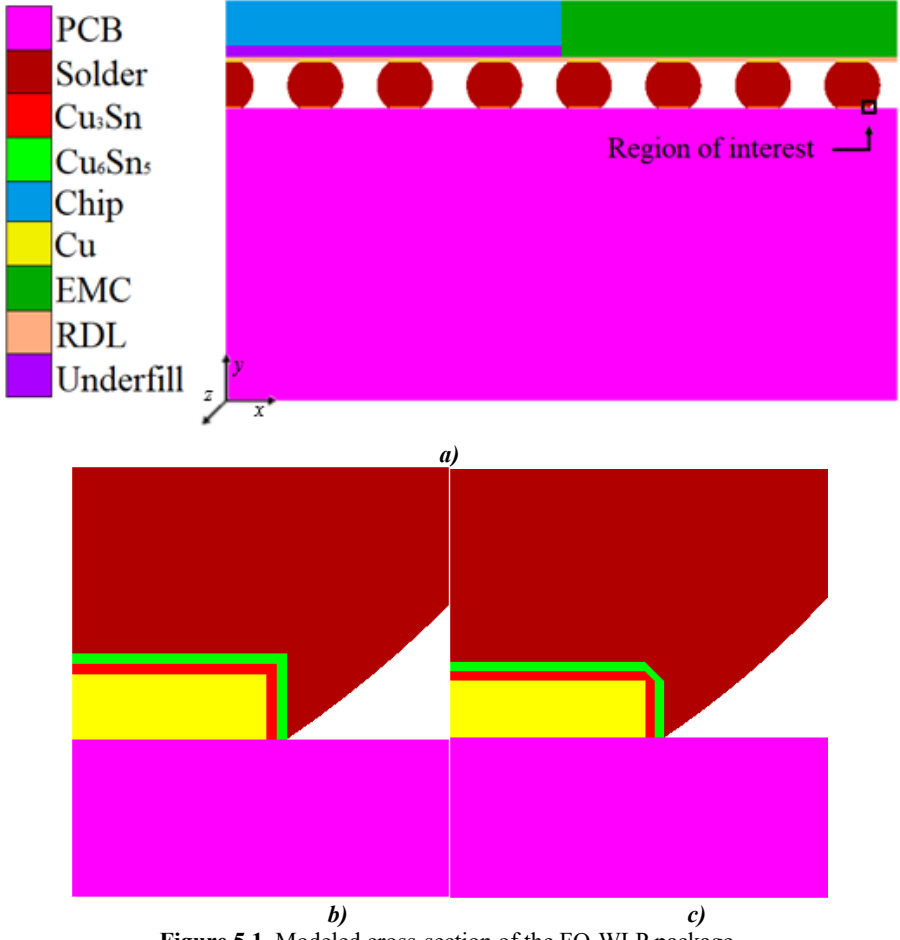


Figure 5.1. Modeled cross-section of the FO-WLP package.
a) Material description; contact pad modeled with b) ideal, or c) real geometry.

Usually, under-bump metallization (UBM) consists of copper coated in noble metals such as gold (Au) [138]. As a simplification, UBM was modeled as pure copper (Figure 3.6). While 3-D modeling provides a more realistic approach, a rough mesh is often used to balance out the high computational costs [139]. A 2-D model allows employment of a fine mesh, which can lead to a more accurate local distribution of results with low computational costs. For the simulation domain, therefore, a 2-D cross-section was modeled in this work, either with 2-D elements with a plane strain condition or with a pseudo-3-D variation, using a linear geometry extension in the out-of-plane direction (Figure 5.2). This pseudo-3-D approach allows the model of the solder with plane stress condition, whereas the other parts of the assembly may remain in plane strain condition. Therefore, overestimations of the stresses in the solder balls, which often arise in pure plane strain conditions [140], are avoided.

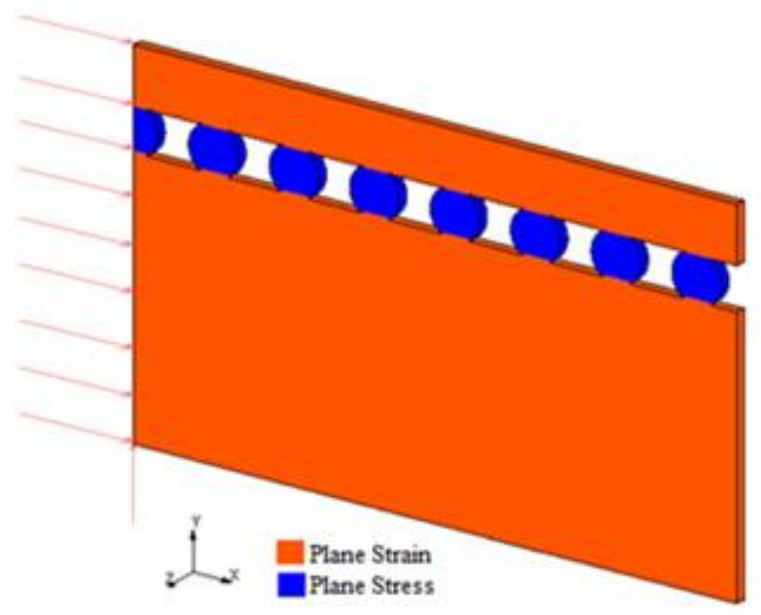


Figure 5.2. Pseudo 3-D model Combined plane strain and plane stress conditions.

The pseudo-3-D model was one element thick, where all planar elements of the 2-D model in Figure 5.1 a were expanded to a thickness equivalent to 20% of the solder ball diameter (100 μ m) with respect to the z-axis.

The finite element mesh for the 2-D model contained plane strain quad elements with a geometric property of unit thickness, while the mesh for the pseudo-3-D domain consisted of full integration hexahedral elements. The complete finite element mesh contained over 27,000 elements.

5.2.2 Material Models and Properties

Materials in the modeled package layout in Figure 5.1 are considered to be linear elastic and temperature independent, except for the solder. For the chip and the substrate, elastic material properties such as Young's Modulus (*E*) and Poisson's Ratio (*v*) are summarized in Table 3.4 with the addition of IMC properties detailed in Table 5.1 [94], [121].

 Table 5.1. IMC Material Properties.

Material	E (GPa)	v (-)	CTE (ppm/K)
Cu ₆ Sn ₅	85.6	0.31	17.6
Cu₃Sn	108	0.30	17.8

The solder was modeled as temperature-dependent elastic-time and temperature-dependent inelastic (creep) material. The dominant deformation is creep, for which the Anand solder model [27] was employed in the simulations. In this model, creep strain

is a function of stress, temperature, and time for describing inelastic deformation. Anand Equations (1.4) - (1.7) comprise nine material parameters previously detailed in section 1.2.5.

For the solder materials, either SAC305 (Sn-3.0Ag-0.5Cu) or SACQ (Sn-4.0Ag-0.5Cu-3.0Bi-0.05Ni) were selected based on our earlier studies on creep behavior, where many data sources were compared for SAC305 [136] and for various SACX soldering materials [137]. The doping for SACQ involves Bi besides Ni [90], which, together with the slightly higher Ag content, results in somewhat higher resistance to creep deformations, while it causes minor differences in elastic behavior [63]. For simplicity, identical elastic behavior was modeled for both alloys, with the temperature-dependent elastic parameters shown in Figure 3.8. The Anand creep model parameters are summarized for both alloys in Table 5.2.

SACQ [95] **Parameter** SAC305 [68] S_0 (MPa) 21 0.405 $A (s^{-1})$ 3501 2.45×10^{8} ξ (-) 4 0.068 0.25 m(-)0.36 180×10^{3} h_0 (MPa) 3521.56 s (MPa) 30.2 0.638 0.0056 n (-) 0.01 a (-) 1.78 1.243 112,313.8 $Q (J \cdot mol^{-1})$ 77,491.14

Table 5.2. Anand parameters for the solder materials.

5.2.3 Boundary conditions

Mechanical constraints regarding the *x*-direction were located along all the nodes on the model's left side. This setup allowed a symmetrical analysis in both cases (2-D and pseudo-3-D). Furthermore, since the differential equation systems require a single solution, all axes were confined to the bottom-left node (see Figure 5.2).

In the case of the pseudo-3-D model, extra constraints in the z-axis were established for all nodes. An exception was considered for the solder material for a free expansion in the z-direction (Figure 5.2), leading to a simulation of plane strain and plane stress.

The mismatch in CTE of the different materials, in combination with the further described thermal load case, leads to stress and mechanical loads. No extra mechanical loads, such as vibration or external forces, were applied.

Previous studies in the field of reliability showed that a creep strain energy density of the first three thermal cycles may be sufficient to estimate the reliability of the solder [97]. An average of creep strain and creep strain energy density can be computed, taking values at the end of the second and third thermal cycles.

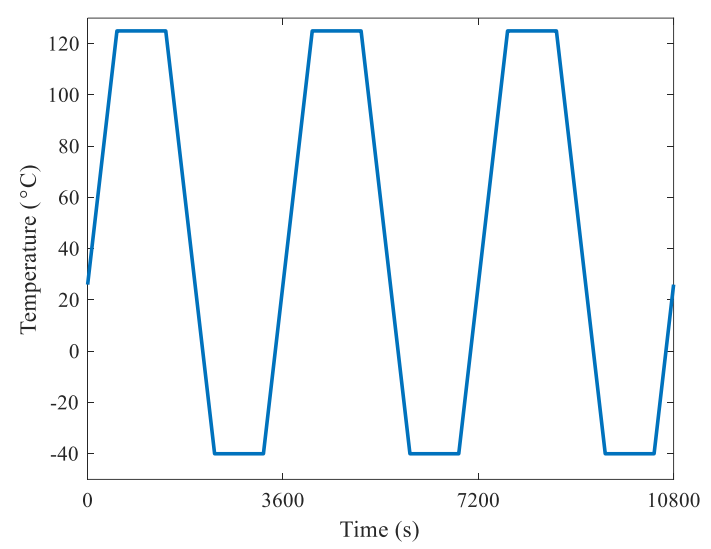


Figure 5.3. Applied temperature load as a function of time.

Regarding the thermal loads, following the Joint Electron Device Engineering Council (JEDEC) standards [141], the maximum temperature should not exceed any of the glass transition temperatures (Tg) of the materials included in the experiment. Therefore, a maximum temperature of 125 °C was defined. Among the cases mentioned in the JEDEC standard, case G suggests –40 °C as the minimum temperature and an approximate number of one to two thermal cycles per hour. Starting the cycling at a high initial temperature would reflect a case when the cycling begins right after the soldering. Thermal testing starts quite a significant time after soldering. Therefore, the solder material has time to relax. Thermal testing then always begins at room temperature at solder stresses higher than zero but lower than right after soldering. We have chosen to neglect the residual stresses in the solder at the start of the thermal testing. Based on similar studies [142], the initial temperature was set at 26 °C, ramp rates were 11 °C/min, and the hold times were 15 min. The isothermal load applied to all the nodes in the model is shown in Figure 5.3.

5.2.4 Summary of Parameters Variation

Four different parameters were considered for the simulations, each with two levels: soldering material, bond pad edge geometry, incorporation of IMC, and the simulation

domain. Altogether, 16 different simulations were carried out, as summarized in Table 5.3. For one simulation, calculation times could reach less than 30 min for either simulation domain, with output file sizes of about 2 MB at ca. 27,000 elements with about 1000 time increments.

Table 5.3. Summary of study cases.

Simulation domain		Solder material		
2-D pseudo 3-D		SAC305	SACQ	
IMC *		Bond pad edge		
NI	I	Sharp	Blunt	

*NI: No IMC layers included, I: IMC layers included

5.3 Results and Discussion

Upon completing 16 simulation replicates, the results were systematically organized based on creep strain and strain energy density metrics, equivalent von Mises stress and shear stress curves, and stress–strain hysteresis loops. These metrics were analyzed regarding the simulation domain, material type, intermetallic compound (IMC) layer characteristics, and bond pad edge conditions. Furthermore, reliability estimates were computed to determine the parameters most significantly influencing lifetime predictions.

5.3.1 General Observations

An example of the distribution of the total equivalent of creep strain (TECS) at the end of the simulation for the case of the SACQ 2-D model with the inclusion of IMC is shown in Figure 5.4. In the contour band graph, the highest strain was found in the vicinity of the bottom left of the outer solder ball. This result was similar in all the studied cases. The principle of the distance to the neutral point [100] suggests such behavior, as well as experimental results where electronic packaging with UBM presented its critical node at the bottom section of the solder bump [116]; therefore, we did not extend the analysis for the upper contact.

Although particular values do not show a significant variation, the contour band distribution reveals a different concentration of strain. Critical values are distributed along the edge of the Cu pad for the blunt case, whereas for the sharp edge case, high values surround only in the close vicinity of the critical location (Figure 5.4).

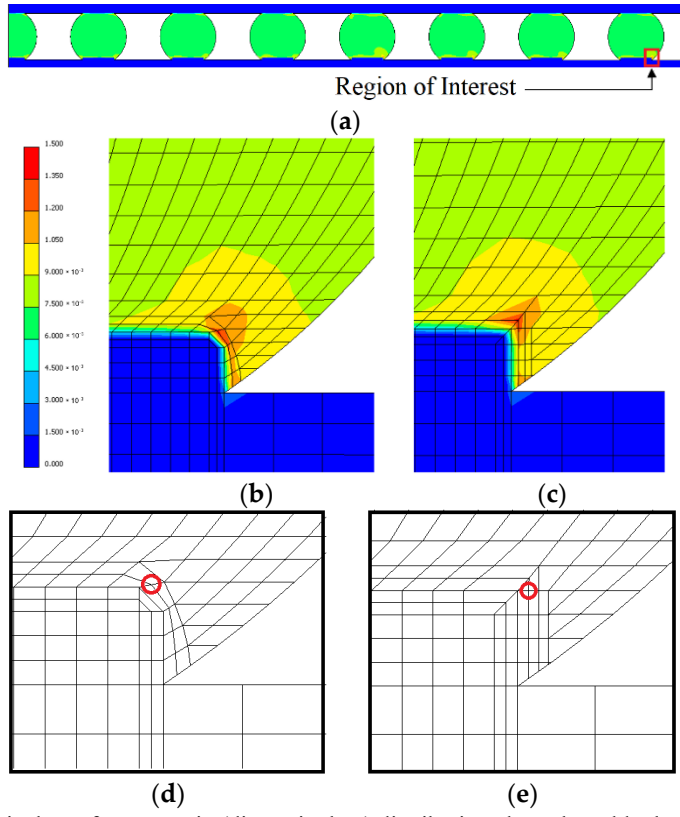


Figure 5.4. Total equivalent of creep strain (dimensionless) distribution along the solder bumps at the end of the three cycles.

(a) cropped image. Augmented contour band graph of TECS distribution at the vicinity of the critical node: (b) blunt and (c) sharp bond pad edge profile. Location of the node of interest: (d) blunt and (e) sharp pad profile.

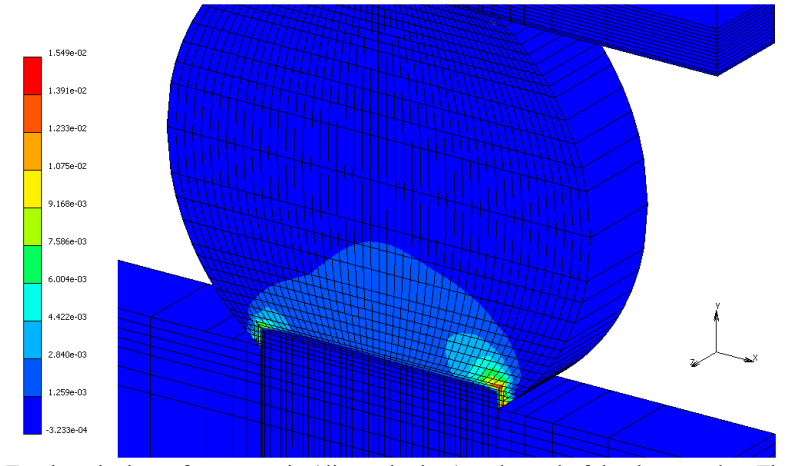


Figure 5.5. Total equivalent of creep strain (dimensionless) at the end of the three cycles. The 3-D-Sharp-SAC305-IMC case is included.

TECS distribution is shown for SAC305, pseudo-3-D, model in Figure 5.5. In contrast with the 2-D models previously detailed, high strain values are located only near the vicinity of the critical location. This last node is on the bottom side of the outer solder ball. After comparing values in the vicinity of the critical node, a constant location was selected for the data collection for all the study cases (see Figure 5.4 d,e).

In the following subsections, results at the critical locations are analyzed in detail: first, creep strain and creep strain energy density values, which are the basis of reliability calculations, followed by detailed stress analyses.

5.3.2 Creep Strain and Creep Strain Energy Density

Data collected from the total equivalent of creep strain (TECS) and creep strain energy density (CSED) are presented for the different cases in Figure 5.6. In accordance with curves from blunt bond pad cases (see Figure 5.7), the case displayed in Figure 5.6 c shows a reduction of over 25% from the 2-D model to the pseudo-3-D model.

Regarding IMC incorporation, a minor difference can be seen in the results. Considering the variation in bond pad shape, TECS curves present slightly higher values for sharp edges, whereas for CSED values, blunt curves are higher. Since reliability models use strain and strain energy density independently, special attention should be paid to selecting the solder material model that describes the true behavior. We have previously conducted an extended study on the effect of the creep material models, including power law and Anand's model [143], and a comparison of solder joint reliability models [135]. Fundamentally, failure prediction based on strain energy density relies on the chosen plastic strain model. Anand's solder creep model for the material model, in combination with Morrow's model for solder joint reliability, can be a preferable choice for reliability predictions.

A thorough comparison of values of TECS and CSED for the eight cases generated from blunt Cu pad is presented in Figure 5.7. Regarding changes due to the simulation do-main (2-D vs. pseudo-3-D), the most significant reduction can be observed in Figure 5.7 c, where both curves decreased by nearly 25% from the 2-D to pseudo-3-D case. It can be noticed that changes due to element type are more evident for SACQ than for SAC305.

In terms of IMC incorporation, minor changes can be observed at the critical location in the solder ball. The largest change takes place in Figure 5.7 b for 2-D elements. A slight reduction of less than 10% can be observed at the end of the three thermal cycles.

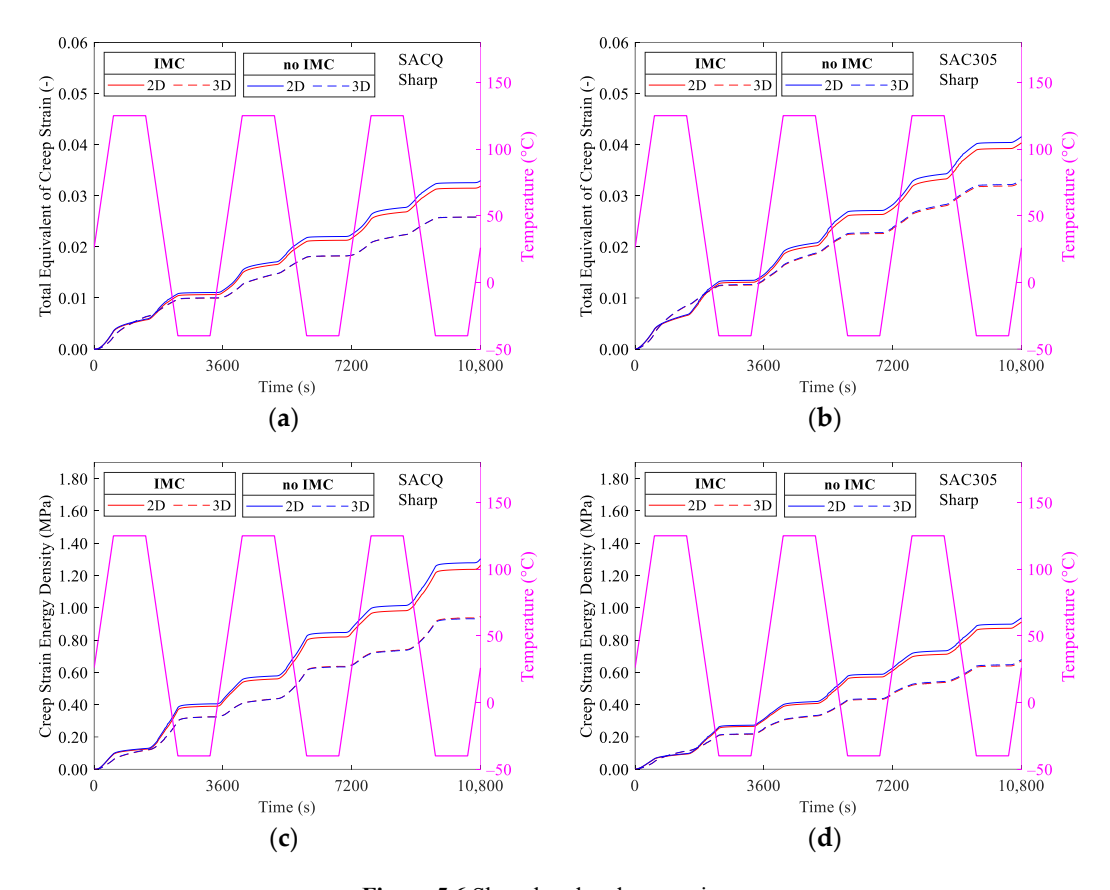


Figure 5.6 Sharp bond pad comparison.

Total equivalent of creep strain: (a) SACQ, (b) SAC305. Creep strain energy density: (c) SACQ, (d) SAC305.

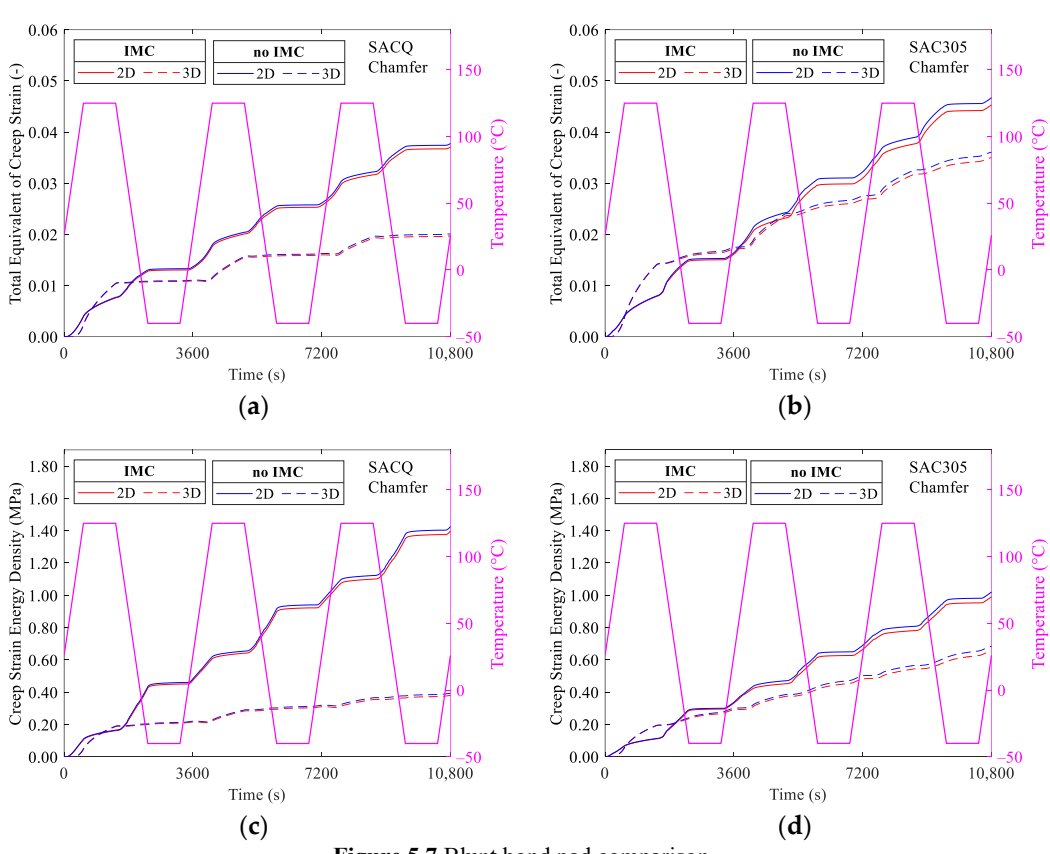


Figure 5.7 Blunt bond pad comparison.

Total equivalent of creep strain: (a) SACQ, (b) SAC305. Creep strain energy density: (c) SACQ, (d) SAC305.

Finally, the change in material properties from SACQ and SAC305 is more evident for 2-D elements rather than pseudo-3-D elements. However, there is a slight inconsistency in CSED curves. Observing TECS curves in Figure 5.7 a,b, all four curves from SAC305 are slightly greater than SACQ. Furthermore, CSED curves in Figure 5.7 c, d for 2-D elements present lower values for SAC305, whereas curves for pseudo-3-D elements display slightly greater values. There is a tendency for SAC305 values to be greater than SACQ, except for 2-D element type in both IMC inclusion scenarios.

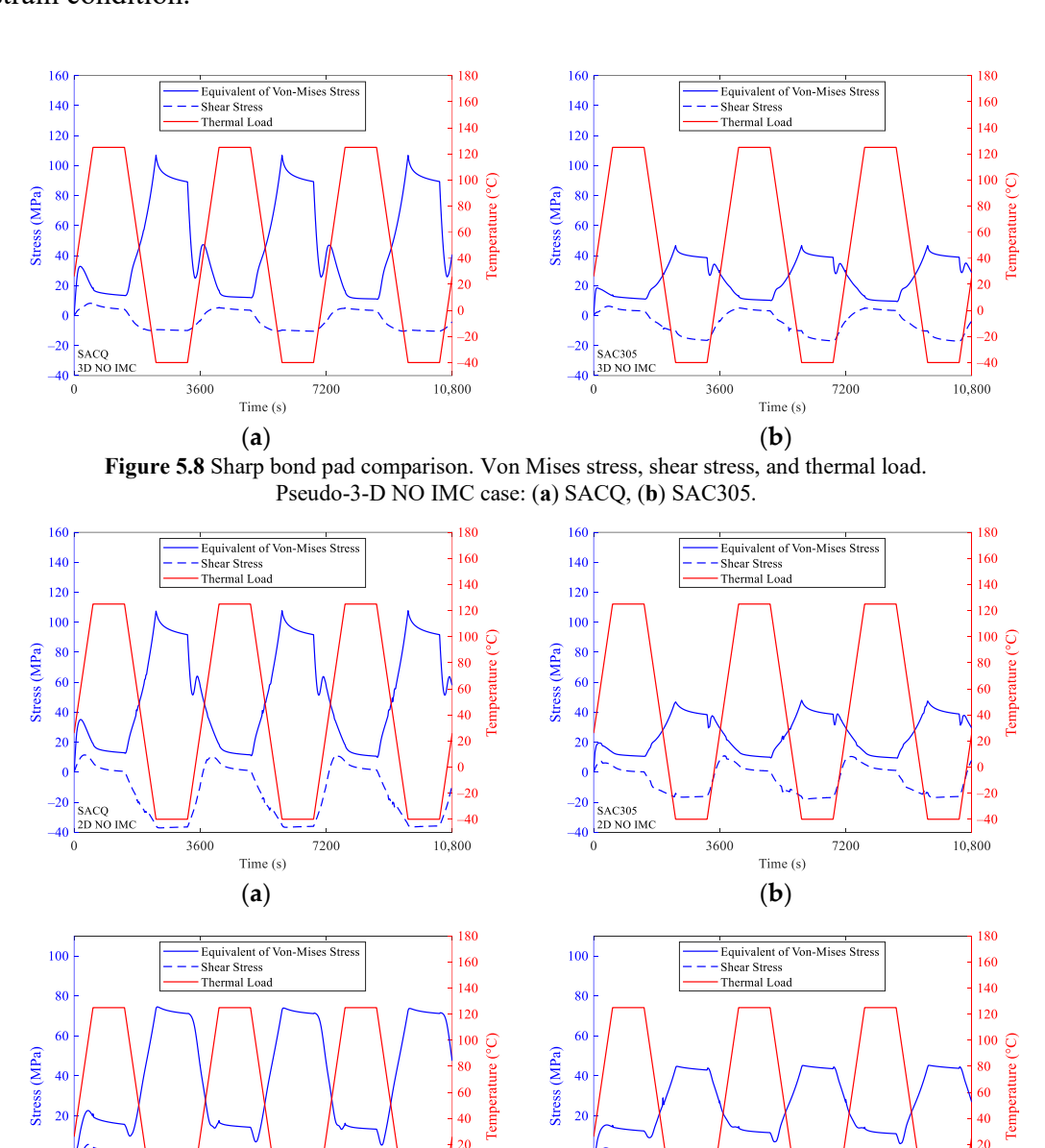
5.3.3 Von Mises and Shear Stresses

Stress vs. time graphs were collected for all cases; nonetheless, for the sharp bond pads, only the pseudo-3-D model without IMC showed relevant differences, as shown in Figure 5.8. In all cases from sharp bond pad geometry, the relaxation curve constantly presented a defined exponential shape during low temperatures. Additionally, the shear stress shows a minimum value of nearly -15 MPa, whereas, for the blunt pad geometries, the same minimum value exceeds -20 MPa (see Figure 5.9).

Von Mises and shear stresses are shown for the blunt pad geometry in Figure 5.9. Four cases were considered for the comparison based on the relevance of changes as compared with curves obtained from the sharp bond pad geometry. The decreasing exponential distribution of values during the low temperature (-40 °C) demonstrates a constant relaxation, like the one shown in the graphs reported by Zhang et al. [132]. This relaxation is visible in both cases with a 2-D model (Figure 5.9 a,b). On the other hand, the relaxation during the high constant temperature presents more stable values in the 2-D element cases compared with pseudo-3-D model cases.

It can be observed that there are small troughs during the second decreasing ramp temperature in both scenarios with a pseudo-3-D model. The same unusual troughs can be observed in both scenarios with 2-D elements when the temperature initiates the second, increasing ramp from -40 °C to 125 °C. A trough is seen for the pseudo-3-D model at cooling, while it is present for the 2-D model at heating, in both cases close to the extreme (high or low, respectively) temperatures. The trough is a local minimum, which might arise when a stress component changes sign. For the 2-D modeling, due to the plane strain condition, very high out-of-plane stress arises, which mainly governs the equivalent stress, while in the pseudo-3-D case, the out-of-

plane stress is zero; therefore, other components govern the equivalent stress. In Zhang's 3-D models [132], such troughs are seen for heating, which means that in the real 3-D case, the out-of-plane (or tangential) (partial) confinement is felt, i.e., stresses are not zero in that direction, but obviously not as high as they would be in a plane strain condition.



(c) (d) Figure 5.9 Blunt bond pad results for von Mises stress, shear stress, and the thermal load as a function of time. The 2-D, NO IMC case: (a) SACQ, (b) SAC305. Pseudo-3-D NO IMC Case: (c) SACQ, (d) SAC305.

40

10,800

7200

SACQ 3D NO IMO

3600

40

SAC305 3D NO IMC

3600

-20

-40

10,800

Overall, the von Mises stress values are nearly 50% smaller for SAC305 than SACQ in both scenarios, 2-D and pseudo-3-D domains. This is due to SACQ being stiffer relative to SAC305; therefore, it has a higher resistance to deformations. SACQ, therefore, deforms somewhat less, as seen in Figure 5.6 and Figure 5.7, and at the same time, its high resistance shows significance at high stress levels.

Regarding von Mises stress, curves agree with values presented by Zhang et al. [132]. The most remarkable change concerns the troughs during the heating ramp (at the beginning of every cycle). The decreasing exponential distribution of values during the low temperature (-40 °C) demonstrates a constant relaxation, like the one shown in the graphs reported by Zhang et al. [132].

5.3.4 Hysteresis Curves

Due to the high thermal load and the difference between the plane strain and plane stress assumptions, cyclic hardening and softening vary significantly in the strain vs. stress curves in Figure 5.10 and Figure 5.11.

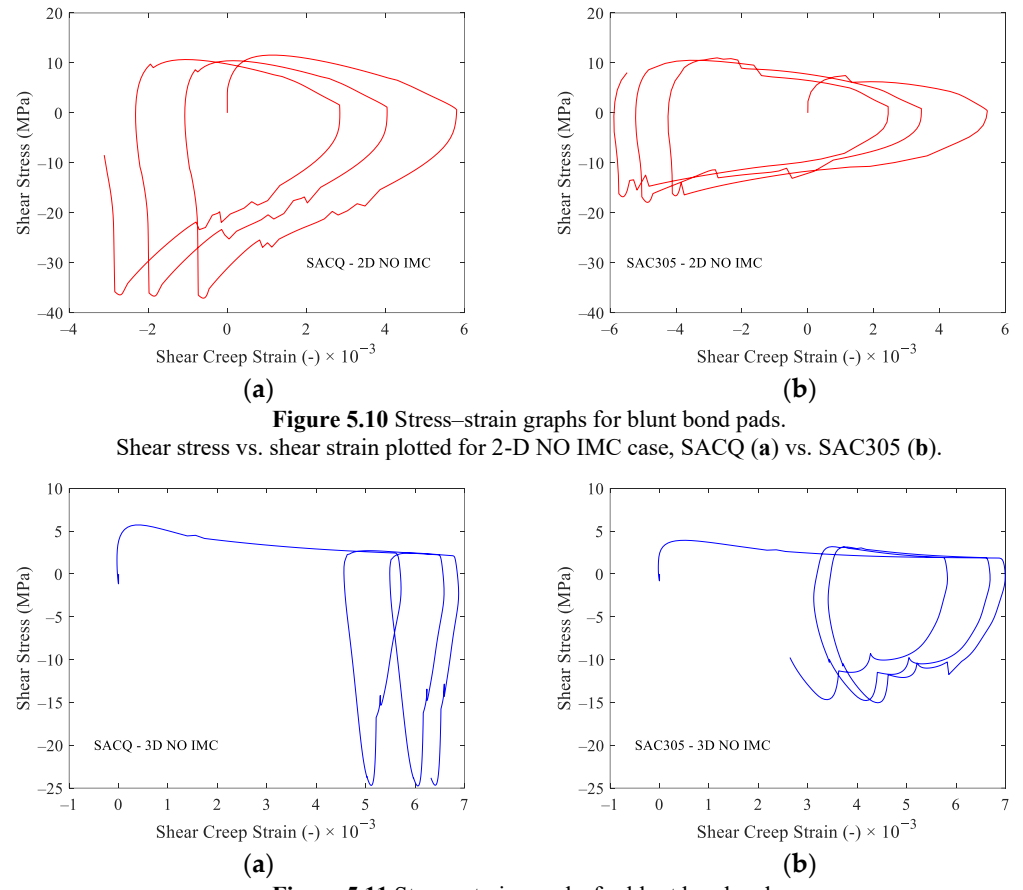


Figure 5.11 Stress—strain graphs for blunt bond pads. Shear stress vs. shear strain plotted for pseudo-3-D NO IMC case, SACQ (a) vs. SAC305 (b).

Variations in the sheer stress range are straightforward from the previous analysis: the range is broader for the high deformation resistant SACQ than SAC305 and narrower for the less confined pseudo-3-D domain than to the 2-D domain.

The main difference is also related to the out-of-plane confinement: in the plane strain model, shear creep strain alternates, while in the plane stress model, it pulsates. In the latter case, there is a large deformation in the first cycle that also pushes the solder in the out-of-plane direction, and then there is no such force that could pull it back completely; nevertheless, it will climb towards the negative shear creep strain direction cycle by cycle.

5.3.5 Reliability-Related Predictions

Che and Pang [97] introduced a method for reliability predictions for the Coffin–Manson strain-based model and Morrow's energy-based models for simulated environments. In general, the number of cycles to failure is inversely proportional to the fatigue indicator, i.e., the lower the inelastic strain range (Δ TECS) for the Coffin–Manson, or strain energy density range (Δ CSED), the higher the number of cycles to failure. The range is calculated in this work between the difference of the parameter at the end of 3rd and the end of the 2nd cycle.

In Table 5.4, both fatigue indicators ΔCSED and ΔTECS are listed for all calculated cases. The table is organized by the simulation domains in the columns 2-D and pseudo-3-D cases, which represent the lower and upper bound for the strain and strain energy-related values, respectively. The higher confinement by the plane strain condition 2-D restricts strains and strain energies, while less confinement in the pseudo-3-D case with the plane stress condition for the solder allows higher strains and, therefore, higher strain energies. In a real scenario, these indicators will fall in between the bounds; hence, the averages are displayed in the third column, and further analysis and conclusions will be based on these average values. In a full 3-D simulation, a volume-averaging scheme would be required for accurate indicators [97].

In terms of material quality, these reliability indicators alone would not provide a valid basis for comparison, as the number of cycles to fracture will also depend on the fatigue ductility coefficient and fatigue exponents. Therefore, sound conclusions cannot be drawn by comparing average $\Delta TECS$ or $\Delta CSED$ between the dissimilar material qualities of SAC305 and SACQ. While the lower average $\Delta TECS$ for SACQ would indicate better fatigue response, average $\Delta CSED$ shows the opposite trend, and the reason is that the strength of SACQ is higher; therefore, the lower strain parameter, while with less deformation, stresses increase, resulting in high strain energy parameters. By calculating the number of cycles to failure, the high-reliability performance of SACQ can be shown [129], [130].

The effect of the IMC incorporation over the Cu bond pad in the simulations shows only minor differences in the fatigue parameters for the solder. Here, IMC will further enforce the already relatively high strength Cu pad at the solder interface, decreasing deformation slightly in the close vicinity of the pad within the solder as shown by the decrease in $\Delta TECS$ values, while stress has less effect; therefore, strain energy density and $\Delta CSED$ will also slightly decrease with a few percent.

The advantage of the realistic bond pad geometry in the simulation can be seen in the decreased Δ CSED values for blunt edges compared to the ideal sharp-edged geometries.

2-D Pseudo-3-D Average (Lower Bound) (Upper Bound) (2-D—Pseudo-3-D) ΔCSED ΔCSED ΔCSED SAC305 ΔTECS ΔTECS ΔTECS (MPa) (MPa) (MPa) w/o IMC 0.0133 0.3105 0.0094 0.2101 0.0114 0.2603 Sharp 0.0093 0.0111 0.2546 w/ IMC 0.0128 0.3016 0.2075 w/o IMC 0.0145 0.3306 0.0086 0.1833 0.0116 0.2570 Blunt w/ IMC 0.32630.00820.1732 0.0113 0.24980.0143ΔCSED ΔCSED ΔCSED **SACQ** ΔTECS ΔTECS **ΔTECS** (MPa) (MPa) (MPa) 0.0105 0.2979 0.0090 w/o IMC 0.4308 0.0075 0.3644 Sharp w/ IMC 0.0101 0.4176 0.0076 0.3001 0.0089 0.3589 0.4622 0.0038 0.0077 0.2683 w/o IMC 0.0116 0.0743 Blunt w/ IMC 0.4528 0.0037 0.0076 0.2612 0.01140.0037

Table 5.4. Summary of study cases.

5.4 Conclusions

In this chapter, an efficient finite element calculation framework was developed for deformation modeling and lifetime predictions of solder interconnects in advanced packaging under cyclic thermal loads. Demonstrations were carried out considering the following variations: modeling domain (2-D and pseudo-3-D), soldering material (SAC 305 and SACQ), incorporation of intermetallic compound (IMC), and bond pad

edge geometry (sharp and blunt). Modeling domain assumptions were thoroughly analyzed, and the stress-strain analysis on the solder showed fundamental differences in the stress cycles. Cyclic hardening and softening vary significantly due to the out-of-plane confinement: in the plane strain model, shear creep strain alternates, while in the plane stress model, it pulsates. Reliability prediction for low cycle fatigue requires strain or strain energy-based reliability indicators; furthermore, an averaging scheme, which was proposed in this work, is dedicated to the modeling framework. The usability of the reliability indicators shows predictions are sound with the energy-based parameter (Δ CSED average) but may be fallacious with the purely strain-based one due to strain (or stress) alone is not sufficient in temperature-dependent cases. The following conclusions are drawn related to the essential modeling elements:

- 1. Efficient planar simulation framework with 2-D and pseudo-3-D meshed geometries provides a quick estimate for lower and an upper bound for the strain, stress and strain energy-related parameters, respectively. In a real scenario, these indicators will fall in between the calculated bounds. This calculation framework can be employed for extensive parameter studies solved rapidly at low computational costs.
- 2. In terms of material quality, simulation results provide a sound insight into the behavior of the structure, showing the stiffer behavior of SACQ compared to SAC305. Nevertheless, the reliability indicators alone would not provide a valid basis for comparison of dissimilar solders, as the number of cycles to fracture will also depend on the fatigue ductility coefficient and fatigue exponents.
- 3. The effect of the IMC incorporation over the Cu bond pad in the simulations shows only minor differences in the fatigue parameters for the solder. IMC will further enforce the already relatively high-strength Cu pad at the solder interface, decreasing deformation slightly in the close vicinity of the pad within the solder.
- 4. Related to the bond pad geometries, the advantage of the realistic blunt bond pad geometry in the simulation is obviously lowering stresses. In the worst scenario, fatigue parameters can be overestimated by over 30% with the ideal sharp-edged geometries.

6. Summary of New Scientific Results

The dissertation findings are summarized in four thesis points. The author's works in which the actual thesis points were published are in square brackets.

Thesis 1 [Publication: J1 and C1]

A virtual test bench was developed that is tailored for strain analysis in solder interconnects. Evaluating lead-free (Sn-3.5Ag, SAC305, SAC387) and SnPb solder behavior in the simplified soldered stack, which was subjected to simulated thermal and mechanical loads in the test bench environment, showed a significant reduction in creep deformations for lead-free solders. It was found that among the lead-free solders, SAC305 exhibits the most favorable performance due to its lower average creep strain, indicating superior mechanical stability under thermal and mechanical loads.

Thesis 2 [Publication: C2 and C3]

Methodology was developed for the evaluation of the goodness of material parameters for simulations of advanced electronic packaging subjected to thermal loads. Out of the six selected Anand solder creep parameter sets describing SAC305, it was found that the favorable set provided accurate and computationally stable simulation results, as evaluated by creep strain and creep strain energy densities, at the lowest computational costs. Additionally, doped SAC solders (SACQ, SACR, InnoLot) showed improved creep strain energy density in the simulations, with SACQ being beneficial due to its lower average creep strain energy density.

Thesis 3 [Publication: J2]

A test bench was developed to evaluate the simplifications of the modeled geometry for interconnects in advanced packaging. Solder—solder pad geometries were examined by varying contact pad edges (fillet, chamfer, and sharp) for Fan-Out Wafer-Level Packaging. It was found that slight changes in geometry reduce stress and thus accentuate differences in creep behavior among soldering materials. Fillet-shaped copper pads resulted in a 16% reduction in creep strain energy density in the contacting solder, which can significantly impact reliability predictions.

Thesis 4 [Publication: J3]

An efficient finite element calculation framework was developed for modeling deformation and predicting the lifetime of solder interconnects in advanced packaging under cyclic thermal loads. Within this simulation framework, planar 2-D and pseudo-3-D meshed geometries provide quick estimates for lower and upper bounds of strain, stress, and strain energy-related parameters. Reliability prediction for low cycle fatigue also requires an averaging scheme that provides reliability indicators. This scheme, proposed in this work, is dedicated to the modeling framework. It was found that the usability of the reliability indicators is sound with the energy-based parameter but may be misleading with the purely strain-based one, as strain (or stress) alone is insufficient in temperature-dependent cases. This calculation framework can be employed for extensive parameter studies, solved rapidly at low computational costs.

7. List of Publications

7.1 Articles in internationally reviewed academic journals.

- [J1] R. S. Vargas Cruz and V. Gonda, "Comparison of creep behavior for lead free solders Sn-3.5Ag, SAC305 and SAC387," Banki Reports, vol. 2, no. 2, pp. 16–21, 2019, [Online]. Available: http://bk.bgk.uni-obuda.hu/index.php/BK/article/view/101
- [J2] R. S. Vargas Cruz and V. Gonda, "Creep and Reliability Prediction of a Fan-Out WLP Influenced by the Visco-Plastic Properties of the Solder," Acta Polytechnica Hungarica, vol. 19, no. 7, pp. 235–254, 2022, doi: 10.12700/APH.19.7.2022.7.13.
- [J3] R. S. Vargas Cruz and V. Gonda, "Efficient Modeling Framework for FO-WLP Solder Interconnect Behavior During Thermal Cycling," Metals (Basel), vol. 15, no. 1, p. 17, Dec. 2024, doi: 10.3390/met15010017

7.2 Papers at international scientific conferences.

- [C1] R. S. Vargas Cruz and V. Gonda, "Comparison of the thermal-mechanical behavior of a soldered stack influenced by the choice of the solder," in 2019 20th International Conference on Thermal, Mechanical and Multi-Physics Simulation and Experiments in Microelectronics and Microsystems (EuroSimE), IEEE, Mar. 2019, pp. 1–6. doi: 10.1109/EuroSimE.2019.8724590.
- [C2] R. S. Vargas Cruz and V. Gonda, "Solder joint reliability based on creep strain energy density for SAC305 and doped SAC solders," MATEC Web of Conferences, vol. 343, p. 02005, Aug. 2021, doi: 10.1051/matecconf/202134302005.
- [C3] R. S. Vargas C and V. Gonda, "Sensitivity of the structural behavior of SAC305 interconnects on the variations of creep parameters," in 2021 IEEE 15th International Symposium on Applied Computational Intelligence and Informatics (SACI), IEEE, May 2021. doi: 10.1109/SACI51354.2021.9465551.

8. Recommendations and Outlook

Soldering materials have evolved drastically since new restrictions were implemented to reduce the use of hazardous substances. The model presented in this research can include more new compositions that are not limited to SAC. Additionally, electronic boards continuously evolve to miniaturize technology. New models could consist of multiple layers in smaller packaging. Finally, a 3D model of one-quarter of the chip should be simulated, and the variation with the pseudo-3D model should be computed to compare and optimize computing resources.

Figures

Figure 1.1 Constant true stress and constant strain rate creep behavior [35]	6
Figure 2.1 Flip Chip placement operation [54].	14
Figure 2.2 Flip-Chip Structural setup and materials description of the sample	16
Figure 2.3 Sinusoidal Structural: Displacement vs Time	17
Figure 2.4 Thermal load: Temperature vs Time.	17
Figure 2.5 Bottom constraints.	18
Figure 2.6 Horizontal boundary condition.	18
Figure 2.7 Point of analysis.	19
Figure 2.8 Equivalent Creep Strain - Comparison.	20
Figure 2.9 Total Equivalent Creep Strain - Comparison	20
Figure 2.10 Total Equivalent Stress.	21
Figure 2.11 Comparison of total equivalent creep strain results	22
Figure 2.12 Total and equivalent creep strain for SAC305	22
Figure 3.1 History of Integrated Circuits [71].	25
Figure 3.2 History of IC Semiconductor packaging evolution [72]	25
Figure 3.3 Semiconductor packaging evolution [75].	26
Figure 3.4 Cross-section of Electronic Packaging [76].	26
Figure 3.5 Comparison of the Cyclic Properties [92].	30
Figure 3.6 Main dimensions of the FO-WLP package section.	30
Figure 3.7 2D Model (Half cross-section of the chip).	31
Figure 3.8 SAC305 temperature-dependent modulus and CTE [63]	32
Figure 3.9 Thermal load.	32
Figure 3.10 Contour band graph.	33
Figure 3.11 ECS and TECS vs time at critical location.	33
Figure 3.12 ECS at critical location.	34
Figure 3.13 TECS at critical location.	35
Figure 3.14 Creep Strain Energy Density.	35
Figure 3.15 Creep Strain Energy Density Comparison.	36

Figure 4.1 Microscopic image of real packaging vs a 2D model [115]42
Figure 4.2 The modelled section:
Figure 4.3 Copper pad filet edge radius
Figure 4.4 . TECS at the end of the three cycles
Figure 4.5. Creep Strain Curves. a) SAC305, b) SACQ
Figure 4.6. Strain Energy Density curves. a) SAC305, b) SACQ47
Figure 5.1. Modeled cross-section of the FO-WLP package
Figure 5.2. Pseudo 3-D model
Figure 5.3 . Applied temperature load as a function of time
Figure 5.4 . Total equivalent of creep strain (dimensionless) distribution along the solder bumps at the end of the three cycles
Figure 5.5. Total equivalent of creep strain (dimensionless) at the end of the three cycles. The 3-D-Sharp-SAC305-IMC case is included
Figure 5.6 Sharp bond pad comparison
Figure 5.7 Blunt bond pad comparison
Figure 5.8 Sharp bond pad comparison. Von Mises stress, shear stress, and thermal load
Figure 5.9 Blunt bond pad results for von Mises stress, shear stress, and the thermal load as a function of time
Figure 5.10 Stress–strain graphs for blunt bond pads
Figure 5.11 Stress–strain graphs for blunt bond pads

Tables

Table 1.1. Thermal environments for solder in several electronic packages [13]	2
Table 1.2. Essential properties of solder alloys [18].	3
Table 1.3. Micro-mechanism of Creep.	8
Table 2.1. Selected studies on lead-free solders.	15
Table 2.2. Composition and melting point of Pb-free solder alloys [56].	15
Table 2.3. Thermomechanical properties.	16
Table 2.4. Material parameters for Anand model	17
Table 2.5. Data set obtained per soldering material.	19
Table 2.6. Main values of equivalent creep and stress	21
Table 2.7. Anand Model vs. Power-law equation.	22
Table 3.1. Some typical SAC Solder Compositions [79].	27
Table 3.2. Anand parameters for SAC305 in various sources.	28
Table 3.3. Doped-SAC solders composition wt% [90].	29
Table 3.4. Material parameters [94].	31
Table 3.5. SAC-X material parameters for the Anand creep model.	31
Table 3.6. Approximation of the Average of Creep Strain Energy Density (MPa).	37
Table 4.1 Overview of solder joint reliability models.	40
Table 4.2 Employed creep and reliability models in highlighted references.	40
Table 4.3 Summary of the main studied parameters.	44
Table 4.4 Total Equivalent of Creep Strain final value variation	47
Table 4.5 Total Strain Energy Density final value variation	48
Table 4.6 Approximation of average of creep strain and energy density	48
Table 5.1. IMC Material Properties.	54

Table 5.2. Anand parameters for the solder materials.	55
Table 5.3. Summary of study cases.	57
Table 5.4. Summary of study cases.	65

References

- [1] R. Chandrappa and D. B. Das, "Waste From Electrical and Electronic Equipment," 2012, pp. 197–216. doi: 10.1007/978-3-642-28681-0_8.
- [2] DIRECTIVE 2002/95/EC Restriction of the use of certain hazardous substances in electrical and electronic equipment, vol. 46. THE EUROPEAN PARLIAMENT AND THE COUNCIL OF THE EUROPEAN UNION, 2003. Accessed: Mar. 25, 2024. [Online]. Available: https://eur-lex.europa.eu/legal-content/EN/TXT/PDF/?uri=CELEX:32002L0095
- [3] T. R. Bieler and T. K. Lee, "Lead-Free Solder," in *Reference Module in Materials Science and Materials Engineering*, Elsevier, 2017. doi: 10.1016/B978-0-12-803581-8.09205-5.
- [4] K. Suganuma, "Advances in lead-free electronics soldering," *Curr Opin Solid State Mater Sci*, vol. 5, no. 1, pp. 55–64, 2001, doi: 10.1016/S1359-0286(00)00036-X.
- [5] H. Ma and J. C. Suhling, "A review of mechanical properties of lead-free solders for electronic packaging," *J Mater Sci*, vol. 44, no. 5, pp. 1141–1158, 2009, doi: 10.1007/s10853-008-3125-9.
- [6] R. W. Johnson, J. L. Evans, P. Jacobsen, J. R. R. Thompson, and M. Christopher, "The Changing Automotive Environment: High-Temperature Electronics," *IEEE Transactions on Electronics Packaging Manufacturing*, vol. 27, no. 3, pp. 164–176, Jul. 2004, doi: 10.1109/TEPM.2004.843109.
- [7] I. E. Anderson, "Development of Sn-Ag-Cu and Sn-Ag-Cu-X alloys for Pb-free electronic solder applications," in *Lead-Free Electronic Solders*, Boston, MA: Springer US, pp. 55–76. doi: 10.1007/978-0-387-48433-4_4.
- [8] K. Seshan, "Reliability Issues," in *Handbook of Thin Film Deposition*, Elsevier, 2018, pp. 43–62. doi: 10.1016/B978-0-12-812311-9.00003-7.
- [9] H. Zhang, F. Che, T. Lin, and W. Zhao, "Stress and reliability analysis for interconnects," in *Modeling, Analysis, Design, and Tests for Electronics Packaging beyond Moore*, Elsevier, 2020, pp. 131–244. doi: 10.1016/B978-0-08-102532-1.00004-4.

- [10] R. Dudek, "Characterization and modelling of solder joint reliability," in *Mechanics of microelectronics*, Springer, 2006, pp. 377–468.
- [11] J. Zhang and G. Q. Zhang, "Advances in LED Solder Joint Reliability Testing and Prediction," in *Solid State Lighting Reliability Part 2*, Springer, 2018, pp. 301–351. doi: 10.1007/978-3-319-58175-0 12.
- [12] D. Charles, "Electrical apparatus and method of manufacturing the same," Dec. 01, 1925
- [13] D. R. Frear, S. N. Burchett, H. S. Morgan, and J. H. Lau, *Mechanics of solder alloy interconnects*. Springer Science & Business Media, 1994.
- [14] D. S. Herman, M. Geraldine, C. C. Scott, and T. Venkatesh, "Health hazards by lead exposure: evaluation using ASV and XRF," *Toxicol Ind Health*, vol. 22, no. 6, pp. 249–254, Jul. 2006, doi: 10.1191/0748233706th266oa.
- [15] EUROPEAN PARLIAMENT; THE COUNCIL OF THE EUROPEAN UNION, "DIRECTIVE 2011/65/EU OF THE EUROPEAN PARLIAMENT AND OF THE COUNCIL of 8 June 2011 on the restriction of the use of certain hazardous substances in electrical and electronic equipment (recast)," Official Journal of the European Union.
- [16] S. Cheng, C. M. Huang, and M. Pecht, "A review of lead-free solders for electronics applications," *Microelectronics Reliability*, vol. 75, pp. 77–95, 2017, doi: 10.1016/j.microrel.2017.06.016.
- [17] S. Yue, "Philips our experience in the introduction of leadfree soldering," in 2004 International IEEE Conference on the Asian Green Electronics (AGEC). Proceedings of, IEEE, pp. 18–25. doi: 10.1109/AGEC.2004.1290859.
- [18] M. Abtew and G. Selvaduray, "Lead-free solders in microelectronics," *Materials Science and Engineering R: Reports*, vol. 27, no. 5, pp. 95–141, 2000, doi: 10.1016/S0927-796X(00)00010-3.
- [19] J. S. Hwang, *Environment-friendly electronics: lead-free technology*. Electrochemical Publications, 2001.
- [20] M. J. Wickham and C. P. Hunt, *Thermal profiling of electronic assemblies*. National Physical Laboratory, 2001.

- [21] B. Salam, C. Virseda, H. Da, N. N. Ekere, and R. Durairaj, "Reflow profile study of the Sn-Ag-Cu solder," *Soldering & Surface Mount Technology*, vol. 16, no. 1, pp. 27–34, 2004.
- [22] H. Ma, "Constitutive models of creep for lead-free solders," *J Mater Sci*, vol. 44, no. 14, pp. 3841–3851, Jul. 2009, doi: 10.1007/s10853-009-3521-9.
- [23] Xu Chen, Gang Chen, and M. Sakane, "Prediction of stress-strain relationship with an improved Anand constitutive Model For lead-free solder Sn-3.5Ag," *IEEE Transactions on Components and Packaging Technologies*, vol. 28, no. 1, pp. 111–116, Mar. 2005, doi: 10.1109/TCAPT.2004.843157.
- [24] Y. Lee and C. Basaran, "A Creep Model for Solder Alloys," *J Electron Packag*, vol. 133, no. 4, p. 044501, 2011, doi: 10.1115/1.4005288.
- [25] Y. Zhang, H. Zhu, M. Fujiwara, J. Xu, and M. Dao, "Low-temperature creep of SnPb and SnAgCu solder alloys and reliability prediction in electronic packaging modules," *Scr Mater*, vol. 68, no. 8, pp. 607–610, Apr. 2013, doi: 10.1016/j.scriptamat.2012.12.017.
- [26] S. Mukherjee, M. Nuhi, A. Dasgupta, and M. Modarres, "Creep Constitutive Models Suitable for Solder Alloys in Electronic Assemblies," *J Electron Packag*, vol. 138, no. 3, p. 030801, 2016, doi: 10.1115/1.4033375.
- [27] J. Thambi, A. Schiessl, M. Waltz, K.-D. Lang, and U. Tetzlaff, "Modified Constitutive Creep Laws with Micromechanical Modeling of Pb-Free Solder Alloys," *Journal of Electronic Packaging, Transactions of the ASME*, vol. 139, no. 3, pp. 1–10, 2017, doi: 10.1115/1.4035850.
- [28] Y. Yao, X. Long, and L. M. Keer, "A Review of Recent Research on the Mechanical Behavior of Lead-Free Solders," *Appl Mech Rev*, vol. 69, no. 4, p. 040802, 2017, doi: 10.1115/1.4037462.
- [29] X. Long, W. Tang, M. Xu, L. M. Keer, and Y. Yao, "Electric current-assisted creep behaviour of Sn–3.0Ag–0.5Cu solder," *J Mater Sci*, vol. 53, no. 8, pp. 6219–6229, Apr. 2018, doi: 10.1007/s10853-017-1967-8.
- [30] V. Ramachandran, K. C. Wu, C. C. Lee, and K. N. Chiang, "Reliability Life Assessment of WLCSP Using Different Creep Models," in 2018 IEEE 68th

- Electronic Components and Technology Conference (ECTC), IEEE, May 2018, pp. 1017–1022. doi: 10.1109/ECTC.2018.00156.
- [31] V. Ramachandran, K. C. Wu, and K. N. Chiang, "Overview Study of Solder Joint Reliablity due to Creep Deformation," *Journal of Mechanics*, vol. 34, no. 5, pp. 637–643, Oct. 2018, doi: 10.1017/jmech.2018.20.
- [32] International Standards Organization, ISO 6303: Method of Extrapolation Used in Analysis of Creep Rupture Dat. 1981.
- [33] A. Di Gianfrancesco, "The European Creep Collaborative Committee: History, structure, activities and last assessments results.," *Journal of Nanomaterials & Molecular Nanotechnology*, vol. 07, 2018, doi: 10.4172/2324-8777-C3-026.
- [34] M. E. Kassner, "Fundamentals of Creep in Materials," in *Fundamentals of Creep in Metals and Alloys*, Elsevier, 2015, pp. 1–6. doi: 10.1016/B978-0-08-099427-7.00001-3.
- [35] M. E. Kassner, Fundamentals of Creep in Metals and Alloys. Elsevier, 2015. doi: 10.1016/C2012-0-06071-1.
- [36] G. Dieter, "Mechanical Metallurgy," 1961.
- [37] M. I. M. Ahmad, J. L. Curiel Sosa, and J. A. Rongong, "Characterisation of creep behaviour using the power law model in copper alloy," *JOURNAL OF MECHANICAL ENGINEERING AND SCIENCES*, vol. 11, no. 1, pp. 2503–2510, Mar. 2017, doi: 10.15282/jmes.11.1.2017.9.0230.
- [38] A. M. Brown and M. F. Ashby, "On the power-law creep equation," *Scripta Metallurgica*, vol. 14, no. 12, pp. 1297–1302, Dec. 1980, doi: 10.1016/0036-9748(80)90182-9.
- [39] S. Spigarelli, "Creep of Aluminium and Aluminium Alloys," *Talat*, p. 26, 1999.
- [40] C. Kittel, *Introduction to solid state physics*, vol. 8. Wiley New York, 1976.
- [41] S. D. Mesarovic, "Lattice continuum and diffusional creep," *Proceedings of the Royal Society A: Mathematical, Physical and Engineering Sciences*, vol. 472, no. 2188, 2016, doi: 10.1098/rspa.2016.0039.

- [42] F. R. N. Nabarro, "Report of a Conference on the Strength of Solids," *The Physical Society, London*, vol. 75, 1948.
- [43] C. Herring, "Diffusional viscosity of a polycrystalline solid," *J Appl Phys*, vol. 21, no. 5, pp. 437–445, 1950.
- [44] G. FANTOZZI, J. CHEVALIER, C. OLAGNON, and J. L. CHERMANT, "Creep of Ceramic Matrix Composites," in *Comprehensive Composite Materials*, Elsevier, 2000, pp. 115–162. doi: 10.1016/B0-08-042993-9/00092-9.
- [45] R. L. Coble, "A model for boundary diffusion controlled creep in polycrystalline materials," *J Appl Phys*, vol. 34, no. 6, pp. 1679–1682, 1963.
- [46] J. Harper and J. E. Dorn, "Viscous creep of aluminum near its melting temperature," *Acta Metallurgica*, vol. 5, no. 11, pp. 654–665, 1957.
- [47] P. Yavari, D. A. Miller, and T. G. Langdon, "An investigation of harper-dorn creep—I. Mechanical and microstructural characteristics," *Acta Metallurgica*, vol. 30, no. 4, pp. 871–879, Apr. 1982, doi: 10.1016/0001-6160(82)90085-2.
- [48] C. R. Barrett, E. C. Muehleisen, and W. D. Nix, "High temperature-low stress creep of Al and Al+ 0.5% Fe," *Materials Science and Engineering*, vol. 10, pp. 33–42, 1972.
- [49] F. A. Mohamed, K. L. Murty, and J. W. Morris, "Harper-dorn creep in al, pb, and sn," *Metallurgical Transactions*, vol. 4, no. 4, pp. 935–940, 1973.
- [50] L. Anand, "Constitutive Equations for the Rate-Dependent Deformation of Metals at Elevated Temperatures," *J Eng Mater Technol*, vol. 104, no. 1, p. 12, 1982, doi: 10.1115/1.3225028.
- [51] D. Lee and F. Zaverl Jr, "A generalized strain rate dependent constitutive equation for anisotropic metals," *Acta Metallurgica*, vol. 26, no. 11, pp. 1771–1780, 1978.
- [52] L. Anand, "Constitutive equations for hot-working of metals," *Int J Plast*, vol. 1, no. 3, pp. 213–231, 1985, doi: 10.1016/0749-6419(85)90004-X.

- [53] S. B. Brown, "An Internal Variable Constitutive Model for the Thixotropic Behavior of Metal Semi-Solid Slurries," 1989.
- [54] G. O'Malley, J. Giesler, and S. Machuga, "The importance of material selection for flip chip on board assemblies," *IEEE Transactions on Components, Packaging, and Manufacturing Technology: Part B*, vol. 17, no. 3, pp. 248– 255, 1994, doi: 10.1109/96.311770.
- [55] J. Shepherd, "Lead Restrictions and Other Regulatory Influences on the Electronics Industry," in *Lead-Free Soldering*, J. Bath, Ed., Boston, MA: Springer US, 2007, pp. 5–19. doi: 10.1007/978-0-387-68422-2 1.
- [56] H. R. Kotadia, P. D. Howes, and S. H. Mannan, "Microelectronics Reliability Review paper A review: On the development of low melting temperature Pbfree solders," *Microelectronics Reliability*, vol. 54, no. 6–7, pp. 1253–1273, 2014, doi: 10.1016/j.microrel.2014.02.025.
- [57] M. Amagai, Y. Toyoda, and T. Tajima, "High solder joint reliability with lead free solders," in 53rd Electronic Components and Technology Conference, 2003. Proceedings., IEEE, 2003, pp. 317–322. doi: 10.1109/ECTC.2003.1216296.
- [58] J. Liang, S. Downes, N. Dariavach, D. Shangguan, and S. M. Heinrich, "Effects of load and thermal conditions on Pb-free solder joint reliability," *J Electron Mater*, vol. 33, no. 12, pp. 1507–1515, 2004, doi: 10.1007/s11664-004-0092-z.
- [59] J.-P. Clech, "Lead-Free Solder Joint Reliability Trends," in *Lead-Free Solder Interconnect Reliability*, D. Shangguan, Ed., ASM International, 2005, pp. 107–125.
- [60] Hongtao Ma, J. C. Suhling, P. Lall, and M. J. Bozack, "Reliability of the Aging Lead Free Solder Joint," in 56th Electronic Components and Technology Conference 2006, IEEE, 2006, pp. 849–864. doi: 10.1109/ECTC.2006.1645757.
- [61] MSC Software Corporation, *Theory and User Information*. 2018.

- [62] National Institute of Standards and Technology (NIST), "Sn-Ag Properties and Creep Data." [Online]. Available: https://www.metallurgy.nist.gov/solder/clech/Sn-Ag Other.htm#Poisson
- [63] T. T. Nguyen, D. Yu, and S. B. Park, "Characterizing the mechanical properties of actual SAC105, SAC305, and SAC405 solder joints by digital image correlation," *J Electron Mater*, vol. 40, no. 6, pp. 1409–1415, 2011, doi: 10.1007/s11664-011-1534-z.
- [64] National Institute of Standards and Technology (NIST), "Sn-Ag-Cu Properties and Creep Data." [Online]. Available: https://www.metallurgy.nist.gov/solder/clech/Sn-Ag-Cu Other.htm
- [65] Q. J. Yang, X. Q. Shi, Z. P. Wang, and Z. F. Shi, "Finite-element analysis of a PBGA assembly under isothermal/mechanical twisting loading," *Finite Elements in Analysis and Design*, vol. 39, no. 9, pp. 819–833, 2003, doi: 10.1016/S0168-874X(02)00134-8.
- [66] J. R. Davis, "ASM specialty handbook," Stainless Steel, vol. 10, 1994.
- [67] N. Bai, X. Chen, and H. Gao, "Simulation of uniaxial tensile properties for lead-free solders with modified Anand model," *Mater Des*, vol. 30, no. 1, pp. 122–128, 2009, doi: 10.1016/j.matdes.2008.04.032.
- [68] M. Basit, M. Motalab, J. C. Suhling, and P. Lall, "Viscoplastic Constitutive Model for Lead-Free Solder Including Effects of Silver Content, Solidification Profile, and Severe Aging," in *Volume 2: Advanced Electronics and Photonics, Packaging Materials and Processing; Advanced Electronics and Photonics: Packaging, Interconnect and Reliability; Fundamentals of Thermal and Fluid Transport in Nano, Micro, and Mini Scales*, ASME, Jul. 2015, p. V002T01A002. doi: 10.1115/IPACK2015-48619.
- [69] J. H. L. Pang, Lead Free Solder, vol. 9781461404. New York, NY: Springer New York, 2012. doi: 10.1007/978-1-4614-0463-7.
- [70] M. Riordan, "The lost history of the transistor," *IEEE Spectr*, vol. 41, no. 5, pp. 44–49, May 2004, doi: 10.1109/MSPEC.2004.1296014.

- [71] G. W. A. DUMMER, "The Development of Components, Transistors and Integrated Circuits," in *Electronic Inventions and Discoveries*, Elsevier, 1983, pp. 3–11. doi: 10.1016/B978-0-08-029354-7.50007-2.
- [72] AnySilicon, "Semiconductor Packaging History and Trends." [Online]. Available: https://anysilicon.com/semiconductor-packaging-history-trends/
- [73] J. H. Lau et al., "Design, Materials, Process, Fabrication, and Reliability of Fan-Out Wafer-Level Packaging," *IEEE Trans Compon Packaging Manuf Technol*, vol. 8, no. 6, pp. 991–1002, Jun. 2018, doi: 10.1109/TCPMT.2018.2814595.
- [74] T. Braun *et al.*, "Opportunities of Fan-out Wafer Level Packaging (FOWLP) for RF applications," in 2016 IEEE 16th Topical Meeting on Silicon Monolithic Integrated Circuits in RF Systems (SiRF), IEEE, Jan. 2016, pp. 35–37. doi: 10.1109/SIRF.2016.7445461.
- [75] T. Braun *et al.*, "Fan-Out Wafer and Panel Level Packaging as Packaging Platform for Heterogeneous Integration," *Micromachines (Basel)*, vol. 10, no. 5, p. 342, May 2019, doi: 10.3390/mi10050342.
- [76] C. Palesko, A. Palesko, and E. J. Vardaman, "Cost and yield analysis of multidie packaging using 2.5D technology compared to fan-out wafer level packaging," in *Proceedings of the 5th Electronics System-integration Technology Conference (ESTC)*, IEEE, Sep. 2014, pp. 1–5. doi: 10.1109/ESTC.2014.6962745.
- [77] L. T. Guan, C. K. Fai, and D. H. S. Wee, "FOWLP electrical performances," in 2016 IEEE 18th Electronics Packaging Technology Conference (EPTC), IEEE, Nov. 2016, pp. 79–84. doi: 10.1109/EPTC.2016.7861447.
- [78] V. S. Rao *et al.*, "Development of High Density Fan Out Wafer Level Package (HD FOWLP) with Multi-layer Fine Pitch RDL for Mobile Applications," in 2016 IEEE 66th Electronic Components and Technology Conference (ECTC), IEEE, May 2016, pp. 1522–1529. doi: 10.1109/ECTC.2016.203.
- [79] K. Seelig and D. Suraski, "A COMPARISON OF TIN-SILVER-COPPER LEAD-FREE SOLDER ALLOYS Karl Seelig and David Suraski AIM, Incorporated," *Lead-free Solder Alloys*, pp. 1–11, 2014.

- [80] M. Osterman and A. Dasgupta, "Life expectancies of Pb-free SAC solder interconnects in electronic hardware," *Journal of Materials Science: Materials* in *Electronics*, vol. 18, no. 1–3, pp. 229–236, Dec. 2006, doi: 10.1007/s10854-006-9017-3.
- [81] H. McCormick, P. Snugovsky, C. Hamilton, Z. Bagheri, and S. Bagheri, "The great SAC debate: comparing the reliability of SAC305 and SAC405 solders in a variety of applications," in *SMTA Pan Pacific Symposium*, Citeseer, 2007.
- [82] G. Iyer, E. Ouyang, W. Kittidacha, S. Tantideeravit, and L. Suresh, "Pb-free Solder: SAC105 vs SAC305 Drop-Test Reliability Data Comparison," in 2007 32nd IEEE/CPMT International Electronic Manufacturing Technology Symposium, IEEE, Oct. 2007, pp. 251–255. doi: 10.1109/IEMT.2007.4417072.
- [83] K. Mysore, G. Subbarayan, V. Gupta, and Ron Zhang, "Constitutive and Aging Behavior of Sn3.0Ag0.5Cu Solder Alloy," *IEEE Transactions on Electronics Packaging Manufacturing*, vol. 32, no. 4, pp. 221–232, Oct. 2009, doi: 10.1109/TEPM.2009.2024119.
- [84] D. Herkommer, J. Punch, and M. Reid, "Constitutive Modeling of Joint-Scale SAC305 Solder Shear Samples," *IEEE Trans Compon Packaging Manuf Technol*, vol. 3, no. 2, pp. 275–281, Feb. 2013, doi: 10.1109/TCPMT.2012.2227481.
- [85] M. S. Alam, K. M. R. Hassan, J. C. Suhling, and P. Lall, "High temperature mechanical behavior of SAC and SAC+X lead free solders," *Proceedings - Electronic Components and Technology Conference*, vol. 2018-May, pp. 1781– 1789, 2018, doi: 10.1109/ECTC.2018.00268.
- [86] P. Lall, D. Zhang, and J. Suhling, "High strain rate properties of SAC305 leadfree solder at high operating temperature after long-term storage," in 2015 IEEE 65th Electronic Components and Technology Conference (ECTC), IEEE, May 2015, pp. 640–651. doi: 10.1109/ECTC.2015.7159659.
- [87] H. H. Yuwen, H. B. Qin, M. B. Zhou, and X. P. Zhang, "The interfacial thermomechanical reliability of 3D memory-chip stacking with through silicon via array," 16th International Conference on Electronic Packaging Technology, ICEPT 2015, pp. 568–573, 2015, doi: 10.1109/ICEPT.2015.7236651.

- [88] Q. Wang, Y. Zhang, L. Liang, Y. Liu, and S. Irving, "Anand parameter test for Pb-free material SnAgCu and life prediction for a CSP," *Proceedings of the Electronic Packaging Technology Conference, EPTC*, vol. 00, 2007, doi: 10.1109/ICEPT.2007.4441437.
- [89] D. T. Janz, "Reliability of discrete power devices with lead free solder joints," 2004, MS dissertation. Institute for Microsystem Technology, Albert Ludwigs
- [90] S. Ahmed, M. Basit, J. C. Suhling, and P. Lall, "Characterization of Doped SAC Solder Materials and Determination of Anand Parameters," in *Volume 2:*Advanced Electronics and Photonics, Packaging Materials and Processing;

 Advanced Electronics and Photonics: Packaging, Interconnect and Reliability;

 Fundamentals of Thermal and Fluid Transport in Nano, Micro, and Mini Scales, American Society of Mechanical Engineers, Jul. 2015, pp. 1–14. doi: 10.1115/IPACK2015-48624.
- [91] M. S. Alam, "Mechanical Behavior and Microstructural Evolution of Lead Free Solder Alloys in Harsh Environment Applications," 2019. [Online]. Available: http://hdl.handle.net/10415/6788
- [92] M. M. R. Chowdhury, N. Fu, J. C. Suhling, and P. Lall, "Evolution of the cyclic stress-strain behavior of doped SAC solder materials subjected to isothermal aging," in 2017 16th IEEE Intersociety Conference on Thermal and Thermomechanical Phenomena in Electronic Systems (ITherm), IEEE, May 2017, pp. 1369–1379. doi: 10.1109/ITHERM.2017.7992641.
- [93] Texas Instruments Incorporated, "MicroStar BGA, Packaging Reference Guide," 2000. Accessed: Sep. 02, 2024. [Online]. Available: https://www.ti.com/lit/pdf/ssyz015
- [94] Z. Chen *et al.*, "Solder Joint Reliability Simulation of Fan-out Wafer Level Package (FOWLP) Considering Viscoelastic Material Properties," *2018 IEEE* 20th Electronics Packaging Technology Conference (EPTC), pp. 573–579, 2019, doi: 10.1109/eptc.2018.8654355.
- [95] T. C. Lui, "Lifetime prediction of viscoplastic lead-free solder: A new solder material, SACQ," in 2017 IEEE International Workshop On Integrated Power

- *Packaging (IWIPP)*, IEEE, Apr. 2017, pp. 1–4. doi: 10.1109/IWIPP.2017.7936754.
- [96] JEDEC Solid State Technology Association 2000, "JESD22-A104-B," 2009, *Arlington*.
- [97] F. X. Che and J. H. L. Pang, "Thermal fatigue reliability analysis for PBGA with Sn-3.8Ag-0.7Cu solder joints," in *Proceedings of 6th Electronics Packaging Technology Conference (EPTC 2004) (IEEE Cat. No.04EX971)*, IEEE, 2004, pp. 787–792. doi: 10.1109/EPTC.2004.1396715.
- [98] J. Morrow, "Cyclic Plastic Strain Energy and Fatigue of Metals," in *Internal Friction, Damping, and Cyclic Plasticity*, 100 Barr Harbor Drive, PO Box C700, West Conshohocken, PA 19428-2959: ASTM International, 1965, pp. 45–87. doi: 10.1520/STP43764S.
- [99] X. Wei, S. Su, S. Hamasha, H. Ali, J. Suhling, and P. Lall, "Fatigue Performance of Doped SAC Solder Joints in BGA Assembly," in 2020 19th IEEE Intersociety Conference on Thermal and Thermomechanical Phenomena in Electronic Systems (ITherm), IEEE, Jul. 2020, pp. 1035–1042. doi: 10.1109/ITherm45881.2020.9190479.
- [100] T. C. Lui and B. N. Muthuraman, "Relibability assessment of wafer level chip scale package (WLCSP) based on distance-to-neutral point (DNP)," in 2016 22nd International Workshop on Thermal Investigations of ICs and Systems (THERMINIC), IEEE, Sep. 2016, pp. 268–271. doi: 10.1109/THERMINIC.2016.7749063.
- [101] J. H. Lau, "The Roles of DNP (Distance to Neutral point) on Solder Joint Reliability of Area Array Assemblies," *Soldering & Surface Mount Technology*, vol. 9, no. 2, pp. 58–60, Dec. 1997, doi: 10.1108/09540919710800674.
- [102] W. Dauksher and W. S. Burton, "An examination of the applicability of the DNP metric on first level reliability assessments in underfilled electronic packages," *Microelectronics Reliability*, vol. 43, no. 12, pp. 2011–2020, Dec. 2003, doi: 10.1016/S0026-2714(03)00219-1.

- [103] X. Li and Z. Wang, "Thermo-fatigue life evaluation of SnAgCu solder joints in flip chip assemblies," *J Mater Process Technol*, vol. 183, no. 1, pp. 6–12, Mar. 2007, doi: 10.1016/j.jmatprotec.2006.09.010.
- [104] J. Clech, "THE COMBINED EFFECT OF ASSEMBLY PITCH AND DISTANCE TO NEUTRAL POINT ON SOLDER JOINT THERMAL CYCLING LIFE Jean-Paul Clech," Rosemont, 2016, pp. 88–98.
- [105] K. C. Norris and A. H. Landzberg, "Reliability of Controlled Collapse Interconnections," *IBM J Res Dev*, vol. 13, no. 3, pp. 266–271, May 1969, doi: 10.1147/rd.133.0266.
- [106] A. Zubelewicz, R. Berriche, L. M. Keer, and M. E. Fine, "Lifetime prediction of solder materials," *American Society of Mechanical Engineers (Paper)*, vol. 111, no. September 1989, pp. 179–182, 1988.
- [107] S. S. Manson and T. J. Dolan, "Thermal Stress and Low Cycle Fatigue," *J Appl Mech*, vol. 33, no. 4, pp. 957–957, Dec. 1966, doi: 10.1115/1.3625225.
- [108] F. C. Monkman and N. J. Grant, "An empirical relationship between rupture life and minimum creep rate in creep-rupture tests," in *Proceedings of the ASTM*, 1956, pp. 593–620.
- [109] R. Darveaux, K. Banerji, A. Mawer, G. Dody, and J. Lau, "Reliability of plastic ball grid array assembly," in *Ball grid array technology*, vol. 13, McGraw-Hill, 1995, pp. 379–442.
- [110] F. X. Che, "Study on board level solder joint reliability for extreme large fanout WLP under temperature cycling," in 2016 IEEE 18th Electronics Packaging Technology Conference (EPTC), IEEE, Nov. 2016, pp. 207–212. doi: 10.1109/EPTC.2016.7861473.
- [111] I. Guven, V. Kradinov, J. L. Tor, and E. Madenci, "Strain energy density criterion for reliability life prediction of solder joints in electronic packaging," *Journal of Electronic Packaging, Transactions of the ASME*, vol. 126, no. 3, pp. 398–405, 2004, doi: 10.1115/1.1773855.
- [112] W. Lin, Q. Pham, B. Baloglu, and M. Johnson, "SACQ Solder Board Level Reliability Evaluation and Life Prediction Model for Wafer Level Packages,"

- Proceedings Electronic Components and Technology Conference, pp. 1058–1064, 2017, doi: 10.1109/ECTC.2017.257.
- [113] U. Rahangdale *et al.*, "Mechanical characterization of RCC and FR4 laminated PCBs and assessment of their board level reliability," *Proceedings of the 16th InterSociety Conference on Thermal and Thermomechanical Phenomena in Electronic Systems, ITherm 2017*, pp. 1111–1118, 2017, doi: 10.1109/ITHERM.2017.7992613.
- [114] J. H. L. Pang, B. S. Xiong, and T. H. Low, "Low cycle fatigue models for lead-free solders," *Thin Solid Films*, vol. 462–463, no. SPEC. ISS., pp. 408–412, 2004, doi: 10.1016/j.tsf.2004.05.037.
- [115] A. Syed, "Accumulated creep strain and energy density based thermal fatigue life prediction models for SnAgCu solder joints," *Proceedings Electronic Components and Technology Conference*, vol. 1, pp. 737–746, 2004, doi: 10.1109/ectc.2004.1319419.
- [116] J. H. Lau, "State of the Art of Lead-Free Solder Joint Reliability," *J Electron Packag*, vol. 143, no. 2, Jun. 2021, doi: 10.1115/1.4048037.
- [117] R. S. Vargas C and V. Gonda, "Sensitivity of the structural behavior of SAC305 interconnects on the variations of creep parameters," in 2021 IEEE 15th International Symposium on Applied Computational Intelligence and Informatics (SACI), IEEE, May 2021. doi: 10.1109/SACI51354.2021.9465551.
- [118] R. S. Vargas Cruz and V. Gonda, "Solder joint reliability based on creep strain energy density for SAC305 and doped SAC solders," *MATEC Web of Conferences*, vol. 343, p. 02005, Aug. 2021, doi: 10.1051/matecconf/202134302005.
- [119] F. X. Che and J. H. L. Pang, "Thermal fatigue reliability analysis for PBGA with Sn-3.8Ag-0.7Cu solder joints," in *Proceedings of 6th Electronics Packaging Technology Conference (EPTC 2004) (IEEE Cat. No.04EX971)*, IEEE, 2004, pp. 787–792. doi: 10.1109/EPTC.2004.1396715.
- [120] Y. Degani, T. D. Dudderar, and K. L. Tai, "Flip chip packaging of memory chips," Nov. 23, 1999, *Google Patents*.

- [121] Y. C. Chiou, Y. M. Jen, and S. H. Huang, "Finite element based fatigue life estimation of the solder joints with effect of intermetallic compound growth," *Microelectronics Reliability*, vol. 51, no. 12, pp. 2319–2329, 2011, doi: 10.1016/j.microrel.2011.06.025.
- [122] R. Al Athamneh, D. B. Hani, H. Ali, and S. Hamasha, "Reliability modeling for aged SAC305 solder joints cycled in accelerated shear fatigue test," *Microelectronics Reliability*, vol. 104, Jan. 2020, doi: 10.1016/J.MICROREL.2019.113507.
- [123] European Commission, "Directive 2002/95/EC of the European Parliament and of the Council of 27 January 2003 on the restriction of the use of certain hazardous substances in electrical and electronic equipment," *Official Journal of the European Union*, vol. 37, pp. 19–23, 2003, Accessed: Sep. 02, 2024.

 [Online]. Available: chrome-extension://efaidnbmnnnibpcajpcglclefindmkaj/https://eurlex.europa.eu/LexUriServ/LexUriServ.do?uri=CELEX:32002L0095:en:PDF
- [124] M. Li, L. Zhang, N. Jiang, L. Zhang, and S. Zhong, "Materials modification of the lead-free solders incorporated with micro/nano-sized particles: A review," *Mater Des*, vol. 197, p. 109224, Jan. 2021, doi: 10.1016/j.matdes.2020.109224.
- [125] O. O. Ogbomo, E. H. Amalu, N. N. Ekere, and P. O. Olagbegi, "Effect of Coefficient of Thermal Expansion (CTE) Mismatch of Solder Joint Materials in Photovoltaic (PV) Modules Operating in Elevated Temperature Climate on the Joint's Damage," *Procedia Manuf*, vol. 11, pp. 1145–1152, 2017, doi: 10.1016/j.promfg.2017.07.236.
- [126] T. A. Woodrow, "NASA-DoD Lead-Free Electronics Project: Vibration Test," in Surface Mount Technology Association International Conference, 2010. Accessed: Nov. 05, 2022. [Online]. Available: https://ntrs.nasa.gov/citations/20100029736
- [127] D. K. Mu, S. D. McDonald, J. Read, H. Huang, and K. Nogita, "Critical properties of Cu 6 Sn 5 in electronic devices: Recent progress and a review," *Curr Opin Solid State Mater Sci*, vol. 20, no. 2, pp. 55–76, Apr. 2016, doi: 10.1016/j.cossms.2015.08.001.

- [128] B. Cal, "Lead-Free Soldering Risks and Reliability Problems in Space Electronics," in 2019 3rd International Symposium on Multidisciplinary Studies and Innovative Technologies (ISMSIT), IEEE, Oct. 2019, pp. 1–8. doi: 10.1109/ISMSIT.2019.8932788.
- [129] S. Su et al., "Fatigue Properties of Lead-free Doped Solder Joints," in Proceedings of the 17th InterSociety Conference on Thermal and Thermomechanical Phenomena in Electronic Systems, ITherm 2018, 2018. doi: 10.1109/ITHERM.2018.8419566.
- [130] M. Raza, L. Shewchenko, A. Olofinjana, D. Kent, J. Mata, and R. Haque, "The effects of Bi substitution for Sn on mechanical properties of Sn-based lead-free solders," *Journal of Materials Science: Materials in Electronics*, vol. 32, no. 17, pp. 22155–22167, Sep. 2021, doi: 10.1007/s10854-021-06691-y.
- [131] J. Albert and Á. Takács, "Optimization Methodology of Thermoelectric Peltier-Modules, for Structural Design and Material Selection, using MCDM and FEM Modelling," *Acta Polytechnica Hungarica*, vol. 21, no. 2, pp. 217–229, 2024, doi: 10.12700/APH.21.2.2024.2.12.
- [132] L. Zhang, J. G. Han, Y. Guo, and C. W. He, "Anand model and FEM analysis of SnAgCuZn lead-free solder joints in wafer level chip scale packaging devices," *Microelectronics Reliability*, vol. 54, no. 1, pp. 281–286, 2014, doi: 10.1016/j.microrel.2013.07.100.
- [133] L. Porkolab and I. Lakatos, "A Simulation System for Testing Side Crashes, in Non-Traditional Seating Positions, for Self-Driving Cars," *Acta Polytechnica Hungarica*, vol. 20, no. 7, pp. 63–82, 2023, doi: 10.12700/APH.20.7.2023.7.4.
- [134] J. H. Lau, "Recent Advances and Trends in Advanced Packaging," *IEEE Trans Compon Packaging Manuf Technol*, vol. 12, no. 2, pp. 228–252, Feb. 2022, doi: 10.1109/TCPMT.2022.3144461.
- [135] R. S. Vargas Cruz and V. Gonda, "Solder joint reliability based on creep strain energy density for SAC305 and doped SAC solders," *MATEC Web of Conferences*, vol. 343, p. 02005, Aug. 2021, doi: 10.1051/matecconf/202134302005.

- [136] R. S. Vargas C and V. Gonda, "Sensitivity of the structural behavior of SAC305 interconnects on the variations of creep parameters," in 2021 IEEE 15th International Symposium on Applied Computational Intelligence and Informatics (SACI), IEEE, May 2021. doi: 10.1109/SACI51354.2021.9465551.
- [137] R. S. Vargas Cruz and V. Gonda, "Creep and Reliability Prediction of a Fan-Out WLP Influenced by the Visco-Plastic Properties of the Solder," *Acta Polytechnica Hungarica*, vol. 19, no. 7, pp. 235–254, 2022, doi: 10.12700/APH.19.7.2022.7.13.
- [138] Y. Degani, T. D. Dudderar, and K. L. Tai, "Flip chip packaging of memory chips," 98303943.9, May 19, 1998
- [139] X.-K. Zhu and B. N. Leis, "Effective Methods to Determine Stress Intensity Factors for 2D and 3D Cracks," in *Volume 2: Pipeline Integrity Management*, American Society of Mechanical Engineers, Sep. 2014. doi: 10.1115/IPC2014-33120.
- [140] H. W. Swift, "Plastic instability under plane stress," *J Mech Phys Solids*, vol. 1, no. 1, pp. 1–18, Oct. 1952, doi: 10.1016/0022-5096(52)90002-1.
- [141] JEDEC Solid State Technology Association 2000, "JESD22-A104-B," 2009, **Arlington.** [Online]. Available: http://web.cecs.pdx.edu/~cgshirl/Documents/22a104b Temperature Cycling.pdf
- [142] L. Zhang *et al.*, "Determination of Anand parameters for SnAgCuCe solder," *Model Simul Mat Sci Eng*, vol. 17, no. 7, p. 075014, Oct. 2009, doi: 10.1088/0965-0393/17/7/075014.
- [143] R. S. V. C and V. Gonda, "Comparison of the thermal-mechanical behavior of a soldered stack influenced by the choice of the solder," in 2019 20th International Conference on Thermal, Mechanical and Multi-Physics Simulation and Experiments in Microelectronics and Microsystems (EuroSimE), IEEE, Mar. 2019, pp. 1–6. doi: 10.1109/EuroSimE.2019.8724590.